Beyond Photodynamic Therapy

Reessing, Friederike; Szymanski, Wiktor

Published in:
CURRENT MEDICINAL CHEMISTRY

DOI:
10.2174/0929867323666160906103223

Publication date:
2017

Beyond Photodynamic Therapy: Light-Activated Cancer Chemotherapy

Friederike Reeßing, Wiktor Szymanski*

Department of Radiology, University of Groningen, University Medical Center Groningen, Hanzeplein 1, 9713 GZ, Groningen, The Netherlands

w.szymanski@umcg.nl

Abstract

Light-activatable cytotoxic agents present a novel approach in targeted cancer therapy. The selectivity in addressing cancer cells is a crucial aspect in minimizing unwanted side effects that stem from unspecific cytotoxic activity of cancer chemotherapeutics. Photoactivated chemotherapy is based on the use of inactive prodrugs whose biological activity is significantly increased upon exposure to light. As light can be delivered with a very high spatiotemporal resolution, this technique is a promising approach to selectively activate cytotoxic drugs at their site of action and thus to improve the tolerability and safety of chemotherapy. This innovative strategy can be applied to both cytotoxic metal complexes and organic compounds. In the first case, the photoresponsive element can either be part of the ligand backbone or be the metal center itself. In the second case, the activity of a known organic, cytotoxic compound is caged with a photocleavable protecting group, providing the release of the active compound upon irradiation. Besides these approaches, also the use of photoswitchable (photopharmacological) chemotherapeutics, which allow an “on” and “off” switching of biological activity, is being developed. The aim of this review is to present the current state of photoactivated cancer therapy and to identify its challenges and opportunities.

Graphical abstract

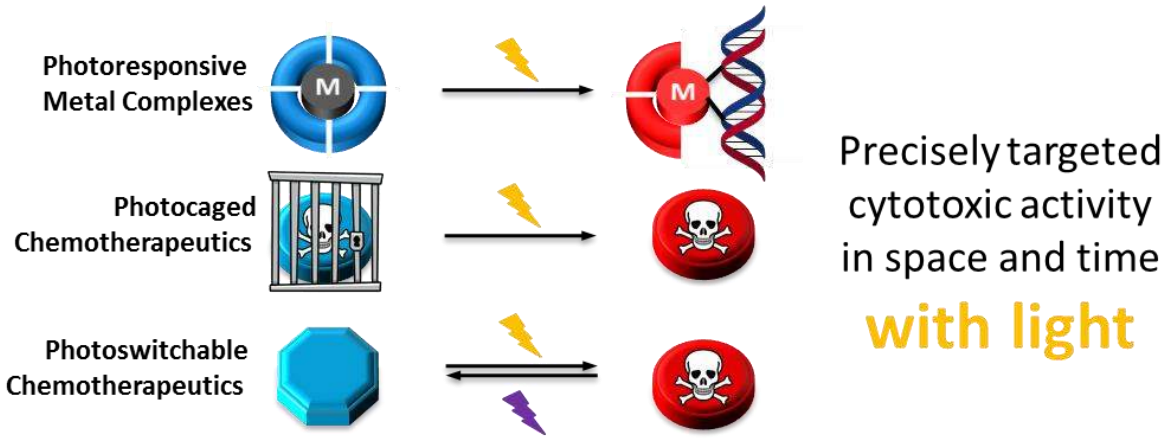

Table of contents

9. References

1. Introduction

Cancer is one of the major causes of death in the western world.[1] Even though new medicines are constantly being developed, standard cancer therapy still faces major challenges, including the high overall toxicity of commonly used cytotoxic agents, which stems from their low specificity towards cancer cells over the healthy ones.[2] This low specificity is caused by the fact that, on biochemical and physiological level, the differences between those types of cells are often very subtle. They are both, after all, human cells that share almost the same genetic information. Healthy cells, especially those that are fast dividing, such as bone marrow or mucosa cells, are affected strongly by chemotherapy, resulting in severe side effects like myelosuppression, nausea, fatigue and stomatitis.[3],[4]

Several attempts have been made to overcome these drawbacks. On one hand, many efforts have focused on the design of drugs that target particular features of tumor cells that do not exist or are not that abundant in healthy cells.[5] Examples are targets that are overexpressed in tumors, including receptors for growth factors (e.g. EGFR, Her2) and hormones (e.g. estrogen receptor in estrogen dependent breast cancer), and mutated tyrosine kinases (e.g. BRAF, ALK). However, a limitation of this strategy is that not every tumor shows one of these unique characteristics and, before initiating the therapy, diagnostic tests have to be done to distinguish between potential responders and non-responders. Furthermore, even a small change in the target molecule can cause resistance of the cells towards those highly specific agents.

On the other hand, the delivery system, and not the drug itself, can be modified to allow selective cancer therapy. Examples of such approach include liposomal formulations, which target affected cells utilizing the enhanced permeability and retention (EPR) effect:[6] a higher uptake of the drug in the tumor cells can be achieved by exploiting the fact that the blood vessels in the tumor environment typically have much bigger fenestrae than those in healthy tissues. Much effort has been devoted to enhancing this method, for example by PEGylation of the liposomes to hinder the uptake by the reticuloendothelial system (RES) or by combining the liposomes with ligands (like folic acid or antibodies against proteins of the surface of the tumor cell) for selective targeting.[6],[7] This general strategy is well established, for example to reduce the cardiotoxicity of Doxorubicin.[8] Undoubtedly, this approach is a major improvement in cancer therapy, but still not free from limitations. For instance, this technique cannot be applied for drugs that migrate easily through the lipid bilayer.[9]

Another approach to minimize the toxic effects on healthy tissues is to activate the cytotoxic drugs exclusively at their desired place of action. Light is well suited for this purpose, as it can be delivered with a very high spatiotemporal resolution. Furthermore, in a wide range of wavelengths, light does not cause any damage to the body. A Light-based technique, known as photodynamic therapy (PDT, Figure 2), is a well-established and clinically applied method to activate cytotoxic activity in a defined place and time.[10] It relies on the use of therapeutic agents, so-called photosensitizers, that form reactive oxygen species upon irradiation with light, resulting in necrosis of the irradiated tissue.[11] This way, the tumor cells can be targeted in a highly selective and precise manner resulting in very limited side effects. The cytotoxic agents are activated in situ and due to the short half live of ROS the damage to the surrounding, non-irradiated tissue is minimal. However, the formation of the cytotoxic species requires the availability of dioxygen, which presents a limitation of PDT, as most internal volume of solid tumors is hypoxic.[12] Thus, new efforts have been made to design photoactivatable drugs. These recent developments, which together with PDT can be described as photoactivatable cancer therapy but rely on another mechanism of cytotoxicity, are the topic of this review.

The objective in the development of photoactivatable drugs is to create compounds that show no, or minimal, cytotoxic activity in their resting state, while their cytotoxicity is activated upon exposure to light of appropriate wavelength. This means that the ratio between the IC_{50} value (half maximal inhibitory concentration) of the resting and the IC_{50} value of the activated compound should be as high as possible. This relation is illustrated in Figure 1. In the following text we will refer to this ratio as the phototherapeutic index.

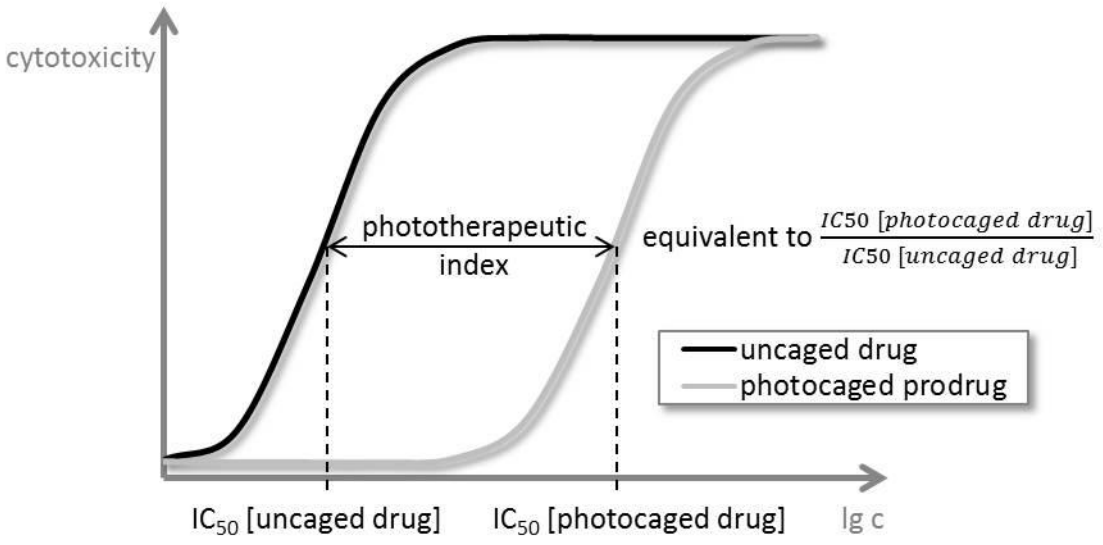

Figure 1: Illustration of phototherapeutic index.

Common challenges presented by these approaches include the following: (i) the design of a molecule that is activated by light of a wavelength in the visible or NIR spectrum (preferably 650-950 nm) to achieve maximal penetration and minimal toxicity[13] and (ii) the molecular design of a modification that "cages" the cytotoxic activity in the resting state in an efficient way and is stable towards *in vivo* factors, like human enzymes, pH shifts etc. Another important issue is the toxic effect of the drug after on-site activation, as it can still cause adverse effects while being cleared from the body.

The following sections introduce the designs, mechanisms of action and biological activities of different groups of photoactivatable anticancer agents published to date, giving special attention to the efficiency of caging the drug's activity and the wavelength dependence of activation. First, an overview of metal complexes, in which the metal center itself participates in a photochemical reaction during the activation process, is given. Subsequently, photoresponsive metal complexes that are activated by a photochemical reaction in the ligand backbone are presented. The final sections focus on photocleavable and photoswitchable organic cancer therapeutics.

2. Metal complexes with photoactivated cytotoxicity

Cytotoxic metal complexes, such as cisplatin, are successfully used in clinical cancer therapy. Also in the field of light-controlled cytotoxicity, photoactivatable variants of metal complexes are the most thoroughly studied compounds .[14],[15] With regards to the mode of action, transition metal complexes used in cancer therapy can be divided into three different classes (see figure 2): [14]

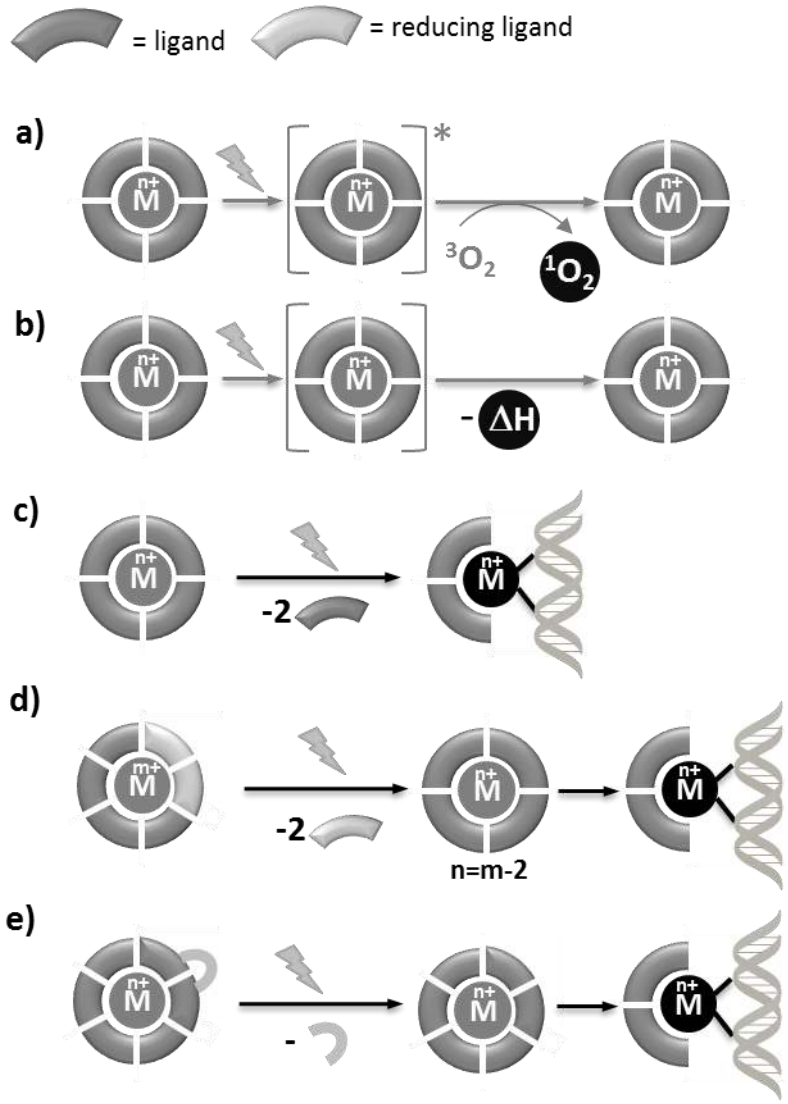

Figure 2: Mechanisms of photoactivated cytotoxicity of metal complexes. a) Photosensitisation, used e.g. in photodynamic therapy, leads to the formation of toxic singlet oxygen; b) Photothermal reaction causes damage due to the local production of heat; c) Photodissociation without changing the oxidation state of the metal, with toxicity due to the subsequent binding to a biomolecule; d) Photoreduction of the metal with subsequent binding to a biomolecule; e) Photocleavage of a part of the bidentate ligand, leading to ligand dissociation and binding to a biomolecule. The elements causing direct damage to the biological system are denoted in black color.

1. Photosensitisation (Photodynamic Therapy, PDT): irradiation leads to the excitation of the metal complex from the S0 state to the S1 state, after which it undergoes intersystem crossing to the T1 state. From there, it relaxes to ground state by reaction with triplet oxygen ($^3O_2$), causing the formation of reactive singlet oxygen ($^1O_2$).

2. Photothermal reaction: the excited state energy of the metal complex is converted into thermal energy, causing damage to the surrounding cells.

3. Photodissociation and/or redox change: upon irradiation, the ligands dissociate from the metal, upon which the metal may form complexes with DNA or other biomacromolecules. This ligand dissociation may also be the consequence of a change of the metal's redox state due to the irradiation (e.g. photoreduction of Pt^{IV} to Pt^{II}).

In this review, we focus on drugs that rely on the third of these mechanisms. For the PDT and photosensitisation processes, the reader is referred to other recent reviews.[16],[17]

2.1 Metals and ligands used in photoactivated chemotherapy

The use of metal complexes in photoactivated chemotherapy is associated with the light-triggered increase in their toxicity, which mainly stems from the cross-linking of double-stranded DNA (see section **2.2** for more detailed discussion on the mechanisms of toxicity). In this context, metal complexes with d^6 configuration are privileged, due to their favourable photophysical properties, relative non-lability under physiological conditions[14] and stable oxidation state with low spin.[18] Electrons in the d shell are a source of useful electronic transitions, which can be addressed with UV and visible light.[14] In particular, for d^6 metals, high extinction coefficients are observed for charge transfers, including metal-ligand charge transfer (MLCT) and ligand-metal charge transfer (LMCT) transitions.[19] For photoactivated chemotherapy, the most studied complexes are those of platinum(IV), ruthenium(II), and rhodium(III).

2.1.1 Platinum(IV)

Pt^{IV} forms octahedral, low spin complexes with $5d^6$ configuration of the metal. These complexes are kinetically inert under physiological conditions, which prevents side reactions in the biological system.[19]–[21] They also show much higher solubility in water in comparison to their activated counterparts, Pt^{II} complexes.[21],[22] For phototriggered cellular toxicity, mainly Pt^{IV} complexes with azide and iodide ligands are used. The photochemistry of such complexes is based on photoreductions (Figure 2d). These processes rely on Ligand-to-Metal Charge-Transfers (LMCTs),[23] which result in homolytic metal-ligand bond cleavage.[14] These processes are in fact reductive eliminations: the ligand is oxidised in an one-electron process, forming a radical, while the metal is reduced to Pt^{III}. The new complex is an even stronger oxidising agent and the oxidation of the second ligand leads to its liberation (in the form of a radical) and formation of planar Pt^{II} complex, which shows increased affinity to DNA. Notably, the liberated ligand radicals often show biological activity as well.

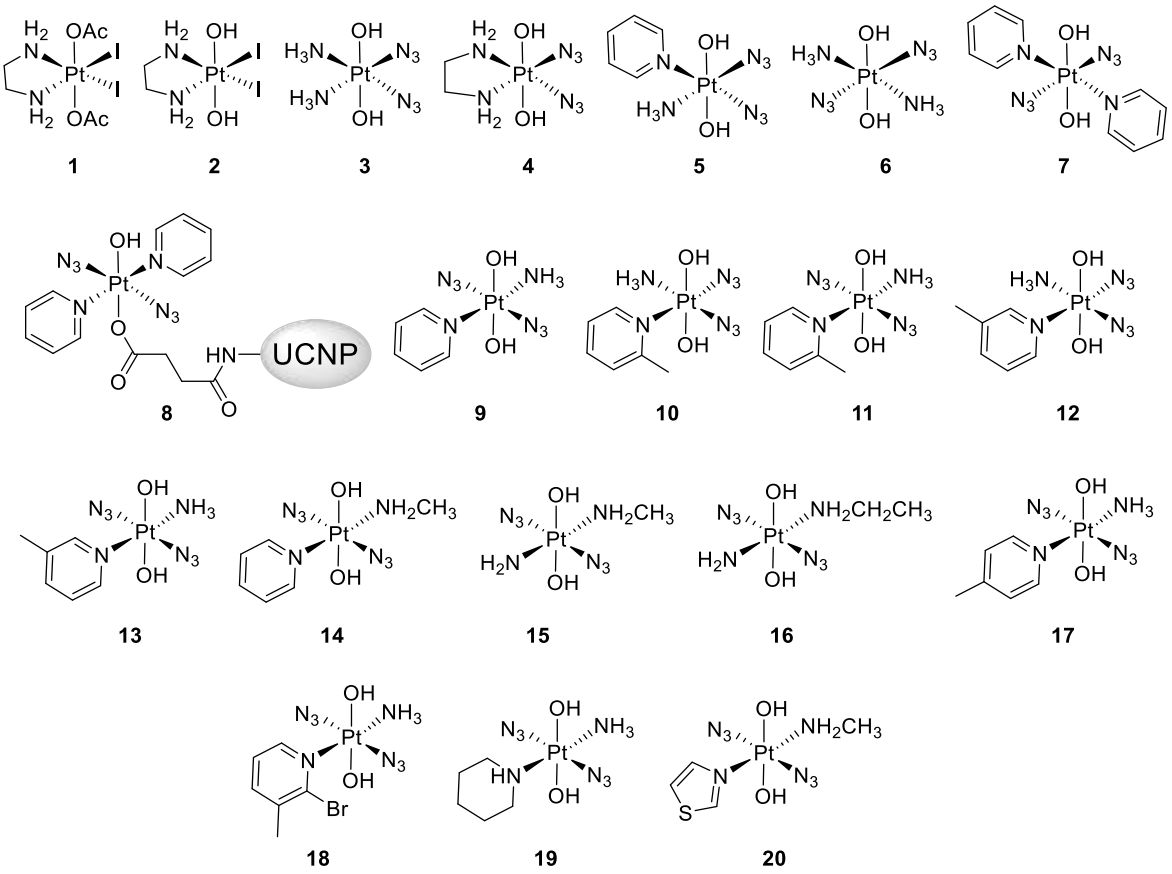

Figure 3. Platinum(IV) complexes with phototriggered cellular toxicity. UCNP = up-converting nanoparticle.

The complexes with iodide ligands, such as **1** and **2** (Figure 3), were developed in the 90's by the group of Bednarski.[24],[25] They featured intense LMCT bands and the irradiation with UV[25] and visible[24] light leads to formation of Pt^{II} complexes that were shown to bind to DNA. However, Pt^{II} complexes with iodide ligands readily undergo reduction by biological thiols (mainly glutathione, GSH), which resulted in their premature activation.[19] Also, their photoactivation is very slow.[26]

The next generation of complexes included azide ligands, introduced in *cis* configuration (compounds **3**,[26] **4**[26] and **5**,[27] Figure 3). These complexes show intense azide-to-Pt^{IV} LMCTs at λ ~ 256 nm. They also featured axial hydroxyl ligands that decrease the reduction potential, rendering the complexes stable in the presence of GSH and thus stabilizing them in biological medium.[19] Subsequently, it was discovered that installing the azide ligands in *trans* configuration leads to a bathochromic shift and increase in the intensity of the LMCT bands, as exemplified[28] by the comparison of *cis* complex **3** (λ_{max} = 256 nm, ε = 13.3 x 10^3 $M^{-1}cm^{-1}$) and *trans* complex **6** (λ_{max} = 285

nm, ε = 19.5 x 10^3 $M^{-1}cm^{-1}$). This relation is valid for all *trans*-azide complexes, which typically show the LMCT at λ = 285-295 nm. They also show higher photoinduced cell toxicity than their *cis*-counterparts (*vide infra*).[27]

Another breakthrough in the design of Pt^{IV}-based light-activatable chemotherapeutics was achieved when pyridines were introduced as the planar σ-donor, π-acceptor nitrogen ligands.[29],[30] They stay strongly bound to the complex even after activation and influence the biological activity, rendering the complexes more potent.[29],[30] Furthermore, they show beneficial effects on the wavelength of light that is used for activation: in complex **7** (Figure 3), a low-intensity, dissociative transition was observed at 414 nm, which was shown by time-dependent density functional theory (TDDFT) calculation to have a mixed ^{1}MLCT/^{1}IL (intraligand) character, involving platinum, azide and hydroxyl ligands[29]. This permitted the use of blue light for the activation, thus avoiding the use of toxic UV irradiation.

Finally, it was recently published[31] that with the use of lanthanide-doped up-converting nanoparticles (UCNPs), it is possible to use near-infrared (NIR) light (λ = 980 nm) to trigger the biological activity in Pt^{IV} complex **8** (Figure 3) by their photoreduction to planar Pt^{II} complexes and liberation from the nanoparticle. UCNPs are designed to absorb the deep-tissue-penetrating NIR light and convert it into photons of higher energy, emitting UV light. Due to these photoluminescent properties, they are an important tool for the future development of light-activated chemotherapeutics.[32]

In general, Pt^{IV} complexes are the most developed and most studied of all the metal-complex-based photoactivated chemotherapeutics, with an established mode of action. There is a wealth of data on their properties, structures and the role of ligands.[14],[15],[23],[33]–[35] The future challenges include the development of complexes addressable in the optical window (λ = 650-900 nm), which was already attempted with the use of up-converting nanoparticles.[31]

2.1.2 Ruthenium(II)

In contrast to Pt^{IV} complexes, whose activity relies on photoreductions, the photochemistry of Ru^{II} complexes used in light-activated therapy is based on ligand substitutions (Figure 2c), in which metal-centred transitions (MC, ^{3}d-d*) play a key role.[36] These substitutions involve the exchange of a nitrogen-containing ligand for a water molecule, to form aqua complexes that bind to DNA. Since the MC transition are (Laporte)-forbidden for octahedral centrosymmetric complexes, they usually give rise to very weak absorptions.[14] Therefore, the metal-centred states often have to be populated from other ones.

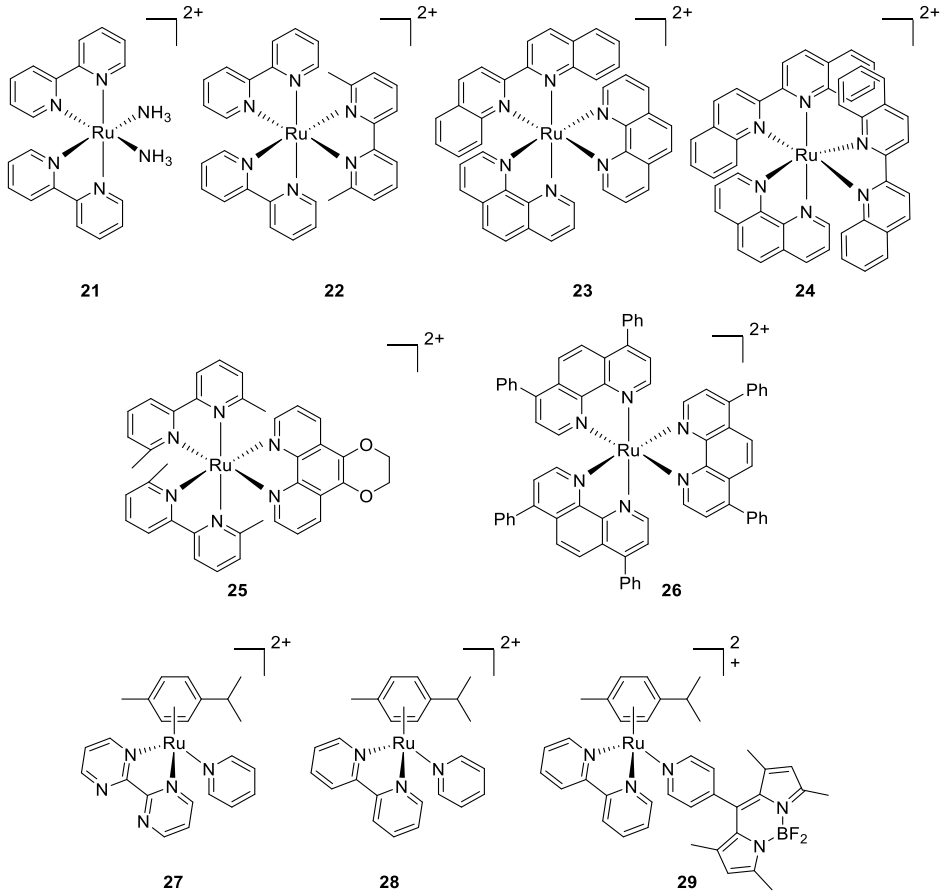

Figure 4. Ruthenium(II) complexes that show light-induced binding to DNA.

The group of Turro introduced an octahedral complex **21** (Figure 4), which in water shows a bpy $\pi \rightarrow \pi^*$ transition at λ_{max} = 290 nm (ε = 55.5 x 10^3 $M^{-1}cm^{-1}$) and Ru-bpy MLCTs at λ_{max} = 345 nm (ε = 7.3 x 10^3 $M^{-1}cm^{-1}$) and λ_{max} = 490 nm (ε = 8.2 x 10^3 $M^{-1}cm^{-1}$).[37] When irradiated at λ = 400 nm, the complex undergoes a substitution of ammonia ligands for water. The loss of ammonia ligands was suggested to originate from the ^{3}MC state, which in **21** is not accessible from the low-lying MLCT state. This explains the lack of reactivity when irradiation at λ > 450 nm is performed. This example highlights the main challenge for Ru^{II}-based agents for photoactivated chemotherapy:[38] the design of visible-light responsive systems requires the lowering of the ^{3}MLCT energy. This, however, increases the energy gap between the ^{3}MLCT and higher-lying dissociative ^{3}MC and impairs the population of the latter, reducing the dissociation efficiency.

The solution to that problem came with the introduction of complexes with distorted octahedral geometry. The distortion lowers the energy of low lying ^{3}MC states and allows their efficient population from ^{3}MLCT, leading to the release of the ligand.[36] This can be exemplified by complex **22**[36] (Figure 4), in which a bulky ligand was introduced to enable efficient activation with visible (λ > 450 nm) light.

This concept was taken further with the introduction of even more sterically-demanding ligands (2,2'-biquinoline) in complexes **23** and **24**.[39] Not only did this lead to efficient photoactivation through the ejection of the bulky ligand, but it also allowed the use of light of longer wavelength for this process. The parent molecule ($Ru(phen)_3$), without any sterically hindered ligands, showed an MLCT band at λ = 450 nm. Introduction of one 2,2'-biquinoline in complex **23** placed this band at λ = 525 nm and the second substitution in complex **24** resulted in a further shift to λ = 550 nm. Impressively, it was possible to efficiently activate the latter compound even with IR light (λ > 650 nm), resulting in a nine-fold increase in its cellular toxicity with respect to the non-irradiated one (Table 1, entries 57-62, *vide infra*).[39]

In parallel to the octahedral Ru^{II} complexes described above, the "piano-stool" complexes were developed by the group of Sadler and evaluated for their binding to DNA and cellular toxicity.[40],[41] In 2009 photoactivated complex **27** (Figure 4) was presented,[42] featuring a monodentate pyridine ligand, which undergoes light-induced substitution with a water molecule to form an aqua complex that binds to DNA. In the UV-Vis spectrum of **27**, two maxima are observed at λ_{max} = 383 nm (ε = 23.1 x 10^3 $M^{-1}cm^{-1}$) and λ_{max} = 254 nm (ε = 2.31 x 10^3 $M^{-1}cm^{-1}$). TDDFT showed that the absorbance tail at 400 nm is composed of mixed ^{1}MC and ^{1}MLCT transitions, partially dissociative due to the contributions from Ru-N(bpm) and Ru-N(py) σ*-antibonding orbitals. At higher energy, pure ^{1}MLCT (Ru-bpm) are found. Excitation, followed by intersystem crossing, leads to lowest energy ^{3}MC state, which is strongly dissociative towards the bipyrimidine ligand. Due to its bidentate nature, this ligand does not dissociate and the observed reactivity is caused by ^{3}MC states of higher energy, which are dissociative towards pyridine.[42]

In 2013, the group of Wang presented[38] an interesting strategy to activate "piano-stool" Ru^{II} complexes with visible light. Substitution of the pyridine ligand in prototypical complex **28** (Figure 4) with BODIPY-Py gave complex **29** (Figure 4). The resulting complex could efficiently be photoactivated to lose the BODIPY-Py ligand with a quantum yield of Φ = 4.1% at λ = 480 nm light irradiation. Having studied the mechanism of the activation, the authors excluded the energy transfer from ^{1}py-BODIPY* to ^{3}MLCT or ^{3}MC states. Instead, they attribute the dissociation to the weakened coordination capacity of ^{1}py-BODIPY*.[38]

In summary, Ru^{II} complexes are well-studied and they offer exciting possibilities for photoactivated chemotherapy. This is highlighted by the possibility of using visible[38] and NIR[39] light for their activation, enabled by the proper choice of ligands. The thorough understanding of the photochemical processes allows the researchers to design complexes that feature both red-shifted spectra and efficient light activation.[36],[39]

2.1.3 Rhodium(III)

The first photoactivated Rh^{III} complexes that showed binding to nucleosides, nucleotides and DNA were published as early as 1992 from the group of Morisson.[18] The majority of those complexes are thermally stable and photochemically labile. As in the case of Ru^{II} complexes, the photochemical process used to evoke cellular toxicity is the light-induced ligand exchange (Figure 2c).[18],[43],[44] This can be exemplified by compound **30**[18] (Figure 5), which shows absorption maxima at λ = 224 and 351 nm (both intraligand transitions) and λ = 380 nm (^{1}MC transition). Upon irradiation at λ = 350 nm, the chloride ligand of complex **30** is substituted to either form the aqua complex, or directly enable the binding to DNA. The ligand dissociation occurs from the lowest-lying ^{3}MC excited state.

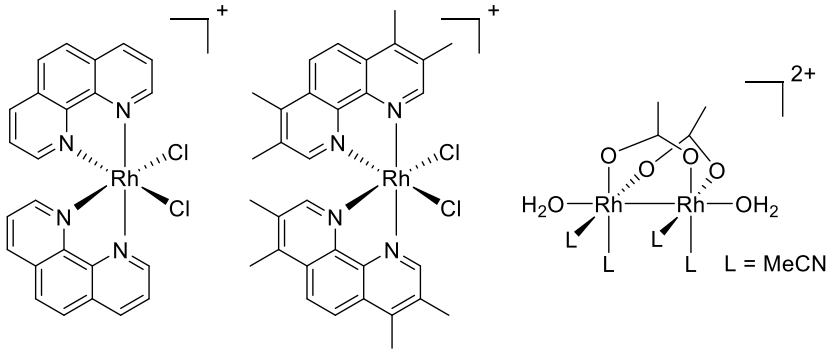

30 **31** **32**

Figure 5. Rhodium(III) complexes that undergo ligand exchange upon photoirradiation, which evokes their binding to DNA.

Introduction of methyl substituents to the phenantroline ligands in complex **30** leads to complex **31** (Figure 5).[44] The methylation renders phenantroline a stronger σ donor, allowing much more pronounced stabilization of either the pentacoordinate species formed upon photo-dissociation of the chloride ligand, or the transition state leading to it. This effect implies more efficient activation of **31** as compared to **30**, and indeed higher disappearance quantum yields have been observed for the methylated complex (at λ = 347nm: Φ_{30} = 0.03, Φ_{31} = 0.63; at λ = 254 nm: Φ_{30} = 0.013, Φ_{31} = 0.061).[44] This example shows how ligand engineering is used to change the quantum yield of the activation, a key and often neglected parameter in light-controlled chemotherapy.

In 2006, the group of Turro introduced complex **32**, the first photoactivated chemotherapeutic agent with a metal-metal bond.[43] It shows a weak absorption maximum at λ_{max} = 555 nm (ε = 160 $M^{-1}cm^{-1}$), which by TDDFT was attributed to be the metal-centred $Rh_2(\pi^*) \rightarrow Rh_2(\sigma^*)$ transition. Moreover, it features a stronger absorption maximum at lower wavelength, which

possesses contributions from $RhL_{eq}(\sigma^*)$ MOs, involving equatorial ligands L_{eq} and $d_{x^2-y^2}$ orbitals of Rh. Irradiation at $\lambda > 455$ nm in aqueous conditions leads to the exchange of equatorial MeCN ligands for water, giving rise to the toxic species. This process shows a wavelength-dependent quantum yield, which was explained by the photochemistry taking place from the excited states, involving the $RhL_{eq}(\sigma^*)$. Populating this orbital results in the dissociation of the equatorial ligands.

In general, complexes of Rh^{III} are much less studied for photoactivated cellular toxicity than the ones of Pt^{IV} and Ru^{II}. It is unclear if it is possible to adjust their structure towards activation in the optical window (λ = 650-900 nm). However, new approaches such as the design of complexes with metal-metal bond,[43] might offer exciting possibilities for the application of Rh^{III}-based therapeutics.

2.2 Molecular mechanisms for the toxicity of photoactivated metal complexes.

The toxicity of metal complexes used for cancer therapy is caused by their binding to DNA. Importantly, this reaction does not depend on the presence of oxygen, which permits the photoresponsive complexes to be activated also under hypoxic conditions. The target for their action is the nuclear DNA and the blueprint for their binding is provided by cisplatin, a clinically-used platinum(II) complex (Figure 6A).[45]

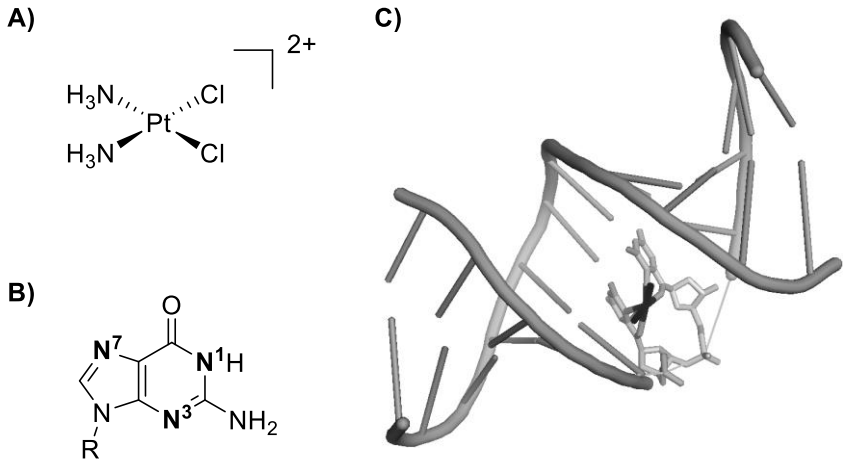

Figure 6. Cisplatin as a prototypical DNA-binding metal complex. A) Structure of cisplatin; B) Nitrogen sites in guanine molecule which can engage in complexes with metals; C) Crystal structure of the adduct of cisplatin(black) to adjacent guanines (light-grey) in a DNA strand (grey). Adapted from a PDB structure 1AIO.[46]

Inside the cells of the human body, cisplatin undergoes ligand exchange of chloride to water, caused by the lower intra- than extracellular concentration of Cl^-. This exchange leads to aqua-complexes that bind preferentially to the N^7-position of guanine in DNA (Figure 6B). The binding

results in the cross-linking of two guanine residues (Figure 6C). This DNA damage impairs RNA synthesis[47],[48] and ultimately leads to apoptosis.[45] The two-point attachment of the complex to DNA is crucial and many monofunctional adducts to DNA do not terminate the RNA synthesis.[47],[48]

The binding of activated metal complexes to DNA and the resulting blocking of RNA-polymerase activity can be assayed in many ways that differ in their complexity and the extent to which they represent the *in vivo* conditions. Most commonly used methods include the following:

1. The reaction of light-activated metal complexes with 9-alkyl-guanine (Figure 6B, R = alkyl) as a model compound, followed by isolation and characterisation of products.[38],[43],[49] This method provides insights into the binding mechanism, but its positive outcome is not an indication if the studied complex will show two-point binding to dsDNA.
2. The reaction of activated complexes with nucleosides, nucleotides and oligonucleotides and spectroscopic analysis of the products.[18],[26],[28],[29],[44],[49],[50]
3. Binding of complexes to short duplex strands of DNA and subsequent analysis of the melting point of the duplex. It is known that the melting point decreases for intrastrand binding and increases for interstrand binding.[37]
4. Reaction of complexes with DNA, followed by the isolation of DNA and determination of the metal content, for example by flameless atomic absorption spectroscopy (FAAS).[30],[47],[51]
5. Reaction of photoactivated complexes with plasmid dsDNA (for example pUC18,[37],[43],[52] pUC19[36],[39] or pSP73KB[47] plasmids) and analysis of their mobility using gel electrophoresis. It is known that a compound that binds to DNA and unwinds the duplex also reduces supercoils in closed circular DNA and thus decreases its mobility on the gel.[47] This simple method is very often used as it provides information on the affinity to dsDNA, although it is not informative with respect to the details of binding on a molecular level.
6. The use of gel electrophoresis to observe lower-mobility cross-linked DNA strands resulting from interstrand binding.[30],[47] The intrastrand cross-links can also be studied in cells, using a Comet assay.[50]
7. Finally, the transcription of DNA by RNA polymerase can be studied using DNA templates which were treated with photoactivated metal complexes (transcription mapping), providing information about the impairment of transcription caused by the binding,[30],[47] and also the preferred sites for addition of complexes to DNA.[50]

2.2.1 Platinum(IV)

The mechanisms behind the photoreactivity of Pt^{IV} complexes in the presence of DNA were presented by the group of Sadler in a series of seminal papers describing the behaviour of *cis*-azide complex **3,**[53],[54] trans-azide complex **6**[21] and pyridine-bearing complex **14**[55] (for structures of

complexes **3**, **6** and **14**, see Figure 3). Important observations that inspired the authors to propose these mechanisms include the detection of azide anions and liberation of O_2 when the reaction was carried out in PBS buffer[54] and the evolution of both O_2 and N_2 gasses when the reaction was performed under acidic conditions.[53]

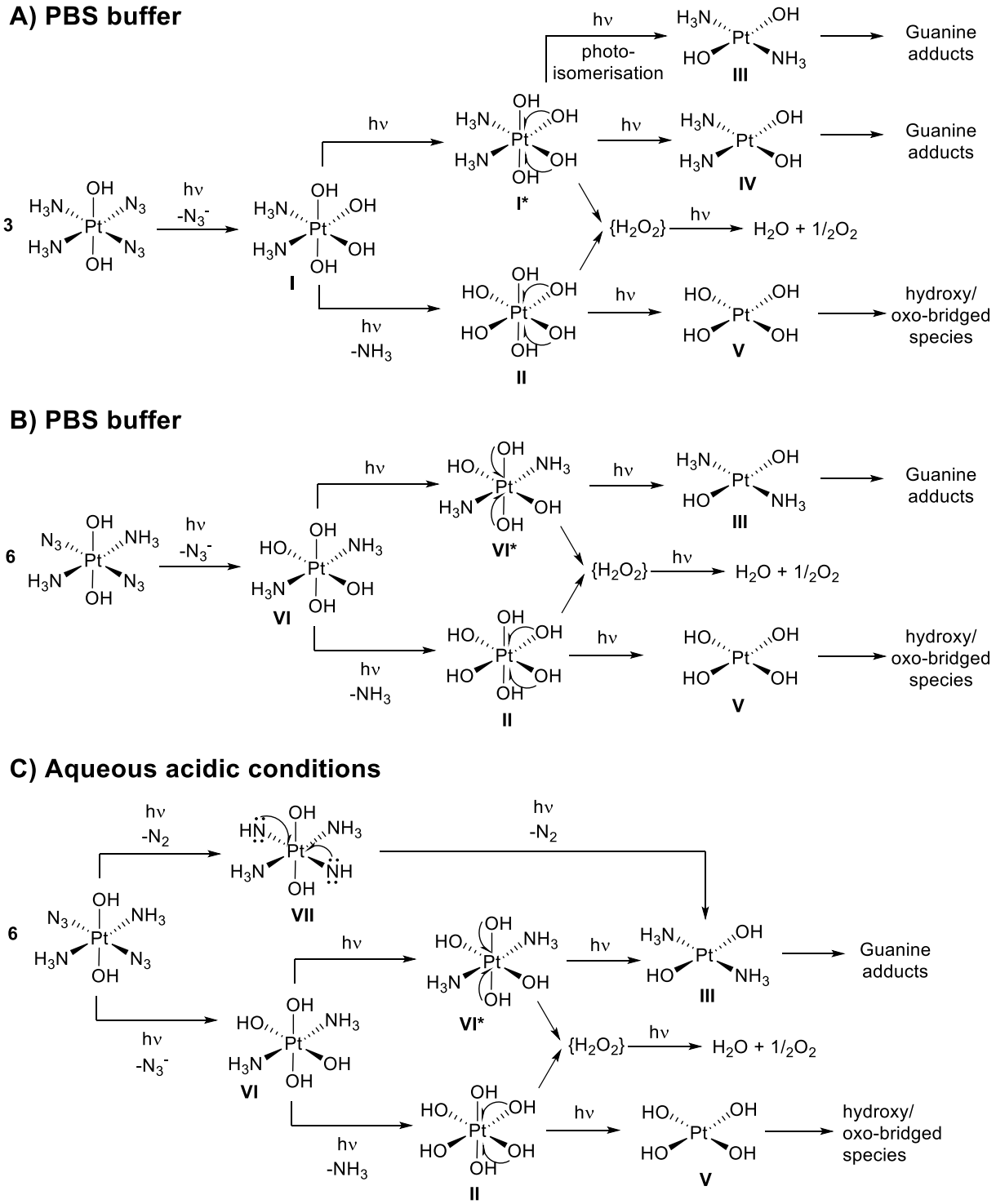

Figure 7. Light-induced reactivity for compounds **3** and **6** in aqueous buffer (A, B) and under acidic conditions (C). Charges were removed for clarity.[21],[54]

In aqueous PBS, complexes **3** and **6** showed similar reaction patterns (Figure 7A and B).[21],[54] The first step is the light-induced exchange of azide ligands to water (hydroxyl) ligands. The formed complexes (**I** and **VI**) undergo photoreduction, in which one-electron transfer from each hydroxyl substituent gives Pt^{II} species (**III** and **IV**) and two hydroxyl radicals. At higher concentration, the latter dimerise to H_2O_2, which at higher pH undergoes light-induced disproportionation to liberate oxygen gas. For the *cis*-complex **3** (Figure 7A), the photoreduction can be accompanied by photoisomerisation, leading to **III**, a common Pt^{II} intermediate with the pathway of compound **6** (Figure 7B). Finally, besides the photoredox and photoisomerisation process, the ammine complexes may undergo photolabilisation, leading to the exchange of ammonia ligands for water in complex **II**, which undergoes photoreduction to Pt^{II} species **V** and ultimately gives rise to insoluble hydroxo/oxo-bridged species.[21]

While the reactivity patterns of isomers **3** and **6** in PBS buffer are similar, their biological activity differs significantly, with **6** showing much higher toxicity.[27] This was explained[21] by: i) formation of additional side products in the reactions of complex **6**, which may be trapped by cellular targets (DNA, proteins) and ii) formation of more insoluble hydroxo/oxo-bridged species in the reactions of compound **3**.

Under acidic conditions, an additional reaction pathway prevails for Pt^{IV} complexes with azide ligands (Figure 7C, shown as an example for complex **6**).[21] The first step is the reduction of **6** to the corresponding Pt^{II} complex **VII** with concurrent oxidation of azide ligands to N_2. This reaction was suggested to proceed *via* nitrene intermediates (Figure 7C), the presence of which was confirmed in trapping experiments.[53] Further reactions proceed in an analogous way to those in PBS buffer.

Yet another reaction pathway was presented for the photoreaction of complex **14** with 5'GMP.[55] This study was inspired by the observation of the oxidised final product **33** in the reaction, which contained 8-oxo-guanine (Figure 8). Two possible mechanisms were proposed, involving singlet oxygen and formation of the nitrene intermediate (Figure 8, pathways B and A, respectively). For other complexes, the formation of azide radicals has been suggested as well.[56]

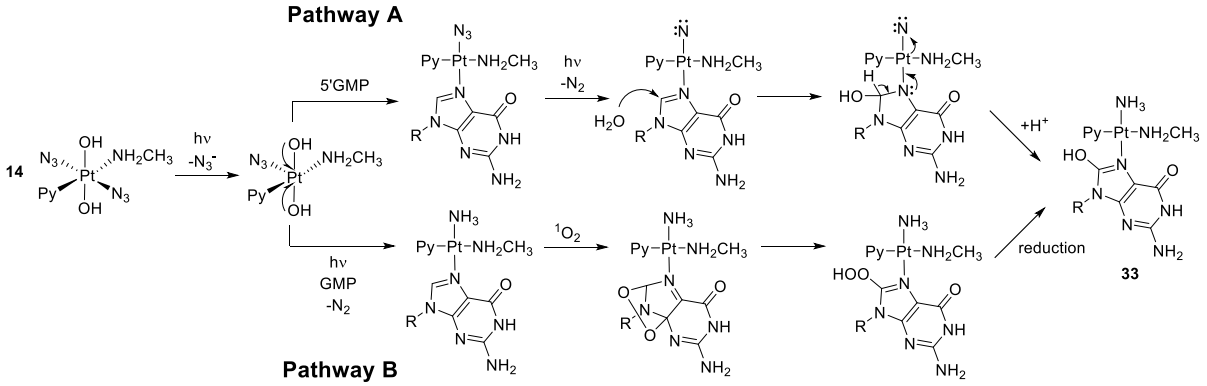

Figure 8. Light-induced reactivity for compound **14** in aqueous buffer, leading to the formation of product **33**. Py = pyridine. Charges were removed for clarity.[55]

The creation of the nitrene intermediate in pathway A (Figure 8) is caused by the loss of N_2 from the common intermediate, analogous to the process described above for compounds **3** and **6** under acidic conditions (Figure 7C). The transfer of electrons from guanine to nitrene results in the oxidation to the final product **33** (Figure 8, pathway A). Alternatively, in a [4+2] cycloaddition, singlet oxygen can react with one of the intermediates, leading to the final product (Figure 8, pathway B). Since singlet oxygen is generated upon irradiation of compound **14** with blue light, no external oxygen source is required and the oxidation process can proceed even under hypoxic conditions.

2.2.2 Ruthenium(II)

The irradiation of octahedral Ru^{II} complexes (**21-26**, Figure 4) leads to the substitution of the nitrogen-ligands with water to form the aqua complexes. Complex **21** loses both ammonia ligands, and the formed diaqua complex reacts further with DNA and its model compounds. Formation of adducts was observed with 9-methyl-guanine, 9-ethyl-guanine, and model single-stranded oligonucleotides.[37]

For "piano-stool" complexes (**27-29**, Figure 4), the irradiation leads to the dissociation of the pyridine ligand and its substitution with water to form the aqua complex.[42],[49] This complex binds to guanine residues in their N^7 position, which was confirmed using NOE measurements[49] on the model adduct to 9-ethyl-guanine (Figure 9).

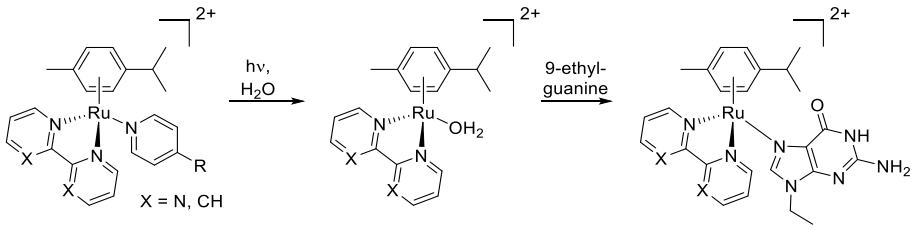

Figure 9. Binding of activated complexes **27-29** to 9-ethyl-guanine.[42],[49]

Importantly, continuous *in situ* irradiation of complex **38** (Figure 15) in the presence of a model nucleotide resulted in a loss of *p*-cymene and formation of an adduct involving two guanines,[49] highlighting the ability of piano-stool Ru^{II} complexes to form complexes in which the DNA is stapled.

2.2.3 Rhodium(III)

The photoinduced binding of Rh^{III} complexes to DNA was studied mainly by using nucleosides and their analogues as models.[18],[43],[44] Irradiation of Rh^{III} complexes **30** and **31** (Figure 5) leads to the liberation of chloride ligands and their substitution with water (Figure 10). It is unclear if the reaction with guanine nucleoside, instead of water, can directly lead to the formation of the adduct.[44]

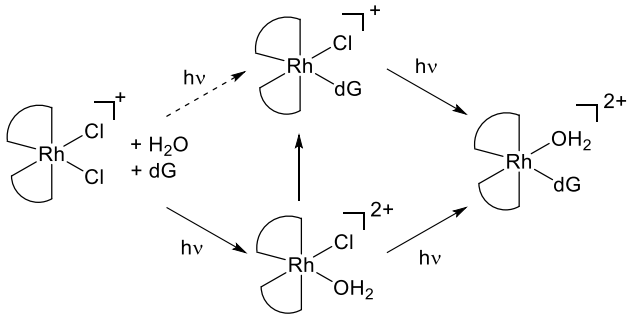

Figure 10. Sequence of events leading to the binding of photoactivated Rh^{III} to nucleosides.[44]

A series of products was observed when complexes **30** and **31** were photoactivated in presence of nucleosides. Mahnken et al.[18] report the isolation and characterisation of two adducts to dG: one of them was assigned to a structure in which guanosine binds to Rh^{III} *via* N1 (complex **34**, R=H, Figure 11), which is different than the binding observed for cisplatin (*via* N^7, Figure 6B). The structure of the second complex has not been assigned, but the authors present compelling evidence that this is not the N^7-adduct either. Furthermore, they report the isolation of complex **35** (Figure 11), formed from **30** and deoxyadenosine nucleoside. In the follow-up report,[44] the group of Morrison isolated additional products of binding of photoactivated complex **31** to dG: besides confirming the presence of N^1-adduct **34** (R=Me), they also isolated the O3-adduct **36** and, in contrast to their previous report, they confirm the formation of a diastereoisomeric mixture of N^7-bound complexes **37** (Figure 11).

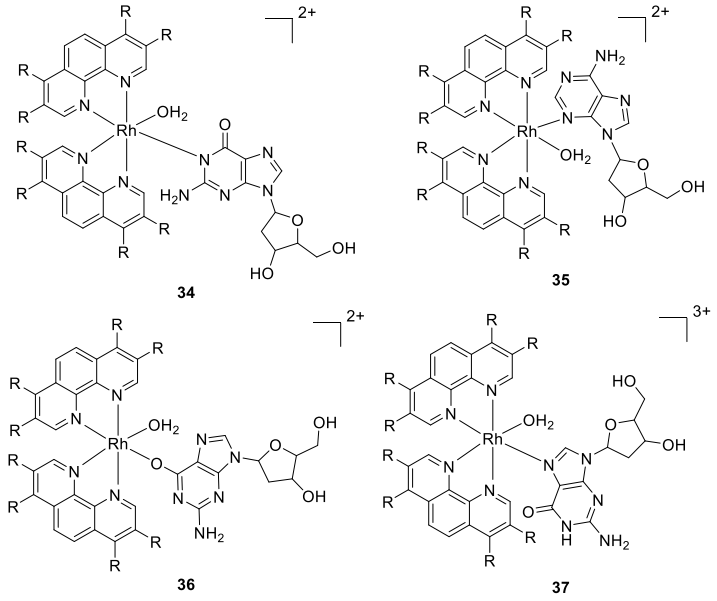

Figure 11. Products of the reaction of photoactivated compounds **30** and **31** with dG and dA.

Importantly, for the cellular toxicity the photoactivated metal complexes must bind to two nucleotides in a double-stranded DNA. With this requirement in mind, Lutterman et al. studied the binding of activated complex **32** (Figure 5) to pUC18 plasmid.[43] These experiments confirmed the decrease in the electrophoretic DNA mobility on agarose gel, indicative of the kinking of DNA induced by the drug.

2.3 Cytotoxicity of photoactivated metal complexes

The Pt^{IV}, Ru^{II} and Rh^{III} complexes, presented in Figures 3-4, were tested for their toxicity on several cell lines, both prior and after photoactivation. The overview of the published results is presented in Table 1, including the cell line type, wavelength of light used for activation, measured IC_{50} values and the phototherapeutic index (PI, a ratio of IC_{50} values for non-irradiated and irradiated complexes). For most of the cell lines, cisplatin (Figure 6A) was used as a reference (Table 1). Since the mechanism of toxicity sometimes differs from that of cisplatin[57] (*vide infra*), cisplatin-resistant cells lines were also often employed for the toxicity testing (Table 1).

Table 1: An overview of the toxicity of photoactivated metal complexes, prior and after irradiation, on selected cell lines. PI = phototherapeutic index.

Entry	cell line	complex	λ / nm	IC_{50} irradiated / μM	IC50 non-irradiated/ μM	PI	ref
1	TCCSUP human bladder cancer	**1**	>375	11.6±1.7	16.5±4.2	1.4	[25]
2		**2**	>375	7.3±1.6	9.4±2.2	1.3	[25]

3	5637 human bladder cancer	**3**	366	49.3±28.1	357±81	7.3	[19]
4		**4**	366	63.0±20.2	440±43	7.0	[19]
5		cisplatin	366	0.78±0.09	0.76±0.18	-	[19]
6	5637-CDDP human bladder cancer, cisplatin resistant	**3**	366	66.8±17.5	>200	>3	[19]
7		**4**	366	79.8±16.6	>200	>2.5	[19]
8		cisplatin	366	3.63±0.93	3.03±0.38	-	[19]
9	OE19 human oesophagal adenocarcinoma	**7**	365	4.7	>212.3	>45	[29]
10		**7**	420	8.4	>212.3	>25	[29]
11	HaCaT human keratinocytes	**3**	365	169.3	>287.9	>1.7	[27]
12		**5**	365	100.9	>244.4	>2.4	[27]
13		**6**	365	121.2	>287.9	>2.3	[27]
14		**7**	365	1.4	>212.3	>151	[29]
15		**7**	420	9.5	>212.3	>22	[29]
16		**9**	365	6.1	>244.3	>40	[30]
17		**9**	420	85.5	>244.3	>2.8	[30]
18		**10**	365	131.0	>236.3	>1.8	[27]
19		**11**	365	54.0	>236.3	>4.3	[27]
20		**12**	365	>236.2	>236.3	ND	[27]
21		**13**	365	22.0	144.1	6.5	[27]
22		**15**	365	65.6	>276.8	>4.2	[27]
23		**17**	365	7.1	97.8	14	[27]
24		**18**	365	61.0	108.0	1.8	[27]
25		cisplatin	365	144	173	-	[30]
26	A2780 human ovarian carcinoma	**3**	365	135.1	>287.9	>2.1	[27]
27		**5**	365	79.6	>244.4	>3.1	[27]
28		**6**	365	99.2	>287.9	>2.9	[27]
29		**7**	365	1.4	>212.3	>151	[29]
30		**9**	365	1.9	>244.3	>128	[30]
31		**10**	365	65.9	>236.3	>3.6	[27]
32		**11**	365	51.0	>236.3	>4.6	[27]
33		**12**	365	63.6	>236.3	>3.7	[27]
34		**13**	365	2.6	26.8	10	[27]
35		**14**	365	2.3	>225	>98	[58]
36		**15**	365	39.8	>276.8	>7	[27]
37		**17**	365	4.2	108.7	26	[27]
38		**18**	365	15.8	31.3	2	[27]
39		**20**	365	3.2	>225	>70	[58]
40		cisplatin	365	151.3	152	-	[30]
41	A2780CIS human ovarian carcinoma, cisplatin resistant	**3**	365	204.9	>287.9	>1.4	[27]
42		**5**	365	108.7	>244.3	>2.3	[27]
43		**6**	365	163.6	>287.9	>1.8	[27]
44		**7**	365	14.5	>212.3	>15	[29]
45		**9**	365	16.9	>244.3	>14	[30]
46		**10**	365	165.2	>236.3	>1.4	[27]
47		**11**	365	59.7	>236.3	>4	[27]
48		**12**	365	>236.3	>236.3	ND	[27]
49		**13**	365	2.9	57.7	20	[27]
50		**15**	365	128.7	>276.8	>2.2	[27]
51		**17**	365	5.4	134.9	25	[27]

52		**18**	365	38.2	54.4	1.4	[27]
53		cisplatin	365	261	229	-	[30]
54	HL60 human leukaemia	**9**	366	35.08±8.37	inactive	high	[59]
55		**19**	366	20.84±0.99	inactive	high	[59]
56		**22**	>450	1.6±0.2	>300	>188	[36]
57		**23**	>400	1.2	52.5	44	[39]
58		**23**	>600	7.6	52.5	6.9	[39]
59		**23**	>650	15.8	52.5	3.3	[39]
60		**24**	>400	2.4	47.3	20	[39]
61		**24**	>600	2.3	47.3	21	[39]
62		**24**	>650	5.1	47.3	9.3	[39]
63		**25**	>400	0.16±0.01	>300	>1880	[60]
64		**26**	>400	0.35±0.18	3.75±0.18	11	[61]
65		cisplatin	>450	3.1±0.2	3.1±0.1	-	[36]
66	A549 human lung cancer	**22**	>450	1.1±0.3	150±7	136	[36]
67		**26**	>400	0.11±0.02	0.62±0.08	8	[36]
68		cisplatin	>450	3.4±0.6	3.5±0.6	-	[36]
69	A549 human lung cancer spheroids	**22**	>450	21.3±0.3	>300	>14	[36]
70		cisplatin	>450	42±3.6	42±3.6	-	[36]
71	HS-27 human skin	**32**	>400	12±2	410±9	34	[43]

Since metal complexes in their non-activated form usually show very low toxicity, the phototherapeutic index observed for them is high (Table 1). Often, it is not possible to determine the precise IC_{50} for the non-irradiated complex, due to e.g. limitations in solubility. In such cases, Table 1 shows the minimum value of PI. The values were obtained in experiments in which cells are grown in the presence of compounds that are either pre-irradiated or irradiated *in situ* for a few minutes[20],[36]-hours[19],[31]. After a certain time (usually in the range of hours[20]-days[19],[31],[36]), the cell survival is assessed. Typical dose-response curves observed in such experiments are presented in Figure 12.

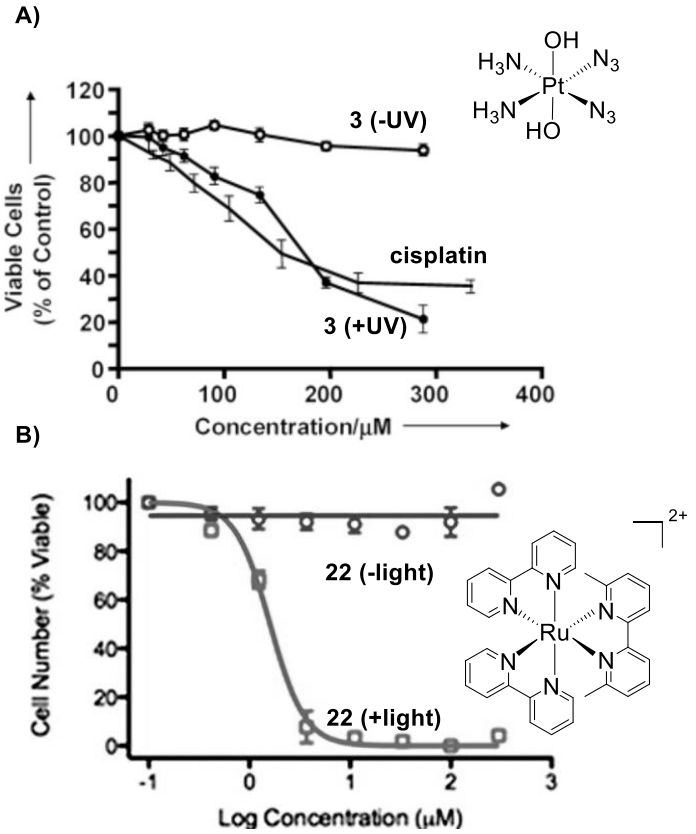

Figure 12. Examples of toxicity measurements for the photoactivated metal complex. A) light-dependent toxicity of Pt^{IV} complex **3** on human keratinocytes; Adapted with permission from ref. 28. Copyright 2006 Wiley-VCH; B) light-dependent toxicity of Ru^{II} complex **22** on human leukemia cells. Adapted with permission from ref. 36. Copyright 2012 American Chemical Society.

2.3.1 Platinum(IV) complexes

The first photoactivated, cytotoxic Pt^{IV} complexes carried iodide ligands in *cis*-configuration (**1** and **2**, Figure 3).[25] They showed high potency towards human bladder cancer cell line, albeit with very low PI (Table 1, entries 1 and 2), which probably stems from their light-independent activation with glutathione.[19] This problem of premature activation was solved by the introduction of azide ligands in *cis*-complexes **3**, **4**, and **5**, for which higher PI values were observed (Table 1, entries 3, 4, 6, 7, 11, 12, 26, 27, 41 and 42). However, these complexes still showed low potency compared to cisplatin (Table 1, entries 3-5), even on cisplatin-resistant cells (Table 1, entries 6-8).

Improved potencies were observed for the *trans*-azide complexes (e.g. **6**,[27] **7**,[29]and **9,**[30] Figure 3). In a seminal publication from the group of Sadler,[27] this general trend was studied in detail by comparison of the *cis* complexes **3**, **10** and **12** with their *trans* isomers **6**, **11** and **13** (Table 1, entries 11, 13, 18-21, 26, 28, 31-34, 41, 44 and 46-49). High potencies were also observed when an ammonia ligand was substituted for methylamine or ethylamine, as in complexes **14**- **16**.[27] Substitution of one of the ammonia ligands in complexes **3** and **6** for pyridine, resulting in complexes

5 and **9**, also showed beneficial influence on potency, with very low IC_{50} values and very high PI values found especially for the trans-azide complex **9** (Table 1, entries 16, 17, 30 and 45).[30] Effects of the substitution on pyridine ligands were assayed by comparison of complexes **9**, **10**, **12**, **13**, **17** and **18** (Figure 3); lowest IC_{50} values were found for the complexes with methyl-substituted pyridine ligands, albeit with compromised phototherapeutic index (Table 1, entries 17-23, 30-34 and 45-52). Finally, substitution of pyridine for piperidine in complex **19**[59] and for thiazole in complex **20** showed only subtle influence on the potency (Table 1, entries 30, 38 and 54-55).

In an attempt at a deeper understanding of the mechanism of cellular toxicity, the group of Sadler studied the influence of cellular accumulation and lipophilicity of complexes **6**, **7**, **9**, **11** and **13-16** on their phototoxicity.[58] The lipophilicity of complexes was derived from their HPLC retention times, revealing that the methyl-pyridine complexes **11** and **13** are the most lipophilic, while the complexes without aromatic ligands (**6**, **15**, **16**) are the most hydrophilic.[58] No correlation was found between the polarity and the cellular accumulation, which was observed to be the highest for complexes **7** and **15**.[58] Based on this observation, the authors postulate that an active mechanism is, at least partially, involved in the membrane transport.[58] Furthermore, neither lipophilicity, nor the cellular accumulation correlated with the toxicity of photoactivated complexes on A2780 cell line, suggesting that other factors, including quantum yield and the mode of interactions of activated complexes with cellular targets, may play a role in determining the toxicity.[58]

Already quite early in the development of the photoactivated metal complexes it has been established that they do not show cross-resistance with cisplatin,[19] suggesting a different mechanism of action. Another difference observed between cisplatin and complexes **3** and **4** (Figure 3) was the effect on the morphology of 5637 human bladder cancer cell lines. While exposure to cisplatin had little influence on the cells and their contacts, the exposure to irradiated complexes **3** or **4** for the same period of time resulted in shrinkage of cells and loss of contact with neighbouring cells and ultimately led to the destruction of the cell nuclei.[19] In the absence of light, complex **3** did not cause any changes in the cell morphology. Furthermore, light was shown to have no effect on platinum uptake to the cells.[19]

Further studies performed with complex **9** shed light on the toxicity mechanism and its distinct differences from action of cisplatin and etoposide, which both cause apoptotic cell death (Figure 13).[20] Observation of cell morphology (Figure 13A) revealed that complex **9** did not induce apoptosis, in contrast to cisplatin and etoposide. Instead, the cells treated with **9** showed only slight swelling.[20] Accordingly, in cell cycle analysis, significant differences to the control group were observed only for cisplatin and etoposide, while the cell cycle phase distribution did not differ between the control and cells treated with complex **9** (Figure 13B).[20] Finally, flow cytometric

measurements (Figures 13C and 13D) further confirmed that the exposure of cells to complex **9** does not lead to apoptosis.

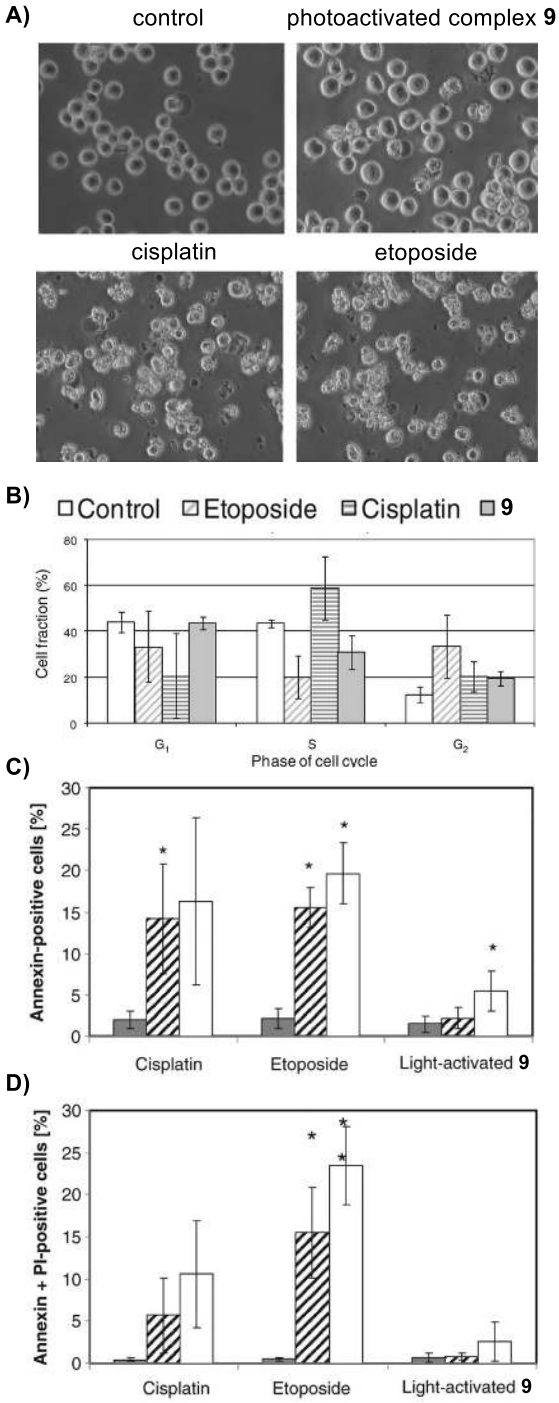

Figure 13. The differences in cellular activity between cisplatin, etoposide and complex **9** on HL60 cells after 48 hours of treatment. A) Phase contrast photos showing the morphology of the cells; B) Cell cycle analysis; C) Flow cytometric distribution of the cells, using Annexin V-FITC to identify apoptotic cells; gray bars: untreated controls, slashed bars: compound at IC_{50}, open bars: compound at IC_{90} (concentration at 90% of maximal inhibition); C) Flow cytometric distribution of the cells, using both Annexin V-FITC and propidium iodide (PI) to identify dead and necrotic cells; gray bars:

untreated controls, slashed bars: compound at IC_{50}, open bars: compound at IC_{90}. Adapted with permission from ref. 20. Copyright 2012 AACR.

Based on these results and earlier observations that complex **9** does not activate caspase-3,[30] the authors convincingly ascertained that apoptosis is not the mechanism by which this complex exerts its cytotoxicity. Instead, they suggested autophagic cell death as predominant pathway, which was supported by the increased levels of LC3B-II, a key protein associated with autophagosome.[20] On the other hand, it has to be noted that experiments on the A2780 cell line toxicity of complex **8** (Figure 3) bound to the up-converting nanoparticles, reported by Min *et al*., revealed that an apoptotic pathway is most probable.[31]

The seminal study on the activity of complex **9**[20] furthermore reported an important experiment performed on nude mice bearing xenograft OE19 tumours. Two important conclusions were drawn from this study. Firstly, the non-irradiated complex **9** administered at dose as high as ten times the maximum tolerated dose of cisplatin did not lead to any behavioural changes of the animals. Secondly, mice treated with irradiated complex **9** showed consistently less tumour growth than the ones treated with non-irradiated one or just irradiated without any drug administered. On day 35 of the experiments, two out of seven treated mice survived, while all the mice from control groups had died. This example[20] highlights the potential of light-activated metal-based chemotherapeutics for *in vivo* applications.

2.3.2 Ruthenium(II) complexes

The cellular toxicity (Table 1, entries 56-70)of Ru^{II} complexes (Figure 4) was studied by the group of Glazer.[36],[39] While their exact mechanism of action has not been elucidated yet, these complexes show very high potency, sometimes even higher than cisplatin (Table 1, entry 56, 57, 60 and 64-67). Complex **22** (Figure 4) stands out due to very high activity (Table 1 and Figure 9B) and fast activation, as it requires only 3 minutes of irradiation by visible light ($\lambda > 450$ nm). Its cytotoxicity has been shown on HL60 human leukaemia cells and A549 human lung cancer cells.[36] Furthermore, its potency is superior to cisplatin also on 3-D tumour spheroids (Table 1, entries 69-70), which mimic the *in vivo* properties of solid tumours, including the hypoxic regions, changes in cell shape and diminished permeability to drugs.

Recently, the group of Glazer reported further attempts to increase the potency of the Ru^{II} agents by ligand engineering.[39],[60]–[62] Complexes **23** and **24** (Figure 4) also show high potency and fast activation. Their application is further enabled by the fact that they can be activated with NIR light (Table 1, entries 57-62).[39] Potency superior to cisplatin, albeit with a low phototherapeutic index, was also observed for complex **26** (Figure 4) upon activation with visible light (Table 1, entries

64, 67).[61] Finally, the most impressive results, regardless of the type of metal used in the complex, were obtained when compound **25**, bearing sterically hindered ligands, was tested on HL60 cells (Table 1, entry 63): a sub-micromolar IC_{50} value was measured, with a phototherapeutic index of >1800. In summary, the research focused on photoactivated Ru^{II} complexes delivers many privileged structures and serves as an important alternative to the use of Pt^{II} complexes. Further developments and mechanistic studies are eagerly awaited.

2.4. Functional ligands: targeted and dual-action metal-based chemotherapeutics

The possibility of using light for local activation of cellular toxicity of metal complexes constitutes an important targeting approach to chemotherapy. For several of the complexes, additional methods to achieve selective accumulation in tumours have been proposed.

Inspired by the fact that the serum of some cancer patients is depleted in L-tryptophan, and recognising the crucial role of this amino acid as an electron transfer mediator, the group of Sadler studied the formation of azidyl radicals from complex **7** (Figure 3) in the presence and absence of L-Trp.[56] A dose-dependent protective effect of L-Trp was observed on A2780 human ovarian cancer cells (Figure 14), suggesting a possible mechanism for the selective targeting of tumour cells by photoactivated complex **7**.

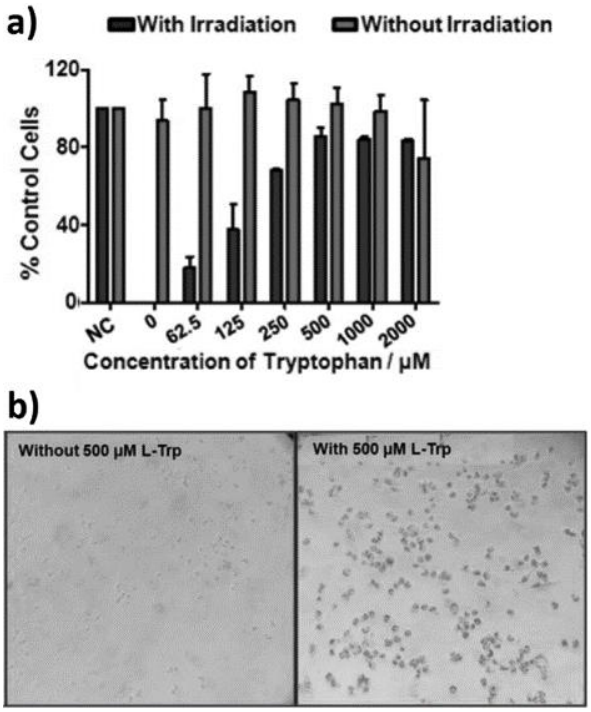

Figure 14. The effect of L-Trp on the toxicity of photoactivated complex **7** for A2780 cancer cell lines. a) Effects of varying the concentration of L-Trp on cell survival in the presence of photoactivated **7**

(42.4 μM); b) A2780 cells with and without L-Trp after treatment with complex **7**. Adapted with permission from ref. 56. Copyright 2012 American Chemical Society.

A more direct approach to tumour-targeting was presented with compound **38** (Figure 15), which was derived from compound **27** (Figure 4) by a modification of the pyridine ligand.[49] Two different peptides were introduced to the ligand: Arg-Gly-Asp (RGD), which is known to bind to the integrins on tumour endothelial cells, and octreotide, which is a cyclooctapeptide analogue of somatostatin and binds selectively to somatostatin receptors in the tumour cell membrane. The modification of the pyridine ligand did not influence the light-induced release of the toxic aqua complex. The experiments on the photoinduced binding of modified metal complexes to native and peptide-modified oligonucleotides revealed that the activated Ru^{II} complex shows preference to DNA over peptidic *N*- and *S*- donor ligands (His and Met, respectively). Importantly, and in contrast to the previous studies on Ru^{II} complexes (Figure 4), in one experiment a chelate was observed, in which the *p*-cymene has dissociated and $\{Ru(bpm)\}^{2+}$ was bound to two adjacent guanines in the DNA sequence, instead of just one. Unfortunately, no studies that would show the targeting effect of the added receptor ligands in an *in vivo* model were presented.

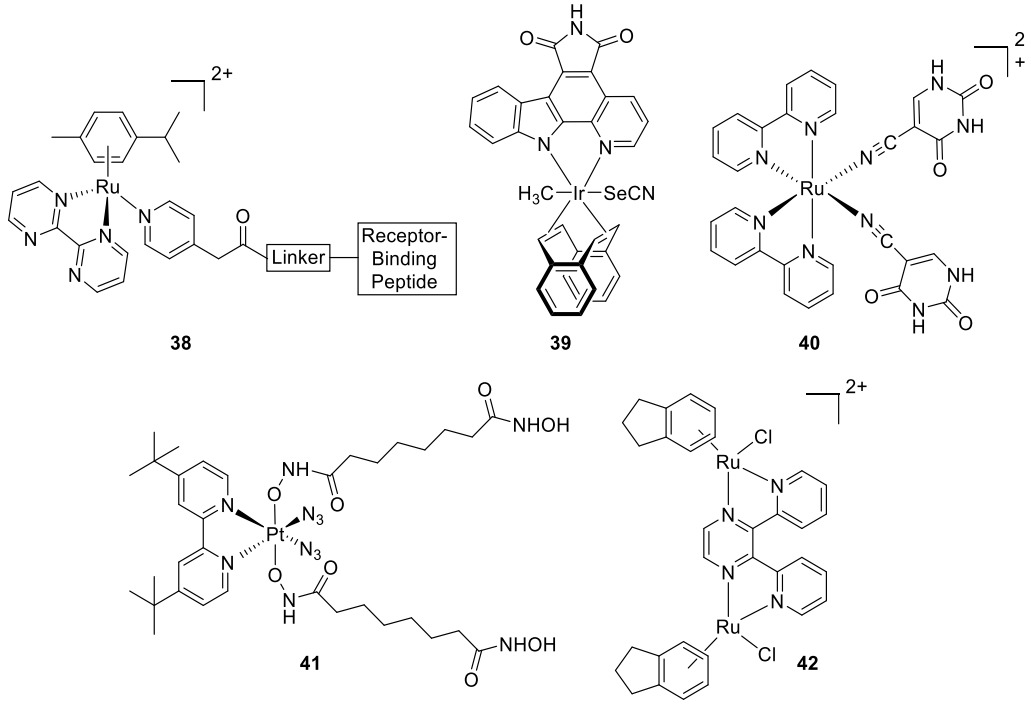

Figure 15. Light-activated metal-based chemotherapeutics that show targeted action (**38**), enable additional treatment modalities constitutively (**39**) or upon photoactivation (**40**, **41**), and can be potentially used for fluorescence imaging (**42**).

The ligands present on the photoactivatable metal-based chemotherapeutic agent can also be used for therapeutic purposes. This is valid both for ligands that dissociate upon photoactivation (in complexes **40** and **41**, Figure 15) and for those that stay in the complex (complex **39**).

Iridium(III) complex **39** was described by the group of Meggers as a potent (IC_{50} = 42±2 nM) inhibitor of VEGFR3 kinase, which could reduce angiogenesis and metastases of the tumour.[49] The pyridocarbazole moiety is responsible for the biological activity, and introduction of a methyl substituent to the nitrogen diminishes the activity. Considering that Ir^{III} is a d_6 complex with potential phototoxicity, the authors measured the influence of compound **39** on the HeLa cells survival prior and after irradiation with λ > 450 nm light (60 min). Phototherapeutic index of 40 was determined (non-irradiated: EC_{50} = 8 μM; irradiated: EC_{50} =0.2 μM). While it was presented that irradiation results in the loss of the selenocyanate ligand,[49] the exact mechanism behind light-induced cell toxicity is yet to be elucidated.

In a couple of cases, the dissociating ligand also acted as a therapeutic agent. The group of Turro presented an example in which the ammonia ligands in complex **21** (Figure 4) were substituted with 5-cyanouracil (5CNU) ligands, giving rise to complex **40** (Figure 15).[52] 5CNU is an inhibitor of pyridine catabolism and an analogue of 5-fluorouracil, which has been used for many years in cancer treatment. Irradiation of complex **40** with λ > 395 nm light led to the release of one equivalent of 5CNU and formation of the monoaqua intermediate, which was shown not to bind to DNA. Further irradiation resulted in the active diaqua complex. When the photolysis was conducted in the presence of linearized pUC18 plasmid, a dose-dependent change of electrophoretic mobility was observed, indicative of covalent binding between DNA and **40**.[52] Unfortunately, no elucidation of cellular activity was presented and it is unclear if the two toxic effects, the one of liberated 5CNU and the one of diaqua complex, are synergistic in nature.

Another case in which the dissociating ligand has biological activity, was presented recently by the group of Kasparkova.[51] Platinum(IV) complex **41** features two ligands, referred to as SBHA, which are based on aliphatic hydroxamic acids and are known to inhibit histone deacetylases (HDACs). This inhibition induces the hyperacetylation of histone proteins and increases the accessibility of DNA in chromatin. Such an effect, besides being already used in cancer treatment,[51] could also lead to a higher accessibility of DNA to the DNA-damaging drugs.

In complex **41**, the metal reactive centre and the hydroxamic acid act as photolabile cages for each other. The complex was not active in the dark, even in the presence of cellular reducing agents. Upon irradiation with UV (λ = 365 nm) or blue (λ = 458 nm) light, the cytotoxic Pt^{II} species are

released, together with the SBHA ligands that inhibit the HDAC activity (Figure 16). The overall cytotoxicity after activation was found to be superior to that of related complexes with biologically-inactive ligands.[51] This impressive example highlights the prospects of combining metal-based photoactivated cancer therapy with other chemotherapeutics in one molecule.

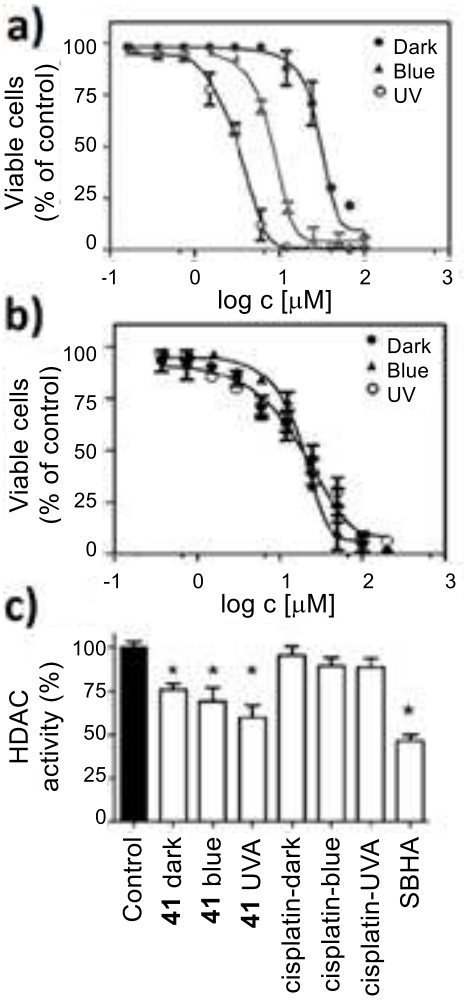

Figure 16. Cellular toxicity and HDAC inhibition for complex **41**. a) Phototoxicity of **41** on human ovarian A2780 cells before and after irradiation with UV (λ = 365 nm) or blue (λ = 458 nm) light; b) Phototoxicity of cisplatin on human ovarian A2780 cells before and after irradiation with UV (λ = 365 nm) or blue (λ = 458 nm) light; c) total HDAC activity in A2780 cells treated with **41**, cisplatin and SBHA. Adapted with permission from ref. 51. Copyright 2015 Wiley-VCH.

Finally, the dissociating ligand can be used for yet another purpose, namely fluorescent imaging. Such design, which would enable the control over location and efficiency of photoactivation, was embodied in complex **42** (Figure 15).[47] Indane was used as a dissociating ligand and it was found that its fluorescence in the liberated form is ~40 times higher than in the complex (λ_{exc} = 260 nm, λ_{em} ~ 290 nm). Already in the dark, the complex underwent a slow exchange of the chloride ligands for

water. Upon irradiation (λ = 365 nm, 60 min), also the indane ligand dissociated and the photoactivated species proved to be a mixture of Ru^{II} complexes with various ratio of Cl and H_2O ligands. A binding to DNA was observed for both the non-irradiated and activated forms of **42**, albeit with much stronger potency to block RNA polymerase observed for the complex formed after photoactivation. Although the wavelengths used for the imaging are far away from the optical window (650-900) nm, this system shows high potential for improvement if more biocompatible fluorescent imaging ligands could be used.

2.4. Summary

Metal complex-based photoactivated chemotherapeutics (Section 2) have been studied for almost three decades now, with first examples of rhodium(III) complexes reported in the early nineties of the previous century. Since then, the attention has shifted to ruthenium(II) and platinum(IV) complexes. Metal-based designs stand out in the field of light-activated chemotherapy due to their very high phototherapeutic indices (Table 1), with the ruthenium(II) complex **25** showing an unprecedented value of PI > 1880. Another important advantage of metal complexes is the fact that in some cases (Table 1) NIR light can be used for activation, allowing deep tissue penetration with negligible toxicity. Important disadvantages of this class of responsive anti-cancer agents are the following: i) the irreversibility of activation, ii) common need for long irradiation times, and iii) limited variety of toxicity mechanism, which relies almost exclusively on dsDNA cross-linking.

3. Photocaged chemotherapeutic agents

Twenty years ago, the first examples of photocaged chemotherapeutics were published.[63],[64] The general design involves an organic or metalorganic cytotoxic agent that carries a photoremovable protecting group (PPG) that cages its activity. To date, development of a wide range of such drugs have been published with studies showing very promising results. However, as mentioned above, a general problem of this strategy is that the released drug may still cause side effects outside its site of action and when being cleared from the body.

3.1. Caged metal complexes

Besides the metal complexes described in section **2**, research also focused on the development of photoactivatable metal complexes that include a photocleavable group in the ligand backbone. In this case, the irradiation leads to decomposition of the original ligand giving rise to a new complex with enhanced biological activity (Figure 2e).

An example, in which this strategy was applied to a Pt^{II} complex, was published by Ciesienski *et al*.[65] The biological activity of the cytotoxic Pt^{II} complex could be efficiently caged with a tetradentate ligand, that includes a photocleavable *ortho*-nitrophenyl (ONP) group (**43**, Figure 17). UV irradiation of this complex resulted in complete disintegration of the ligand within two minutes (with a quantum yield of Φ = 0.75) and gave complex **43** together with nitroso by-products. The photoactivated product showed significantly higher toxicity on MCF-7 cells than the respective prodrug. Interestingly, the photoresponsive ligand alone was found to be cytotoxic as well, which was even more pronounced upon UV irradiation. These results confirm a mutual caging of the metal and the ligand and suggest a synergistic mechanism of action. In order to elucidate this mechanism, the electrophoretic mobility of DNA treated with complex **43** prior and after photoactivation was analysed. Changes in mobility were not observed, indicating a different mode of action than that of cisplatin (Figure 6A). Accordingly, the binding to a peptide fragment of a transport protein, which is known to bind to cisplatin and its analogues and to induce the dissociation of its ligands, was studied.[66] The caged complex did not react with the peptide, in contrast to the activated compound. Reaction of the latter with the peptide led to the formation of Pt-adducts. As these results did not provide an explanation of the cytotoxicity of activated **43**, it is of paramount importance to perform further studies that elucidate the mechanism of action in order to assess the potential of the described complex as a future chemotherapeutic agent.

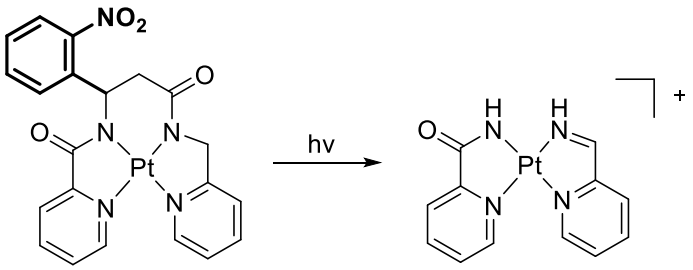

43

\+ Nitroso by-products

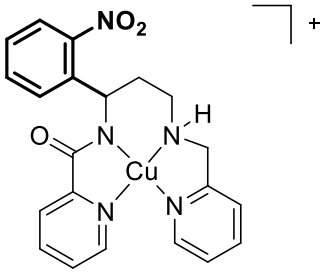

44

Figure 17: Structures of platinum complex **43** and its photoactivated product; structure of copper complex **44.** The photocleavable *ortho*-nitrophenyl group is highlighted.

The authors applied the same strategy to copper complexes, proposing the use of Cu^{II} as a cytotoxic agent.[67]–[69] By optimization of the ligand structure, complex **44** (Figure 17) was designed. The binding affinity between Cu^{II} and the ligand is very high, with a dissociation constant in the femtomolar range, which is a crucial characteristic for possible application as a photocaged prodrug, since human serum albumin binds to copper with a very high affinity. UV irradiation of **44** for 15 s was sufficient to release 43.3% of the copper ions from the complex (quantum yield Φ = 0.43). Moreover, studies on the formation of hydroxyl radicals were performed, as it was proposed[67] that this is the mechanism behind Cu^{II} cytotoxicity.[70] In the presence of ascorbic acid and H_2O_2, the intact complex prevented 70% of radical formation compared to free Cu(II). In contrast, the photolysed product caused enhanced hydroxyl radical formation in comparison to Cu(II) alone. In addition, studies on the biological activity on different cell lines (HeLa, MCF-7 and HL-60 cancer cells) revealed an increase in cytotoxicity of the drug after UV irradiation, albeit with a low phototherapeutic index (PI = 2). Moreover, control cells that were treated with $CuCl_2$ showed enhanced proliferation. Another study confirmed elevated levels of copper in tumor tissues,[71] giving rise to the question if Cu^{II} complexes are suitable candidates for cancer therapy. In conclusion, it was shown that introduction of a photocleavable group into the ligand backbone is a feasible strategy to create metal complexes that undergo a change in activity after irradiation. With regard to the described copper complex, it is, however, doubtful to which extent copper, usually used as a coating of intrauterine devices for contraception, represents a future drug in cancer therapy.

The aim of the research presented by Leonidova *et al.* was to develop a multifunctional light-activatable drug by combining a PDT agent with different biologically active groups via a photocleavable linker.[72] As it is known that Re(I) tricarbonyl bis(quinolinolyl) ("MC-NH_2", Figure 18) possesses photosensitizing characteristics and allows cellular imaging,[73] this complex (Figure18) was chosen as a starting point for the synthesis of the novel prodrugs. The complex was coupled to either a nucleus localization signalling peptide (NLS, Figure 18) or a bombesin moiety (Figure 18) via a bifunctional, ONP-derived photocleavable linker giving complexes **45a** and **46a**. Including bombesin in the design of the chemotherapeutic enables targeting of cancer cells that overexpress receptors of the bombesin family, such as gastrin-releasing peptide receptor (GRPR) on prostate cancer cells. Photocleavage studies showed that both **45a** and **46a** can be completely cleaved with UV light with a relatively low irradiation dose (1.2 J cm^{-1}), and a quantum yield around 10%. Subsequently, the cytotoxicity of the photocleavable compounds, and their analogues **45b** and **46b** that did not contain a photocleavable linker, was tested on several cell lines: (i) HeLa cells, (ii) non-cancerous MRC-5 cells,

and (iii) PC3 cells (GRPR-overexpressing prostate cancer cells). In general, irradiation increased the cytotoxicity of all tested compounds, but in each case also the dark toxicity was elevated compared to the Re(I) complex alone. As expected, bombesin derivatives showed enhanced toxicity on PC3 cells. They were, however, not included in further evaluation,[72] since both the photocleavable (**46a**) and the photo-stable (**46b**) compound showed a comparable cytotoxicity profile, indicating that only the PDT effect is relevant for toxicity. NLS derivatives **45a** and **45b**, however, showed a lower phototherapeutic index (<2), but a significant difference in biological activity of the photocleavable (**45a**) and non-photocleavable (**45b**) was observed. Fluorescence microscopy was used to examine the localization of **45a** in the cells. Results showed that the complex is primarily located in the nucleoli, with 25% of the intracellular drug situated in this organelle. Overall, 50% was taken up into the cell. Since NLS has a high positive charge, it was expected that the peptide interacts with DNA. In fact, gel electrophoresis experiments showed that irradiation of **45a** leads to the relaxation of supercoiled DNA plasmid.[72] Interestingly, changes in DNA shape were observed in the dark as well. Besides that, the effect on RNA was examined, as it is the major content of nucleoli. Experiments showed the formation of RNA agglomerates irrespective of exposure to light. This finding provides a possible explanation for the high dark toxicity of the NLS derivatives. Lastly, the mechanism of cell death was investigated by transmission electron microscopy and staining of markers for both apoptosis and necrosis. Clear indication for late stage apoptosis and also for necrosis were observed, supporting the hypothesis of a dual mechanism of action, including a PDT effect and DNA/RNA damage.

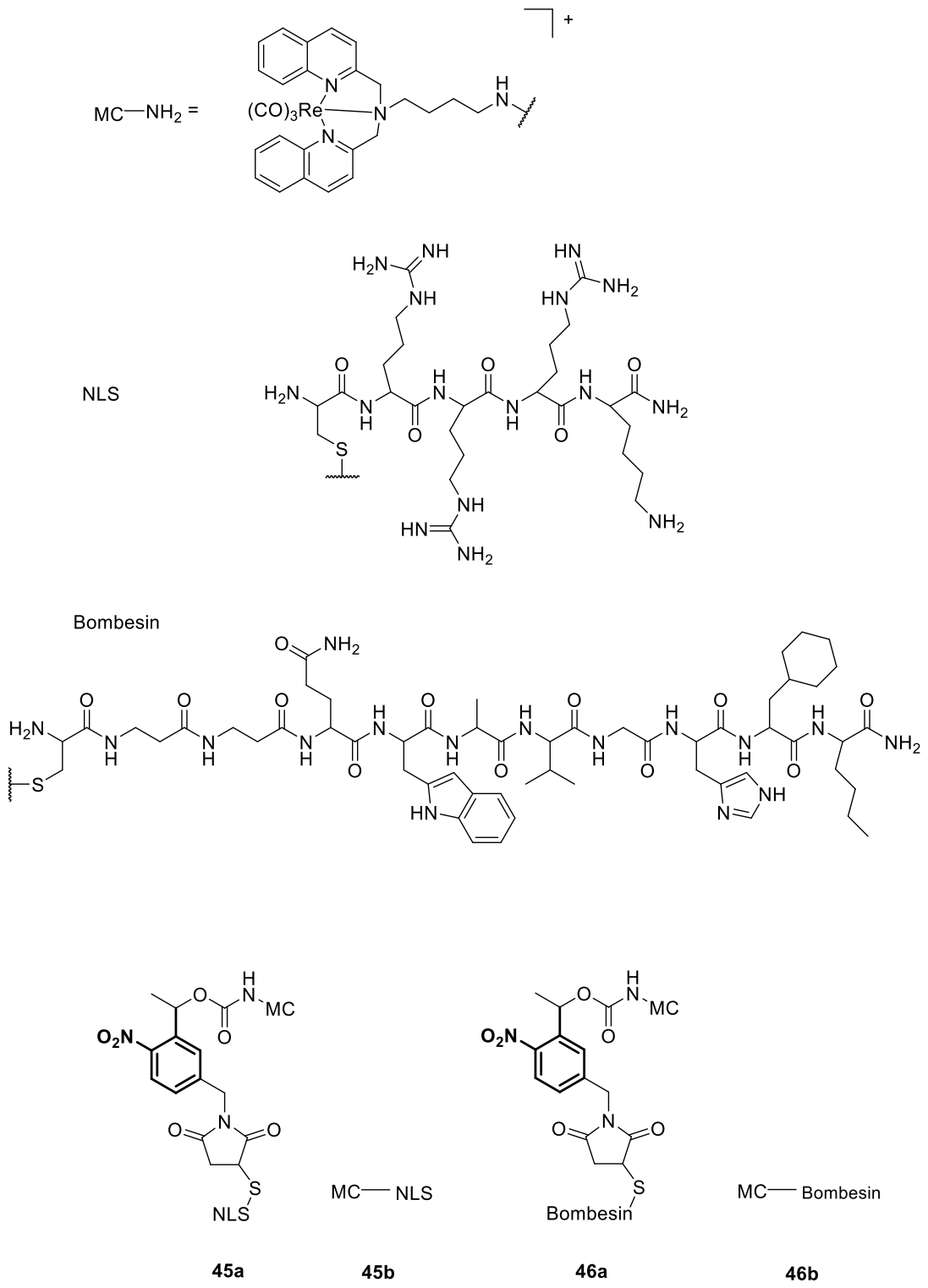

Figure 18: Structures of photocleavable Re(I) compounds with either NLS or bombesin as a peptidic moiety. The photocleavable *ortho*-nitrophenyl group is highlighted.

As presented in **Section 2**, Ruthenium complexes are potential agents for chemotherapy. Joshi *et al*.[74] published an example of a photoactivatable complex containing a PPG in the ligand backbone, which is responsible for the photoactivation step (Figure19). The prodrug was developed

based on structure-activity relationship studies of cytotoxic complex **47**, which indicated that the carboxylate group is crucial for biological activity. Thus, the authors decided to cage this functionality with a photocleavable dimethoxy-*ortho*-nitrophenyl group in complex **47a**. Photocleavage studies showed almost complete release of **47** from prodrug **47a** after 20 min of light exposure (λ = 350 nm). The biological activity was examined on HeLa and on bone cancer (U2OS) cells, confirming the efficient caging of cytotoxic activity, as complex **47a** did not show toxic effects on neither cell lines in the dark. In contrast, after irradiation with λ=350 nm light, a clear increase in cytotoxicity was observed with a potency comparable to the one of **47** in the dark (IC_{50}[**47a**activated]= 17 μM; IC_{50}[**47**]= 16-31 μM). However, complex **47** also showed enhanced cytotoxicity after irradiation, attributed to the Ru(II) complex acting as a PDT agent. Nevertheless, the cleavage of the PPG upon irradiation was considered the crucial step in the photoactivation process.[74] As the mechanism of (photo-)toxicity still needs to established, further analysis is awaited but, in principle, this work shows the successful photocaging of a metal complex applicable in the field of cancer therapy.

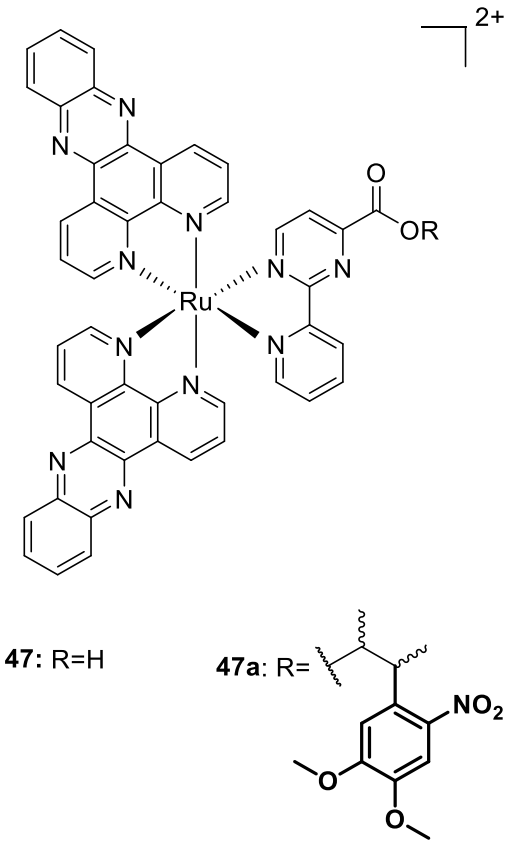

Figure 19: Structure of active Ru(II) complex **47** and photocaged derivative **47a**. The photocleavable ONP-based moiety is highlighted.

Another example of a photoactivatable Pt(II) complex, in which the platinum itself is not involved in the photochemical reaction, was published by Mitra and co-workers,[75] who employed

curcumin as a ligand. Curcumin is a naturally-occurring compound with anti-inflammatory and anti-cancer properties.[76] Unfortunately, it is poorly soluble in water, unstable under aqueous conditions and it shows low bioavailability.[77] Curcumin is furthermore characterized by its preferential cytosolic localization in cells. Therefore, a combination of curcumin with a platinum complex could lead to selective targeting of mitochondrial DNA, instead of nuclear DNA.[75] Moreover, combined therapy with curcumin promises an additional PDT effect, as irradiation of curcumin results in the formation of reactive oxygen species (ROS).[78] With this aim in mind, the authors designed complex **48** (Figure 20), which provided significantly higher stability for curcumin (bold, Figure 20). Photoactivation studies showed efficient release of both curcumin and a cisplatin analogue from the complex after irradiation (λ = 400-700 nm), while in the absence of light no curcumin was released. Furthermore, eight hours of light exposure led to single and double adducts to GMP, whereas in the dark the addition was only observed after 30 hours. DNA-crosslink formation was shown to be in agreement with these findings, as irradiation led to Pt-DNA adducts of mainly (98%) bifunctional character.[75] In addition, DNA melting point studies showed that **48** has no influence on the melting point in the dark, whereas after photoactivation a similar shift to the one measured with cisplatin (1 K) was observed and elevated levels of platinum were detected in ICP MS (inductively coupled plasma mass spectrometry) analysis of the light-treated sample. Subsequently, the cytotoxic activity was examined on different cancerous and non-cancerous cell lines employing an MTT assay. Results showed a minimal phototherapeutic index of 11 with IC_{50}[dark] > 200 μM and IC_{50}[irradiated] = 12-18 μM. Interestingly, curcumin alone had a comparable cytotoxic potency to the irradiated samples (IC_{50}[curcumin] = 10-13 μM). Next, the PDT effect of the photoactivatable prodrug was analysed on HaCat cells (immortalized transformed skin keratocytes). As expected, ROS were detected only after light exposure. Further experiments revealed that 83% of the cells exposed to both the drug and light were in stage of early apoptosis, whereas only 13% of the cells in the dark showed similar morphology. Moreover, more than half of the irradiated cells were arrested in sub G_1 phase. It was also shown that light exposure (λ = 457 nm) led to formation of nicked circular form of DNA when a model plasmid was treated with **48**. This effect could be significantly reduced (up to 50%) by the addition of certain singlet-oxygen quenchers, which indicated that mainly the hydroxyl radicals were involved in the process. Finally, fluorescence microscopy proved that complex **48** is primarily located in the cytosol and additionally it revealed a higher cellular uptake of **48** compared to cisplatin. In conclusion, a photoactivatable complex with dual cytotoxic activity was designed and evaluated. Coordination to platinum led to enhanced stability of curcumin and therefore increased its potential for applications in cancer therapy.

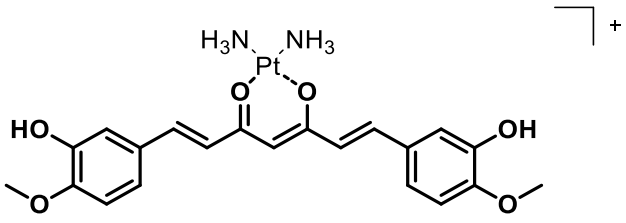

48

Figure 20: Platinum complex **48** with curcumin (highlighted) as a ligand.

3.2 Caged organic chemotherapeutic agents

This section focuses on photocaged organic cytotoxic agents. In the general design, a known cytotoxic agent is linked to a photocleavable protecting group (PPG), and in some cases a moiety for specific tumor targeting is introduced as well. When deciding which position in the original drug the PPG is to be introduced, one should consider structure reactivity relationships of the drug to ensure efficient caging of the biological activity, in order to obtain a prodrug with minimal cytotoxic activity, whereas the corresponding activated drug shows high activity

Apart from a few exceptions,[79]–[81] all the published designs use an *ortho*-nitrophenyl (ONP) moiety, or its analogue, as a caging group. The advantage of this PPG is the high uncaging quantum yield and the fact that it can be easily introduced into the structure of bioactive compounds.[82] However, the deprotection is achieved only upon irradiation with a wavelength around λ = 350 nm, which presents a major drawback, due to the low tissue-penetration and high toxicity of UV light. Another limitation is the possible formation of toxic nitroso byproducts upon cleavage.[83] To expand the available wavelength range and to allow NIR-light release, some approaches use upconverting nanoparticles [31],[84] or combine the photocleavable group with a photosensitizer.[79],[80]

3.2.1. Cytotoxic drugs with DNA alkylating activity

One of the first photocaged chemotherapeutics was reported by Reinhard and Schmidt[63], who presented derivatives of phosphoramide mustard (**49a,b** and **50,** Figure 21). Phosphoramide mustard is the active metabolite of cyclophosphamide and is cytotoxic due to its ability to alkylate DNA. In order to photocage the active compound, an *ortho*-nitrophenyl moiety (Figure 21, in bold) was used as a PPG, allowing cleavage and release of the active drug with UV irradiation (λ = 300-400 nm). *In vitro* DNA alkylation studies of the prodrugs **49a,b** and **50**, using 4-(4-nitrobenzyl)pyridine as a model for DNA (NBP assay), were performed in order to analyze the efficiency and the rate of photocleavage. In all cases, an increased alkylating activity was observed after photoactivation, with

the water-soluble prodrugs **49a** and **49b** showing the fastest cleavage and highest alkylating activity. Unfortunately, the published data is not sufficient to draw conclusions about the toxicity of the caged compounds and to determine the phototherapeutic index.

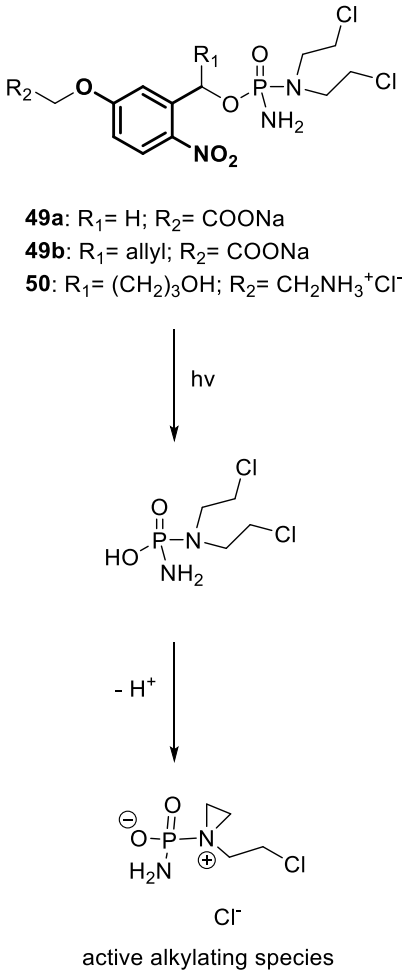

Figure 21: Prodrugs **49a**, **49b**, and **50** and the mechanism of their photoactivation. The photocleavable ONP-based moiety is highlighted.

Tietze *et al.* also exploited the idea of constructing a photocaged DNA alkylating agent, using analogues of Duocarmycin (**51a-c** and **52a,b**, Figure 22), which is a natural antibiotic.[85] Through the introduction of an ONP-based moiety in the seco drug (Figure 22) the authors obtained five light-activatable prodrugs. An *in vitro* human tumor colony-forming ability test with human bronchial carcinoma cells (A459) was used to analyze the photochemical and cytotoxic properties and revealed complex **52a** as a promising candidate for photoactivatable chemotherapy. For this derivative, the phototherapeutic index (after irradiation with λ = 365 nm light for 30 min) of PI > 3000 was determined. A surprising result found in this study is that the prodrugs that contain a free carboxylic acid in the benzyl position of the *ortho*-nitrophenyl derived group (**51c**, **52b**) showed even higher toxicity before irradiation than after. As an explanation for this enhanced toxicity, an active transport

mechanism of this compound to the active site was proposed[85], but this presumption was not investigated further.

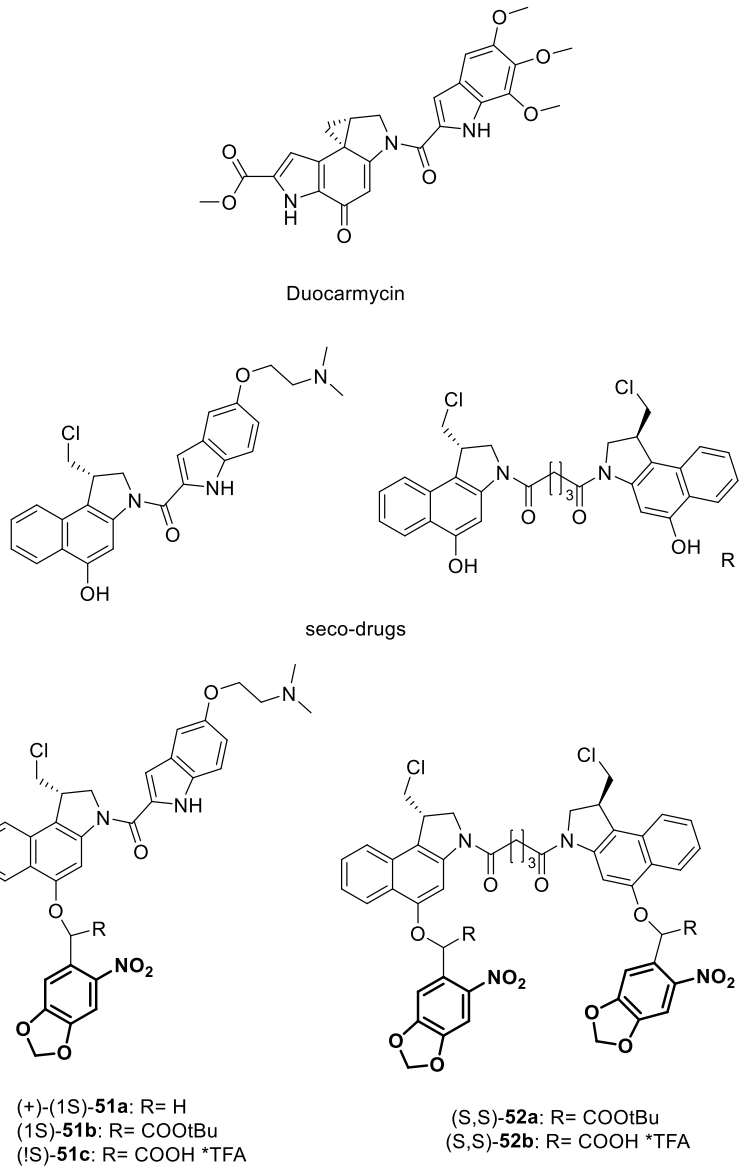

Figure 22: Duocarmycin and the respective seco-drugs. Photolabile prodrugs **51a-c** and **52a** and **52b** derived from the seco-drugs. The photocleavable ONP-based moieties are highlighted.

3.2.2. Antimetabolites

Wei *et al*. reported a photoprotected chemotherapeutic based on the antimetabolite 5-fluorouracil (compound **53**, Figure 23).[64] 5-Fluorouracil (5-FU) inhibits the thymidylate synthase and acts as a false building block in the DNA synthesis after the *in vivo* attachment of a deoxyribose and subsequent monophosphorylation. The protecting group (4,5-dimethoxy-2-nitrobenzyl, bold in **53**, Figure 23) was linked to 5-fluorodeoxyuridine via a carbamate linker in 5' position of the drug, preventing the phosphorylation. Besides photochemical studies, which showed the cleavage of all

compounds upon irradiation with λ = 300-400 nm light, *in vitro* cytotoxicity studies were carried out on *E. coli* cells showing a "slight growth inhibition"[64] when treated with the non-irradiated compound, which was compared to growth that "was almost completely inhibited"[64] after irradiation with λ = 350 nm light. It is, however, arguable to what extent the growth inhibition of bacterial cells is representative for cytotoxic activity on human tumor cells.

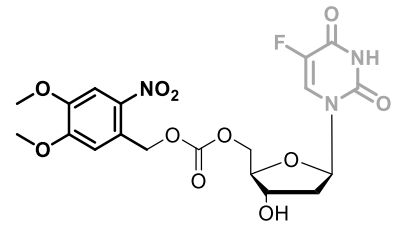

53

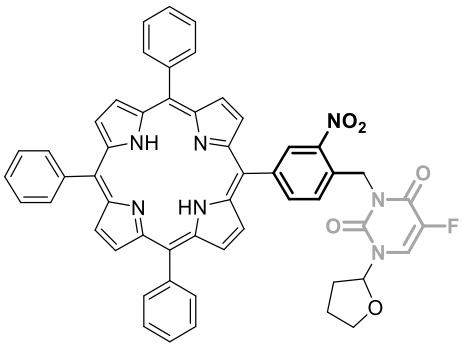

54

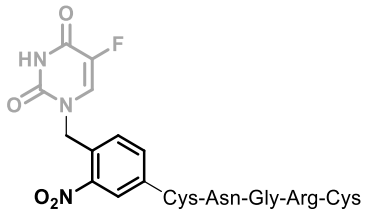

55

Figure 23: Photocaged prodrugs of 5-Fluorouracil. 5-Fluorouracil is highlighted in gray and the photocleavable ONP-based moieties are highlighted in bold.

Another prodrug design based on 5-fluorouracil (5-FU) was published by Lin *et al*.[86] Compound **54** (Figure 23) is composed of three parts: the 5-fluorouracil prodrug (tegafur),[87] a porphyrin, and a linker based on the ONP scaffold. The porphyrin was included in the design because of its affinity for tumor cells.[88] An MTT (3-(4,5-dimethylthiazol-2-yl)-2,5-ditetrazolium bromide) assay with MCF-7 mammary cancer cells was performed in order to assess the biological activity. In the dark, compound **54** caused 7% cell death. After activation with UV light (λ = 350 nm), however, 67% cell death was observed. In comparison, tegafur alone induced 91% cell death at the same concentration. As porphyrin is known to have cytotoxic effects after light activation due to the production of reactive oxygen species, an analogue of **54** with a non-cytotoxic uracil, instead of the

tegafur, was tested in the assay to investigate the effect of porphyrin on cell viability. From the result (6% cell death with the control compound) it can be concluded that the toxicity of prodrug **54** stems mainly from the release of active 5-fluorouracil.

The group of Zhang published another 5-fluoruracil prodrug, compound **55**[89] (Figure 23), caged with an ONP moiety in 1-position of the pyrimidine, which prevents the attachment of a deoxyribose *in vivo*. A cyclic peptide (Cys-Asn-Gly-Arg-Cys), with a disulfide bond between the two cysteines), which is known to recognize a specific tumor marker overexpressed on the surface of tumor blood vessels, was linked to the molecule to provide selective targeting.[90] Photoactivation studies showed that after the exposure of compound **55** to light (λ= 365 nm for 6 hours), 60% of the caged 5-FU was released, along with unknown byproducts. Overall, 80% conversion of the prodrug was observed. However, this method of analysis has limitations as the assay was performed in acetonitrile, which is not always representative for physiological conditions. Unfortunately, no studies on the biological activity of the released drug and the byproducts were presented, making it difficult to evaluate the therapeutic potential of the designed prodrug.

Another chemotherapeutic from the group of antimetabolites is the folic acid analogue Methotrexate (MTX, Figure 24), which is not only used in cancer therapy but also plays an important role in the therapy of rheumatic diseases.[91] At concentrations used in cancer therapy, it inhibits dihydrofolate reductase, thus hindering the formation of thymidine for DNA synthesis. Choi *et al*. [92] described the attempt to design a light-activatable prodrug of MTX. The concept involved the creation a dendrimer nanoconjugate, with both the drug and folic acid (FA, Figure 24) attached to it, to specifically target tumor cells overexpressing the folic acid receptor. As a starting point, a 5th generation (G5) polyamidoamine (PAMAM) dendrimer was used; MTX and FA were covalently attached to the surface of the dendrimer via a photocleavable linker based on ONP (**56**, Figure 24). The release of MTX from the nanoconjugate upon irradiation (λ = 365 nm) was studied, and the results confirmed a complete uncaging of the drug after 6 min of irradiation. Unfortunately, when the inhibition of the dihydrofolate reductase was analyzed, the results indicated that the caged compound **56** is nearly as potent as free MTX. Also *in vitro* cytotoxicity studies of the nanoconjugate **56** and the released drug using FA-receptor-overexpressing KB cells (a sub-line of HeLa cells) confirmed that **56** is nearly as cytotoxic as free MTX. Furthermore, prolonged irradiation (14 min) even decreases the biological activity of the drug, probably due to degradation of MTX. In conclusion, an efficient photocaging of MTX was not accomplished, but further tests, performed by the authors, indicated that a shorter linker between the dendrimer and the methotrexate might decrease the dark toxicity.

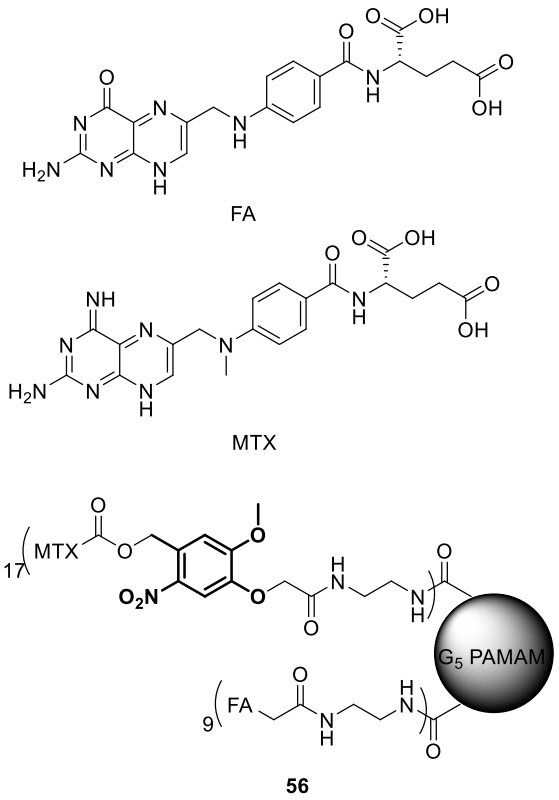

Figure 24: Structures of folic acid (FA), methotrexate (MTX), and dendrimer conjugate **56.** The photocleavable ONP-based moiety is highlighted.

3.2.2. Anthracyclines

The strategy applied to MTX (*vide supra*) has been applied with more success by the same group for the photocaging of doxorubicin (Figure 25).[93] Doxorubicin (Dox) is a very potent anticancer drug from the class of anthracyclines, whose cytotoxic activity is mainly attributed to intercalation with the DNA and inhibition of topoisomerase II, which prevents replication and transcription.[94] Furthermore, a mechanism of action based on the formation of free radicals has been proposed.[95] Unfortunately, the therapy with doxorubicin is limited by severe adverse effects, such as cardiotoxicity.[96] Similarly to the approach discussed above, the active drug and folic acid were attached to the surface of a G5-PAMAM dendrimer via a photocleavable linker. As an attachment point in Doxorubicin, the amino group was chosen. Additionally, a fluorescein moiety was added to the nanoconjugate to allow the studying of cellular binding and uptake of nanoparticles. Three different types of Dox-containing nanoconjugates (compounds **57, 58,** and **59,** Figure 25) have been synthesized. Photochemical studies confirmed the time-dependent release of Dox from **57** after irradiation with UV light (λ = 365 nm, max. 14 min). Furthermore, in order to investigate the influence of the conjugated FA on the uptake of the nanoparticle into FA-receptor overexpressing cells,

competitive binding assays with the fluorescein-containing compounds **58** and **59** and FA were performed on KB cells. The results suggested a ligand-specific uptake of **58**, which was further confirmed by confocal microscopy. Finally, *in vitro* analysis of the biological activity of conjugate **57** showed that the prodrug is inactive prior to irradiation, while 80% reduction of cell growth was observed after activation with UV light (λ = 320-400 nm) for 30 min. In comparison, free Dox inhibited 85% of cell proliferation, and after 30 min irradiation the activity decreased to 70% inhibition, presumably due to light-induced inactivation. Although further investigation is required, for instance on the cytotoxicity of the dendrimer conjugate with FA alone, this work presents a promising approach to increase selectivity and reduce the toxicity of doxorubicin.

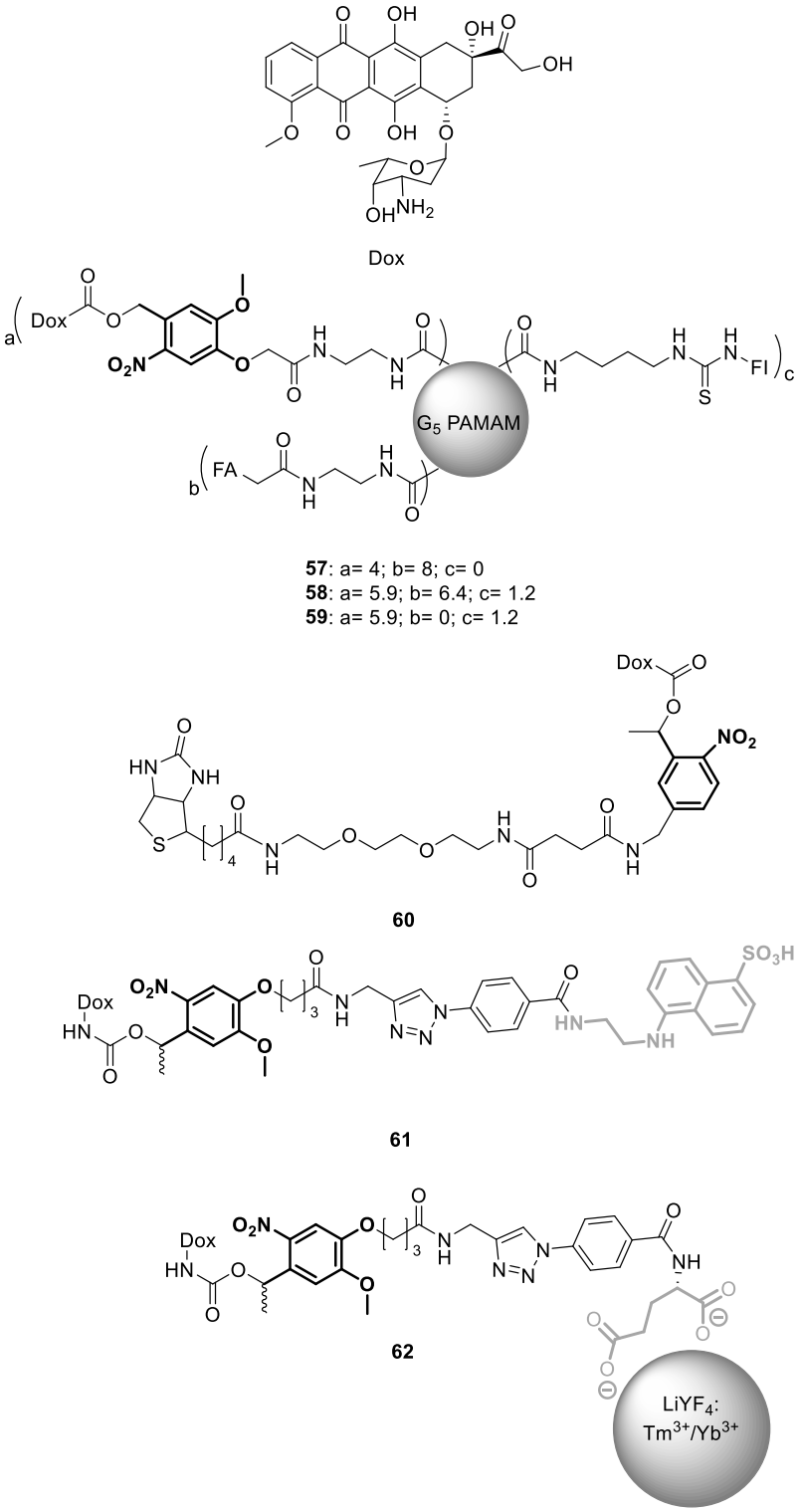

Figure 25: Structure of Doxorubicin (Dox) and its photactivatable prodrugs **57**-**62.** The photocleavable ONP-based moieties are highlighted in bold.

Another design for a photocaged prodrug of doxorubicin was proposed by Ibsen *et al.* (compound **60**, Figure 25).[97] To provide a handle for further functionalization, a biotin moiety was attached via a short PEG chain to the ONP group, which was introduced on the amine group of Dox. Studies on the photocontrolled activation of **60** showed that the active compound was released after

UV irradiation (λ = 330-380 nm), and the amount of uncaged product was linearly dependent on the UV exposure. Under the described conditions (1.9 mW/cm^2), a release rate of 1.8 μM/min was determined. Next, the uptake into cells and cellular localization of compound **60** was investigated using PTK2 epithelial cell line. The localization of the compounds was analyzed by fluorescence microscopy, exploiting the red fluorescence of doxorubicin and its caged derivative. The test showed that free doxorubicin accumulated in the nucleus and bound to the DNA, whereas the prodrug was mainly located in the cytosol surrounding the nucleus. Moreover, it was observed that free Dox caused abnormal-appearing mitosis in contrast to the prodrug, which did not affect mitosis even though it was administered at a ten-fold higher concentration. Irradiation (λ = 330-380 nm) of the cells treated with the photocaged drug resulted in an accumulation of red fluorescence in the nucleus. The same phenomenon was observed when the cells were treated with the pre-irradiated prodrug. Furthermore, cytotoxicity studies were carried out on human bronchial cancer cells (A549). The results showed a 200-fold decrease in potency of the photocaged drug (IC_{50} = 250 μM) in comparison to free doxorubicin (IC_{50} = 1.2 μM), indicating an efficient caging of the cytotoxic activity. In order to analyze the efficiency of photoactivation, the prodrug was exposed to UV light (λ = 330-380 nm) for different periods of time prior to incubation with the cells. After 60 min of irradiation, the IC_{50} value decreased to 3.5 μM. Finally, metabolic studies using human liver microsomes were performed, and no metabolic activation of the prodrug to doxorubicin was detected. Two other metabolites were identified, whose biological activity remains to be analyzed, although it is known that similar compounds are significantly less toxic than doxorubicin.[98]

In the subsequent publication,[99] the same group examined the *in vivo* activation of the prodrug and the light penetration of a λ = 365 nm LED/fiber optic delivery system in tumor tissue (*ex vivo*). Towards this end, suspensions of A549 cells were injected into the left and right flanks of five athymic nude nu/nu mice, and the tumors were allowed to grow until they reached a size of 1 cm^3 (1 month of growth) in order to obtain enough tumor mass for *ex vivo* and *in vivo* studies. The light penetration studies showed an attenuation of radiation of 0.38 over a 0.2 mm path length in the tumor tissue. This attenuation not only stems from absorption but also from light scattering. Having measured the light penetration from different angles, and taking into account the previously determined uncaging rates, the authors estimated that, using their setup, circa 5.7% of the prodrug in the tumor surroundings might be activated based on a tumor diameter of 9 mm. Subsequently, *in vivo* experiments were carried out. It should be noted that the addition of a solubilizing agent (Captisol® Cyclodextrin) was required in order to dissolve the prodrug **60** in water for injection. For pharmacokinetic studies, the concentration of doxorubicin was determined in the blood serum and urine after injection of **60** into two mice. Results showed a circulation half-life of 10 min, and no prodrug was found in the urine collected over 24 hours. Furthermore, no free doxorubicin was

detected in either urine or serum at any time, which supports the findings of previous studies that no metabolic activation of the prodrug to active doxorubicin is manifest. Thereafter, the activation of **60** in tumors of two living mice was investigated (Figure 26). Ten minutes after injection of the prodrug, one of the tumors was irradiated with λ = 365 nm light for 30 min from the center of the tumor using a LED optic fiber. Quantification of free doxorubicin in the tumor tissues indicated a six-fold higher concentration in the tumors that were irradiated than in the ones that were not exposed to light. Trace amounts of doxorubicin were found in the control tumor, but as no doxorubicin was detected in circulation of the mice, the authors assumed that some of the UV light reached the control tumor leading to an uncaging of the prodrug. This assumption seems logical since the distance between the two tumors was only 10 mm. In summary, a very promising candidate for photoactivatable chemotherapy was presented by Ibsen *et al.* and further studies on the *in vivo* cytotoxic activity of the prodrug are awaited.

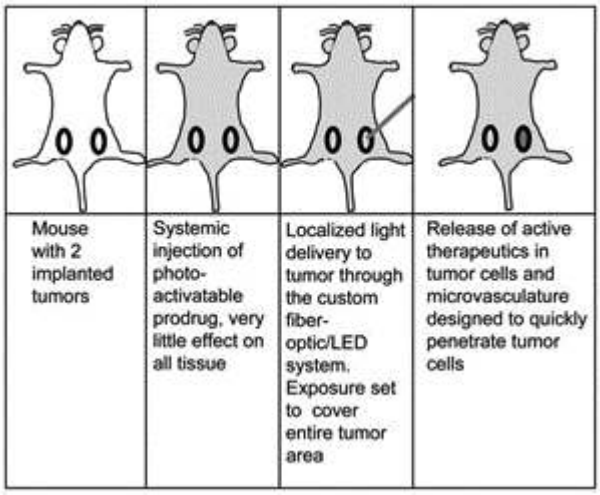

Figure 26: Schematic setup of *in vivo* experiments examining the activation of prodrug **60** in mice tumors. Reproduced with permission from ref. 99. Copyright 2013 Wiley-VCH.

Yet another photocaged prodrug of doxorubicin was presented by the group of Dcocna.[100] In this approach, the drug was connected to 5-((2-Aminoethyl)amino)naphthalene-1-sulfonic acid (EDANS, Figure 25, highlighted in gray in compound **61**) via an ONP-containing linker giving compound **61** (Figure 25). The attachment of EDANS hinders the cellular uptake of the drug and therefore cages its activity. The authors refer to this unique strategy as "photocaged permeability". After photocleavage studies that showed the time-dependent release of doxorubicin upon irradiation with UV light (λ = 365 nm), the effect of the attachment of EDANS was investigated using JH-EsoAd1 cells (a Barrett's esophagus-associated adenocarcinoma cell line). The cell penetration of **61** prior to and after photoactivation was analyzed by flow cytometry and confocal microscopy (Figure 27). Both tests showed a significant increase in cellular doxorubicin fluorescence after exposure to light (Figure

27). Lastly, an MTT assay with the same cell line was performed in order to examine the biological activity. In the assay, free doxorubicin showed an IC_{50} value of 1.0±0.4 μM. In contrast, prodrug **61** did not inhibit cell growth at all up to the highest concentration tested (16 μM), whereas irradiation of **61** (λ = 365 nm) led to significant increase in activity with an IC_{50} value of 1.6±1.0 μM. Therefore it can be concluded that photocaging of doxorubicin was successful, but further investigation of the dark toxicity of **61** is needed in order to evaluate the caging efficiency. The use of photocaged permeability might become a general strategy in designing photocaged drugs. This strategy could be especially useful when it is impossible to identify an easily modified functionality which is responsible for the activity of the original drug and whose photocaging would yield a light-activatable compound.

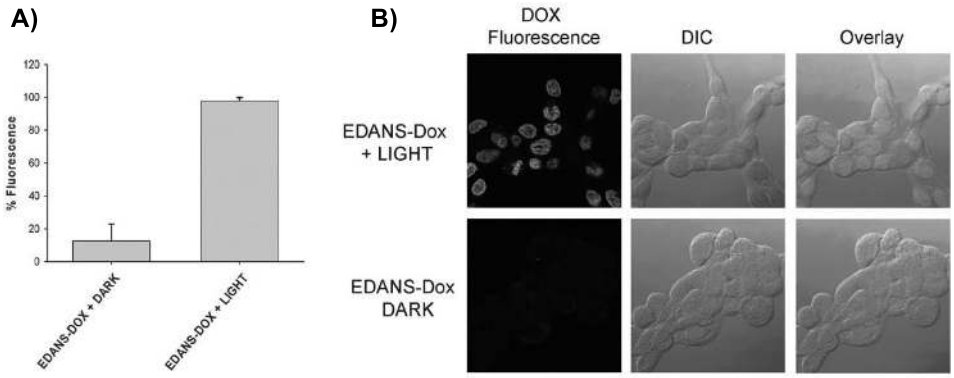

Figure 27: Results of analysis of the activity of compound **61**: A) Quantification of Doxorubicin fluorescence in the dark and after irradiation using flow cytometry; B) confocal images of JH-EsoAd1 cells treated with **61** with and without irradiation. Adapted with permission from ref. 100. Copyright 2012 Royal Society of Chemistry.

More recently, the same group published another approach to photoactivate a caged doxorubicin, using upconverting nanoparticles (UCNP) (compound **62**, Figure 25).[84] This strategy has the advantage that photoactivation can be performed with NIR light, which allows much deeper tissue penetration and lower toxicity (see Figure 28). Doxorubicin was modified with a photocleavable linker containing a glutamate (Figure 25, highlighted in gray), which is used to bind to the surface of the nanoparticles. As the anthraquinone structure of doxorubicin is also a good ligand for coordination to the UCNP, it was necessary to form a saturated complex of Mn^{2+} with the doxorubicin prior to the loading on nanoparticles. Irradiation with NIR light resulted in a 40% release of doxorubicin after 60 min. A surprising finding is that absorption spectra of the released drug suggested that free doxorubicin, and not the Mn^{2+}-complex, was released. It is possible that the liberated doxorubicin is able to bind to the surface of the UCNP, which provides an explanation for the incomplete uncaging. Unfortunately, no cytotoxicity studies were performed, limiting an assessment of this approach for the use in photoactivated chemotherapy.

Figure 28: Mechanism of drug release: Incoming light (λ = 980 nm) excites the upconverting particles, which release light (λ = 360 nm) that leads to cleavage of the photocleavable linker and release of Dox. Adapted with permission from ref. 84. Copyright 2015 Royal Society of Chemistry.

3.2.4. Protein kinase inhibitors

A relatively new group of cancer therapeutics are protein kinase inhibitors (PKI), which are primarily used in individualized therapy.[101] The work of Peifer and co-workers[102] recently focused on the development of photoactivatable PKIs, including imatinib[103] and vemurafenib.[104] Imatinib (Figure 29) inhibits several protein kinases, such as Abelson murine leukemia viral oncogene homolog 1 (ABL1) and platelet-derived growth factor receptor (PDGF-R). *In silico* molecular modeling studies on ligand-protein interactions of the inhibitor and PDGF-Rβ were performed in order to identify suitable positions to introduce a PPG. Inspired by the results of this study, and having performed preliminary photocleavage studies, the authors defined the amide function as most suitable for modification. The photochemical properties were tested of two derivatives, with different PPGs, a coumarinymethyl- (**63**) and an 4,5-dimethoxy,2-nitrobenzyl- (**64**) groups, attached to the amide function. Results showed that after irradiation with λ = 365 nm light for 12 min, only 10% of **63** was activated, whereas 10 min were sufficient to efficiently release imatinib from prodrug **64**. Therefore, only the biological activity of compound **64** was investigated further. For this purpose, an enzymatic PDGF-Rβ assay was performed, showing that imatinib is able to inhibit PDGF-Rβ with an IC_{50} value of 0.059 μM, while prodrug **64** is less potent, giving an IC_{50} value of 5.8 μM. After exposure to light (λ = 365 nm, 10 min) biological activity was restored (IC_{50} = 0.089 μM). Notably, the authors state that the remaining activity of prodrug **64** stems from contamination with uncaged imatinib. Therefore further studies are required to prove the potential of the designed drug, as a higher phototherapeutic index is desirable for efficient photocaging. Additionally, only the inhibition of one drug target was examined to analyze the biological activity and the final cytotoxicity may differ from the potency to inhibit PDGF-Rβ.

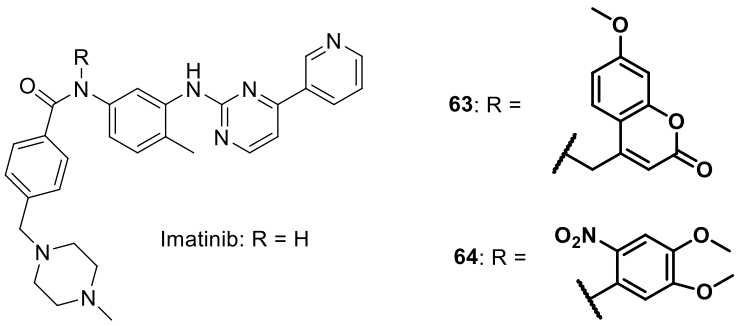

Figure 29: Structures of imatinib and its prodrugs **63** and **64.** The photocleavable groups are highlighted.

An elaborate work on the development of another photocaged PKI, derived from vemurafenib, was published by the same group.[105] This serine/threonine kinase inhibitor targets the $BRAF^{V600E}$ mutant and is used for personalized therapy of cancer. Similarly to the example described above, suitable position for the introduction of a PPG were identified by analysis of the binding mode, using molecular modeling. Both NH moieties were defined to be suited for this purpose. Consequently, three derivatives of vemurafenib were synthesized, utilizing an 4,5-dimethoxy,2-nitrobenzyl-group for photocaging (Figure30, compounds **65-67**). Experiments using UV light (λ = 365 nm) revealed efficient photocleavage of all three derivatives with 90% release of the drug after less than 1 min of irradiation. Thereafter, the biological activity of the three derivatives in comparison to vemurafenib was examined. Determination of the binding affinity towards $BRAF^{V600E}$ showed that vemurafenib has the highest affinity (K_D = 10 nM), but also compounds **66** and **67** featured a moderate binding affinity (K_D = 77 nM and K_D = 79 nM, respectively). In contrast, derivative **65** showed the lowest affinity with a K_D value of 440 nM. Additionally, the selectivity of **65**, **67** and vemurafenib for the target kinase over 140 other kinases was tested. Under the test conditions (10 µM concentration), vemurafenib inhibited more than 70% activity of 32 kinases. However, prodrug **67** inhibited 13 kinases and prodrug **65** inhibited only two kinases. Subsequently, cellular growth inhibition of different melanoma cell lines carrying the $BRAF^{V600E}$ mutation was analyzed. As expected, vemurafenib showed high cytotoxic activity on these cells (IC_{50} = 0.17 µM for SKMel13 cells), whereas the caged prodrugs exerted cytotoxic activity only at higher concentrations: IC_{50} = 4.3 µM for **66** and IC_{50} = 2.6 µM for **67** (both results for SKMel13). In line with the affinity studies, compound **65** did not show any cytotoxic effects under the test conditions. After irradiation, all compounds showed an increase in cytotoxicity (IC_{50} = 1.5 µM for **65**, IC_{50} = 0.46 µM for **66** and IC_{50} = 0.35 µM for **67**). The authors also tested the biological effects of the products formed from the photocage part of the molecule upon irradiation. To that end, a non-toxic, Boc-protected alanine and the corresponding photoprotected derivative were chosen as model compounds. The control assay

showed that photoactivation of the caged compound resulted in growth inhibition, but at much higher concentrations than for compounds **65**-**67**. Thus, the authors conclude that the effects of the PPG can be discarded. As a last assay to confirm the biological activity of the designed prodrugs, the influence on $BRAF^{V600E}$ signaling was tested, using the phosphorylation of ERK (extracellular signal-regulated kinase) as a marker. At concentrations higher than 0.01 μM, vemurafenib blocked the phosphorylation completely. In comparison, even concentrations of the prodrug higher than 10 μM did not lead to a full inhibition of BRAF signaling. After exposure to UV light, all prodrugs showed similar activity to vemurafenib, whose activity was not influenced by irradiation.

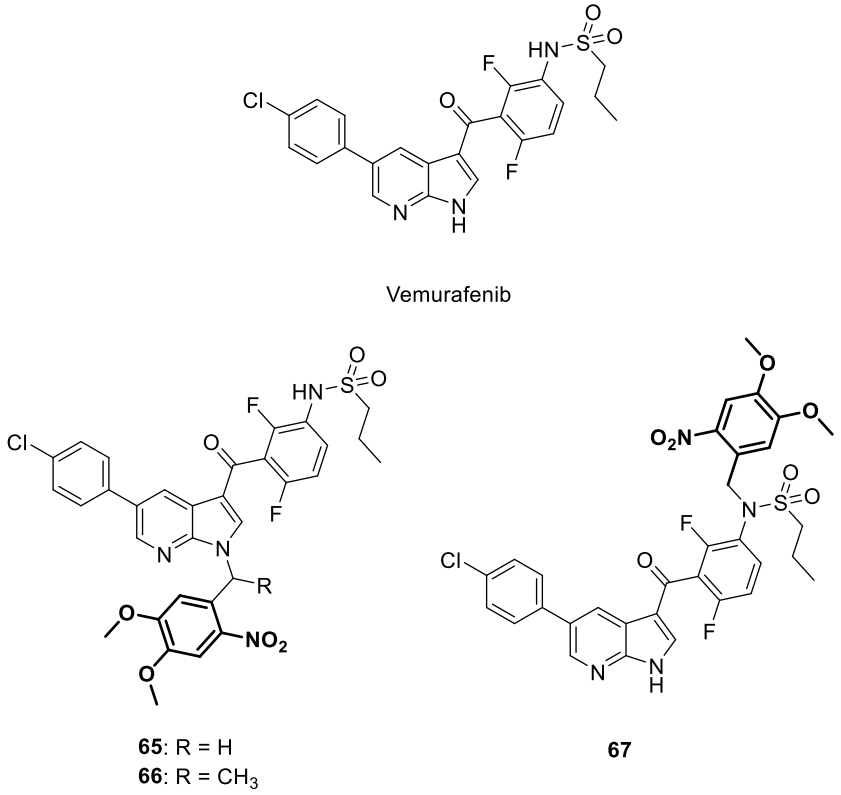

Figure 30: Structures of vemurafenib and the designed prodrugs **65**-**67.** The photocleavable ONP-based moieties are highlighted.

3.2.5. Inhibitors of tubulin (dis-)assembly

The group of Noguchi *et al*. worked on the development of photoactivatable prodrugs of paclitaxel.[81] Paclitaxel is a clinically-used mitosis inhibitor which blocks the disaggregation of microtubules in G_2 phase. One major disadvantage is the low solubility of this natural product and the requirement for solubilizing agent Cremophor EL, which accounts for hypersensitivity reactions. The first photactivatable paclitaxel derivative published by the Noguchi group (**68**, Figure 31) held a coumarinyl moiety as a PPG, and showed the same problem of water insolubility.[106] Therefore, the

group focused on improving the design of the PPG in order to enhance the water solubility of the prodrug. For this purpose, additional positively charged groups were introduced into the coumarinyl moiety. Employing this PPG, the two prodrugs **69** and **70** (Figure 31) were synthesized. Both derivatives were at least 400,000-fold more water soluble than paclitaxel. However, compound **69** is not stable in the dark and therefore is not a candidate for photoactivated chemotherapy.[81] In contrast, compound **70** showed excellent dark stability and was used for further examination. Photocleavage studies with a pulse laser (λ= 355 nm) showed an immediate release of derivative **71**, which was converted to paclitaxel via spontaneous intramolecular O-N acyl migration. The delay in paclitaxel formation after irradiation ($t_{1/2}$= 15.1 min) could present a problem in selectivity *in vivo*. Moreover, with this setup the yield of liberated paclitaxel was only 24% after 4 min irradiation time. The reason for this low recovery rate is probably the high instability of the prodrug. This assumption is supported by the fact that the PPG alone decomposed completely after 0.5 min of irradiation. However, irradiation with λ = 365 nm with a UV lamp with weaker intensity resulted in a much higher yield of paclitaxel (69%), with 50% conversion after 4 min. Still, further analysis of the photoactivation is necessary as the formation of an unknown byproduct was observed, which probably stems from decomposition of the PPG. In conclusion, a water soluble prodrug of paclitaxel was synthesized, allowing the administration of the drug without solubilizing agents. Unfortunately, no information about the cytotoxicity of the prodrug is available, and extensive studies on the biological activity in the dark and after exposure to light are essential to assess the potential of the prodrug for photoactivatable chemotherapy.

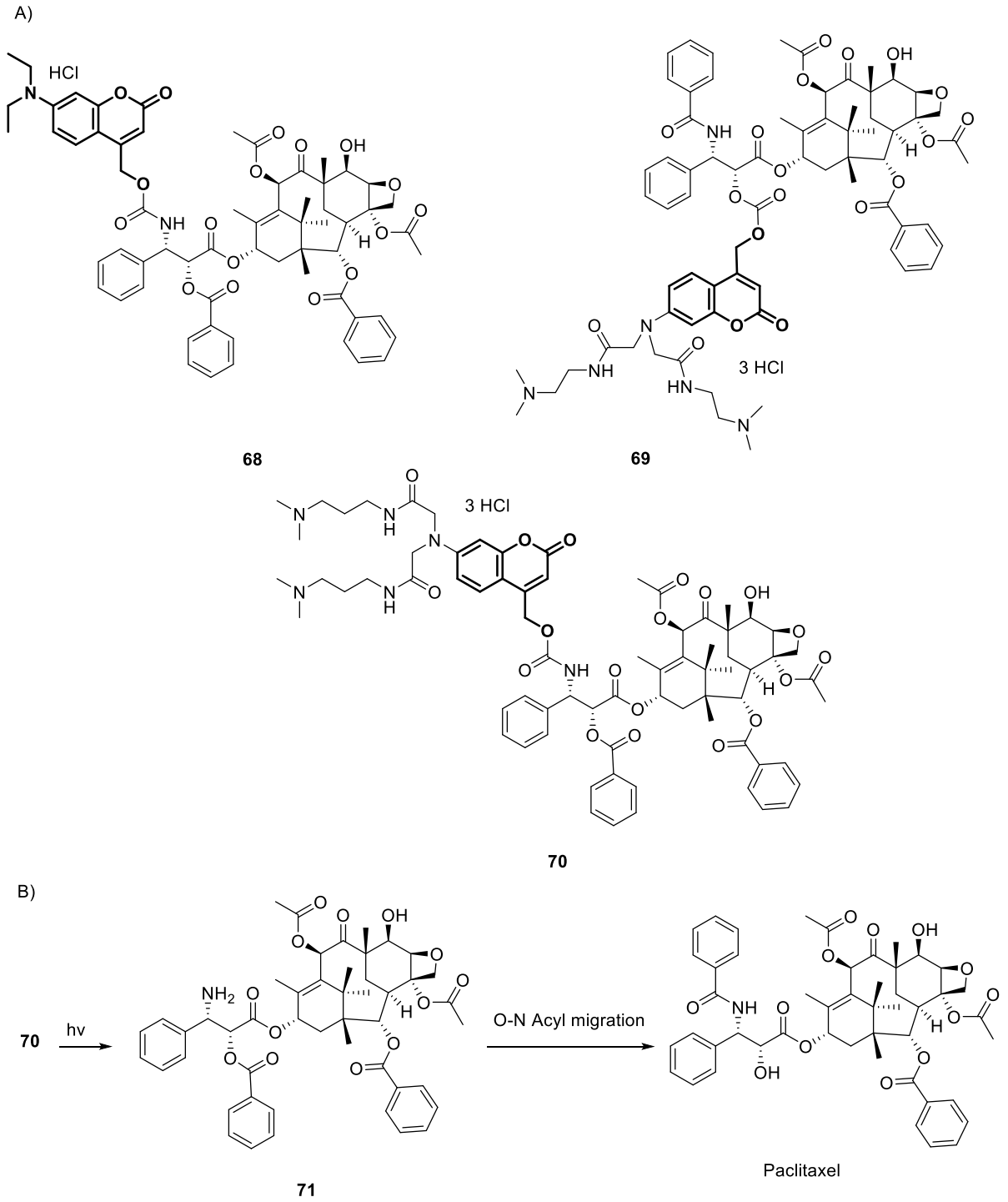

Figure 31: A) Structures of prodrugs **68-70**. B) Release mechanism of Paclitaxel from compound **70** via intermediate **71.** The photocleavable coumarinyl moieties are highlighted.

Bio *et al*. developed a new approach that combines photoactivated chemotherapy with PDT.[80] Towards this end, they combined the tubulin assembly inhibitor combretastatin A4 (CA4) with a core-modified porphyrin (CMP) via an amino-acrylate linker. Upon irradiation with λ = 690 nm, CMP produces singlet oxygen species, which does not only have a cytotoxic effect by itself but also

leads to the cleavage of the linker and subsequent release of CA4 (Figure 32B). Three different (pseudo) prodrugs were synthesized in order to analyze the biological activity of the construct (Figure 32A): (i) the target compound **72**, (ii) compound **73**, with a non-cleavable linker and (iii) compound **74**, containing fluorescent rhodamine instead of CA4. First, the inhibition of tubulin polymerization was analyzed *in vitro.* CA4, paclitaxel and a probe without any active compound were used to define the inhibitory activity of compound **72** and **73**. While CA4 completely inhibited tubulin polymerization, the tested derivatives showed only a limited inhibition (6% for **72**, 9% for **73**). Unfortunately, no data for the inhibitory activity of the activated compounds are available. Secondly, the cytotoxicity of the **72** and pseudo-prodrug **73** were examined on MCF-7 cells using an MTT-assay. Results show that, without activation, the two tested compounds are less toxic than CA4 (IC_{50}[CA4] = 9 nM, IC_{50}[**72**] = 164 nM, IC_{50}[**73**] = 1802 nM). After exposure to light (λ = 690 nm), both compounds showed higher cytotoxicity (IC_{50}[**72**] = 28 nM, IC_{50}[**73**] = 1063 nM). As pseudo-prodrug **73** cannot release CA4 the authors assume that the increase in cytotoxicity only stems from the PDT effect. In comparison, the increase in cytotoxicity of light-activated prodrug **72** is higher than of compound **73**, which indicates a dual mechanism of action. This assumption is supported by fact that the dose response curve has a different shape than the dose response curve of CA4.[80] Next, the bystander effect of photoactivated compound **72** was examined in order to examine the mechanism of action. As reactive oxygen species have a short half-life, the PDT effect only affects the cells that are exposed to light and not in neighboring cells, whereas released CA4 is able to have cytotoxic effects on surrounding cells as well. Results showed that **72** inhibited growth of surrounding cells after light activation, while the CMP photosensitizer alone damaged only the irradiated cells. The *in vivo* cleavage of the photocleavable linker was analyzed with a FRET probe. Compound **74** was injected into a mouse and the fluorescence of released rhodamine was measured as a function of irradiation time. As the irradiation time increased from 10 to 30 minutes, an increase in fluorescence was observed indicating the light-induced cleavage of the linker. Yet, it is worth mentioning that the rate of non-selective *in vivo* activation remains to be examined. Last, the *in vivo* antitumor efficacy was analyzed (Figure 33). For this experiment, colon 26 cells were injected into BALB/c mice to generate sc tumors. Five different probes were tested: (1) control; (2) prodrug **72** + CA4, non-irradiated; (3) pseudo-prodrug **73** + CA4, irradiated; and (4) and (5) prodrug **72** in different concentrations, irradiated. On three consecutive days the respective compounds were administered *via* intraperitoneal injection and after 1.5 h the tumors were irradiated with a diode laser (λ = 690 nm). The antitumor efficacy was evaluated based on the tumor size. All probes showed an inhibition of tumor growth compared to the control group (Figure 33). The combination of CA4 with non-irradiated prodrug **72** possessed least antitumor efficacy, followed by the combination of CA4 with irradiated pseudo-prodrug **73**. The higher activity stems from the PDT effect recognizable by the

signs of necrosis. Surprisingly, the tumors of mice that were treated with prodrug **72** and with light (group 4 and 5) were smaller than the ones of mice exposed to the PDT effect of **73** and the same concentration of CA4 administered separately (group 3).

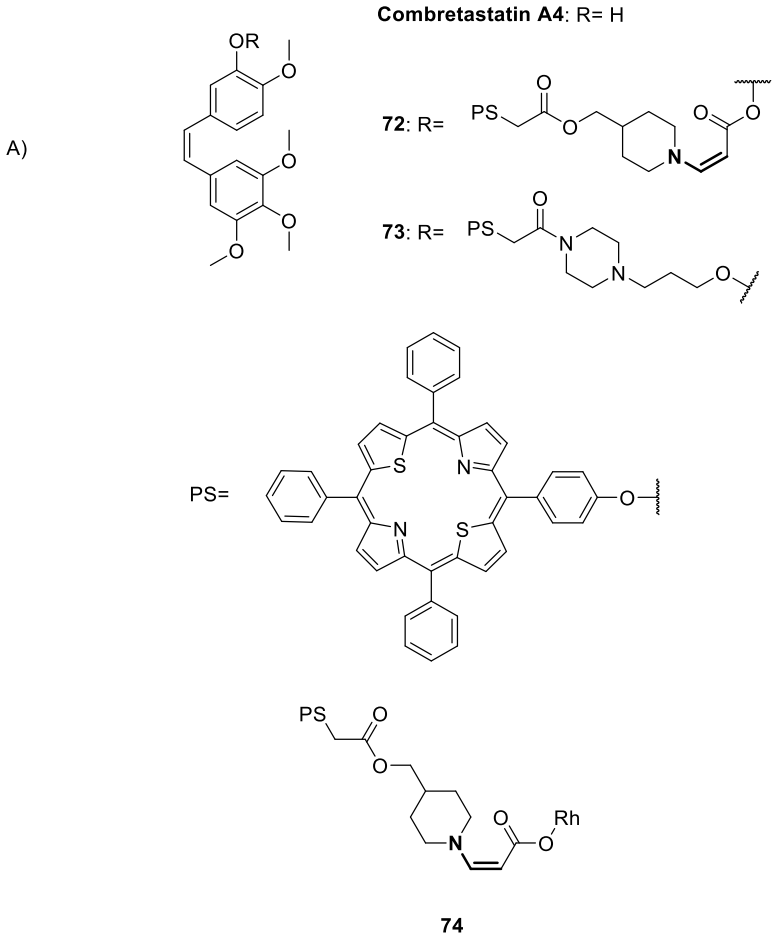

Figure 32: Photoactivated analogues of Combretastatin A4.[80] A) Structures of Combretastatin A4, its prodrug **72,** pseudo-prodrug **73**, and fluorescent probe **74**. Rh = rhodamine. The photocleavable aminoacrylate linker is highlighted. B) Mechanism of drug release: Upon irradiation, the photosensitizer produces reactive singlet oxygen, which leads to the cleavage of the aminoacrylate linker.

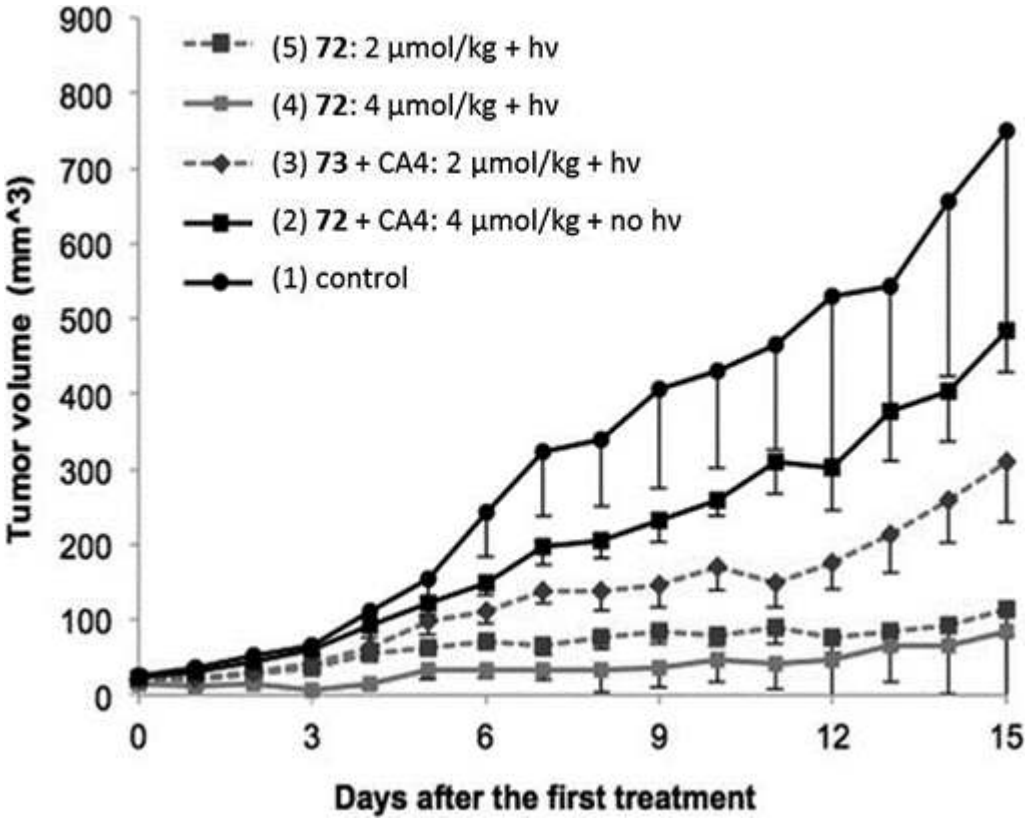

Figure 33: Results of antitumor efficacy experiments presented as tumor growth curves. (1) tumor volume of control mice; (2) tumor volume of mice treated with photoactivatable prodrug **72** and CA4 without irradiation; (3) tumor volume of mice treated with pseudo-prodrug **73** and CA4 with irradiation; (4) and (5) tumor volume of mice treated with photoactivatable prodrug **72** in different concentrations with irradiation. Adapted with permission from ref. 80. Copyright 2013 American Chemical Society.

Later, a similar design was published by the same group (Figure 34).[79] It employed fluorescent phthalocyanine (PC) as a photosensitizing agent, allowing *in vivo* fluorescent imaging. A prodrug with a photocleavable amino acrylate linker (**75**, Figure 34) and one pseudo-prodrug with a non-cleavable linker (**76**, Figure 34) were synthesized. Furthermore, poly(ethyleneglycol)-poly(D,L-lactide) (PEG-PLA) micelles were utilized in order to enhance selective targeting via the EPR effect, to extend circulation time and to solubilize the prodrug.[107] After characterization of the micelles, the effects on tubulin polymerization were examined. Both compounds show a significantly lower tubulin inhibition than CA4 at the same concentration (**75**: 23 %, **76**: 17% of CA4 activity at 3 µM). Similar results were observed when testing the *in vitro* cytotoxicity on MCF-7 cells. Prior to irradiation, compounds **75** and **76** were less toxic than CA4 (IC_{50}[CA4] = 9 nM, IC_{50}[**75**] = 173 nM, IC_{50}[**76**] = 916 nM), whereas exposure to light (30 min, λ = 690 nm) lead to a significant increase in cytotoxicity (IC_{50}[**75**] = 6 nM, IC_{50}[**76**] = 34 nM). The bystander effect was also analyzed: in the probe treated with

pseudo-prodrug **76** only the cells that were irradiated were damaged, whereas in the probe treated with prodrug **75** all the cells were damaged upon irradiation. Next, the *in vivo* distribution and the effect of the micelle formulation was evaluated. To that end, PEG-PLA micelles containing the compounds were prepared, together with solutions in 5% Cremophor EL used as a control. The formulations were injected retro-orbitally in Balb/c mice with sc tumors created via injections of colon-26 cells. Imaging of the phthalocyanine fluorescence at different time points showed accumulation of each formulation in the tumor regions, but the micelles seemed to persist longer in the tumor compared to the formulations with Cremophor EL. Finally, the antitumor efficacy was examined, using the same type of mice. The following samples were tested: (1) CA4, non-irradiated; (2) pseudo-prodrug **76**, irradiated; (3-5) prodrug **75** in different concentrations, irradiated with different energy of light, and (6) control. 24 hours after retro/orbital injection of one of the samples into each mouse, the tumors were irradiated with a diode laser (λ = 690 nm) for 30 min. The tumor size was taken as an indication for efficacy of the treatment. As expected, the tumors from the control group showed most extensive tumor growth. In comparison, the tumors in mice treated only with CA4 were significantly smaller. It is noteworthy that the PDT effect of irradiated pseudo-prodrug **76** inhibited tumor growth more than CA4 in the first three days, but afterwards tumors grew back at a similar rate like in the control group. In contrast, the tumor size in groups (3)-(5) treated with irradiated prodrug **75** shrank to unmeasurable size until day 15. In conclusion, the authors developed a new strategy to combine PDT and *in vivo* optical imaging with photoactivated chemotherapy, activatable with far-red or NIR light, which presents a major advantage of this approach. However, the requirement of oxygen for the PDT effect and bond cleavage is unfavorable as the internal volume of most tumors is hypoxic. Further mechanistic studies are awaited to explain the outstanding antitumor effects, which exceeded the combination of the cytotoxic effect of CA4 and the photosensitizer phthalocyanine or core modified porphyrin respectively.

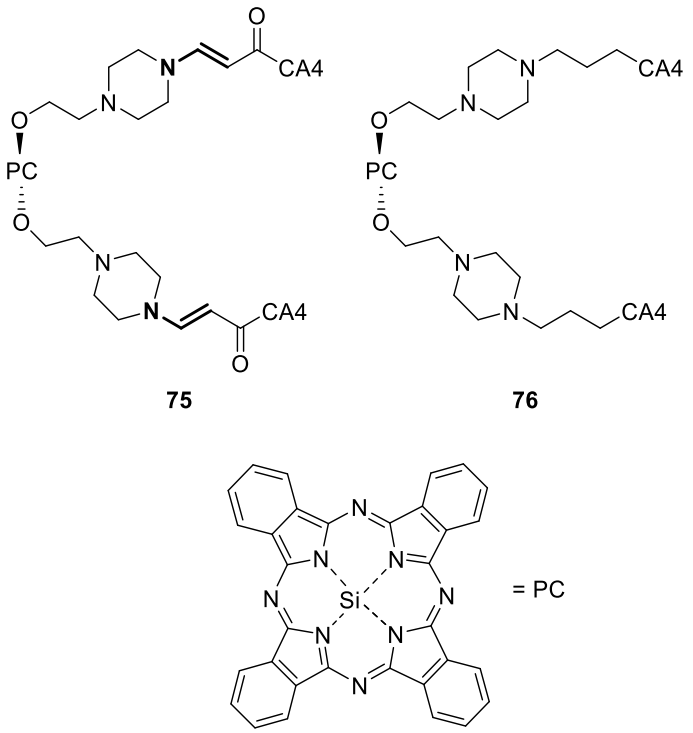

Figure 34: Structures of **75** and **76**. PC=phthalocyanine. The photocleavable aminoacrylate linker is highlighted.

In summary, a wide range of prodrugs that release an active chemotherapeutic upon irradiation have been designed and synthesized as shown in an overview in Table 2. This concept can be applied to a variety of drugs with different cytotoxic mechanisms ranging from relatively unselective DNA alkylation/intercalation to selective inhibition of mutated protein kinases. Photoprotecting groups (PPGs) derived from *ortho*-nitrophenyl are the most often employed. In most cases, it was possible to achieve a very high phototherapeutic index which is crucial in order to reduce unwanted drug effects. Another prospect is offered by the wavelength-selective deprotection of multiple PPGs,[108] which could allow the use of multiple chemotherapeutics and their selective activation in space and time. A weakness of the PPG-based approach is the irreversibility of activation. Undoubtedly, side effects will be reduced but the activated drug will still be able to damage healthy tissues of the body after leaving its site of action. For this reason, recently another modality is being developed using photoswitchable drugs, which offers not only an “on” but also “off” switching of the cytotoxic activity and will be described in the next section.

Table 2: Overview over photocaged organics including corresponding phototherapeutic indices

Original cytotoxic agent	Target / mechanism of action	Compound	Phototherapeutic index	activation λ [nm]	Methods	Ref.
Pt^{II} complex	DNA	**43**	-	UV	*In vitro* cytotoxicity study on MCF-7 cells	[65]
		48	> 11	400-700	*In vitro* cytotoxicity study on HaCaT, BT474, T47D, and Hep3B cells	[75]
Cu^{II}	Production of ROS	**44**	2	UV	*In vitro* cytotoxicity study on MCF-7, HeLa HL-60 cells	[67]–[69]
Re^{I} complex	Production of ROS	**45a**	2	350	*In vitro* cytotoxicity study on MRC-5 and HeLa cells	[72]
		46a	> 5	350	*In vitro* cytotoxicity study on MRC-5, PC3 cells, and HeLa cells	
Ru^{II} complex	DNA	**47a**	> 6	350	*In vitro* cytotoxicity study on HeLa cells and U2OS cells	[74]
Phosphoramide mustard	DNA (alkylation)	**49a-b, 50**	-	300-400	*In vitro* alkylating studies, no IC_{50} values	[63]
Duocarmycin	DNA (alkylation)	**51a-c, 52a-b**	≤ 3000-82000 (for **52a**)	UV-A	*In vitro* cytotoxicity study on A549 cells	[85]
5-Fluorouracil/ Tegafur	Antimetabolite (pyrimidine analogue)	**53**	-	350	*In vitro* cytotoxicity study on E. coli DH5α cells	[64]
		54	7% vs. 67% cell death	350	*In vitro* cytotoxicity study on MCF-7 cells	[86]
		55	-	365	No studies on biological activity	[89]
Methotrexate	Antimetabolite (folic acid analogue)	**56**	Cytotoxicity of prodrug in the same range as for free MTX	365	*In vitro* cytotoxicity study on KB cells	[92]

Doxorubicin	DNA, topoisomerase II	**57**	No activity vs 80% reduction of cell growth	365	*In vitro* cytotoxicity study on KB cells	[93]
		60	71	330-380	*In vitro* cytotoxicity study on A549 cells (No IC_{50} values obtained from *in vivo* studies)	[97]
		61	> 10	365	*In vitro* cytotoxicity study on JH-EsoAd1 cells	[100]
		62	-	980	No studies on biological activity	[84]
Imatinib	Several protein kinases	**63, 64**	65 (for **64**)	365	Inhibition of PDGF-Rβ	[102]
Vemurafenib	$BRAF^{V600E}$ mutant	**65**	No toxicity vs IC_{50}= 1.5 μM	365	*In vitro* cytotoxicity study on melanoma cell line SKMel 13 (carrier of $BRAF^{V600E}$ mutation)	[105]
		66	9			
		67	7			
Paclitaxel	Inhibition of tubulin disaggregation	**69, 70**	-	365	No studies on biological activity	[81]
Combretastatin A4	Inhibition of tubulin assembly	**72**	6	690	*In vitro* cytotoxicity study on MCF 7 cells (No IC_{50} values obtained from *in vivo* studies)	[80]
		75	29	690	*In vitro* cytotoxicity study on MCF 7 cells (No IC_{50} values obtained from *in vivo* studies)	[79]

3.3. Summary

Photocaged organic chemotherapeutics (Section 3) have been synthesized based on drugs with different mechanisms of action, including DNA alkylating agents, enzyme inhibitors and antimetabolites (Table 2). This approach has been employed since late nineties of the 20th century and has resulted in many designs, which are characterized by reasonably high PI values (Table 2) and efficient uncaging. Besides the introduction of new PPGs, the use of up-converting nanoparticles is being studied and is expected to provide solutions for NIR light activation. However, the main problem associated with photocaged drugs, similarly to the of photoactivated metal complexes, is the irreversibility of activation, which would result in systemic toxicity of the activated drug outside its intended site of action.

4. Photoswitchable chemotherapeutic agents

In the following section, we present the design and studies on biological activity of photoswitchable chemotherapeutics. This recent approach to controlling biological activity of drugs with light came to be known as "photopharmacology" and has been recently defined with its strategies, challenges and opportunities.[109],[110] In contrast to photocleavable prodrugs, only a few examples of photoswitchable chemotherapeutics have been published. One major advantage over the use of photocleavable drugs is that the activation of photopharmacological agents is reversible, which may lead to a significant reduction in adverse drug reactions. In general, this strategy uses molecules that can be efficiently excited to the more active form and spontaneously reisomerize to the less active isomer. Therefore the half live of the active form is of crucial importance. On one hand, this form has to be stable enough to exert the desired effect but, on the other hand, the inactivation should succeed as soon as possible to prevent cytotoxic effects on other organs.

To date, three different groups published the work on photoswitchable CA4 analogues. It is known that the *cis* form of CA4 is biologically active,[111] and isomerization of the olefinic bond results in a significant loss in activity. Exchanging the stilbene structure for an isosteric azobenzene leads to a photoswitchable analogue of CA4 (Figure 35). Azobenzenes are well-established photoswitches for biological applications[112] due to synthetic accessibility and robustness of photoswitching. Generally, the *trans* isomer is thermodynamically more stable than the *cis* isomer. Upon irradiation with an appropriate wavelength, it is possible to switch the molecule from the *trans* to the less stable *cis* form. The equilibrium ratio between *cis* and *trans* isomer under irradiation is called the "photostationary state" and is aimed to be as high as possible for medical applications. Isomerization back to the *trans* state will then proceed spontaneously or can be accelerated by exposure to light of

a suitable wavelength. The photochemical properties of azobenzene derivatives, including the wavelength dependence of the switching and the half-life of the unstable isomer can be influenced by careful choice of substituents.

Following this strategy, Borowiak *et al*. synthesized various analogues of CA4, called "photostatins" (Figure 35).[113] All derivatives could be switched to the active *cis* form using UV and blue light (λ = 380-420 nm), whereas irradiation with light of longer wavelength or dark thermal adaptation resulted in back-isomerization to the *trans* form. The half-lives for the thermodynamically unstable *cis*-isomers ranged from 0.8 to 119.0 min (**77**: 6.2-8.4 min). Evaluation of the biological activity of compounds **77** and **78** was performed on different cell lines, including MDA-MB-231 (breast adeno carcinoma epithelial cells), HeLa cells, and Jurkat (T cell lymphoma cells). Results showed a significant increase in cytotoxicity of the derivatives when exposed to light (λ = 390 nm, different pulse schemes), with IC_{50} values in the low micromolar range, which is comparable to the potency of CA4 phosphate. Further studies confirmed toxic effects of activated compound **77,** such as membrane disintegration, depletion of nuclear DNA content, and cleavage of PARP into catalytic fragments serving as an indication for apoptosis. In contrast, under dark conditions such effects were not apparent at the same concentrations. Subsequently, the authors investigated the influence of **77** on tubulin organization (Figure 36). Irradiation and treatment with **77** lead to an arrest in G_2/M phase, typical for tubulin inhibitors. In the dark, and also after applying a "rescue regime" involving a light pulse at λ = 390 nm (activation) followed by a λ = 515 nm (inactivation) pulse, the G_2/M phase arrest was significantly reduced. Additionally, a scintillation proximity assay (SPA assay) of competitive binding of radiolabeled colchicine and **77** confirmed that photoactivation results in competitive binding of **77** to the colchicine binding site on tubulin with an EC_{50} of 30 μM. In comparison, CA4 showed an EC_{50} of 0.16 μM. Similarly, the *cis* isomer showed an inhibitory effect (IC_{50} = 5 μM) on tubulin polymerization of purified tubulin whereas the *trans* isomer was not active (IC_{50} >> 40 μM). These findings were supported by immunofluorescence imaging of tubulin in living HeLa cells in the presence of **77** (see Figure 36C) and by analysis of tubulin organization using EB3 which was labeled with a fluorescence tag. Finally, several *in vivo* studies were performed. Firstly, the cell cycle of transgenic *C. elegans* embryo cells in the presence of compound **77** was analyzed. A fluorescent group was attached to cell membrane marker PH and histone H2B allowing tracing of the different stages of mitosis. Cells that were exposed to light (λ = 405 nm) in the presence of **77** were arrested in metaphase, while neighboring cells that were not irradiated showed normal mitosis. Furthermore, cells that were exposed to an inactivating light pulse of λ = 514 nm right after photoactivation with λ = 405 nm did not show variance in the normal cell cycle either. Next, the biological activity in living mice was evaluated. For this purpose, dissected cremaster muscles of the mice were superfused with a solution of the test substance. In this case, the CA4 phosphate analogue

78 was used because of its higher solubility in water. The muscles were either irradiated with λ = 390 nm or kept in the dark as a control. As further controls, other muscle samples were perfused with buffer and then underwent the same treatment. Subsequently, the tissue was removed for immunohistochemistry analysis using anti-α-tubulin antibody. Similarly to the previous results, the samples that were exposed to λ = 390 nm showed disassembly of microtubules, whereas in the dark control normal microtubule organization, consistent with the control tissues without active compound, was observed.

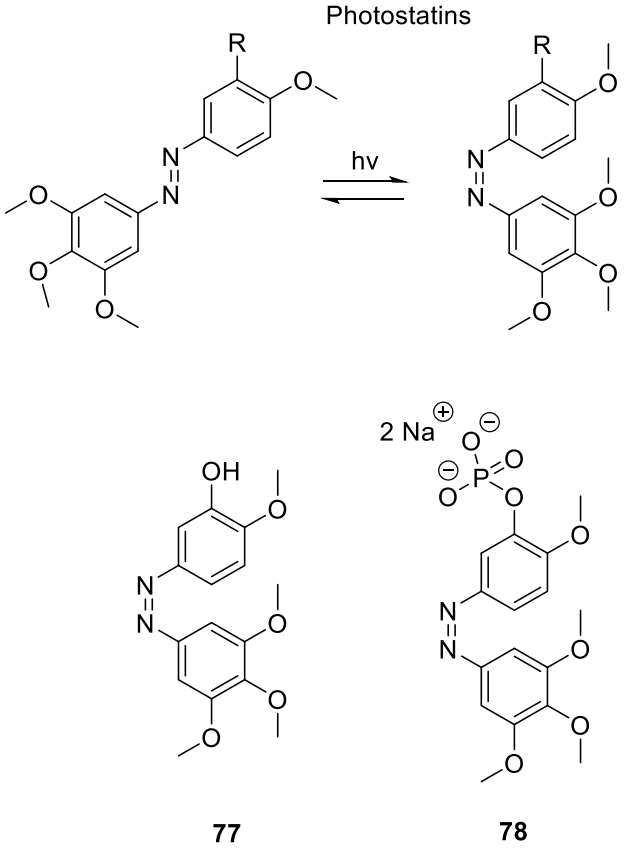

Figure 35: General structure and isomerization of the designed photostatins. **77**: aza-analogue of CA4, **78**: aza-analogue of CA4 phosphate.

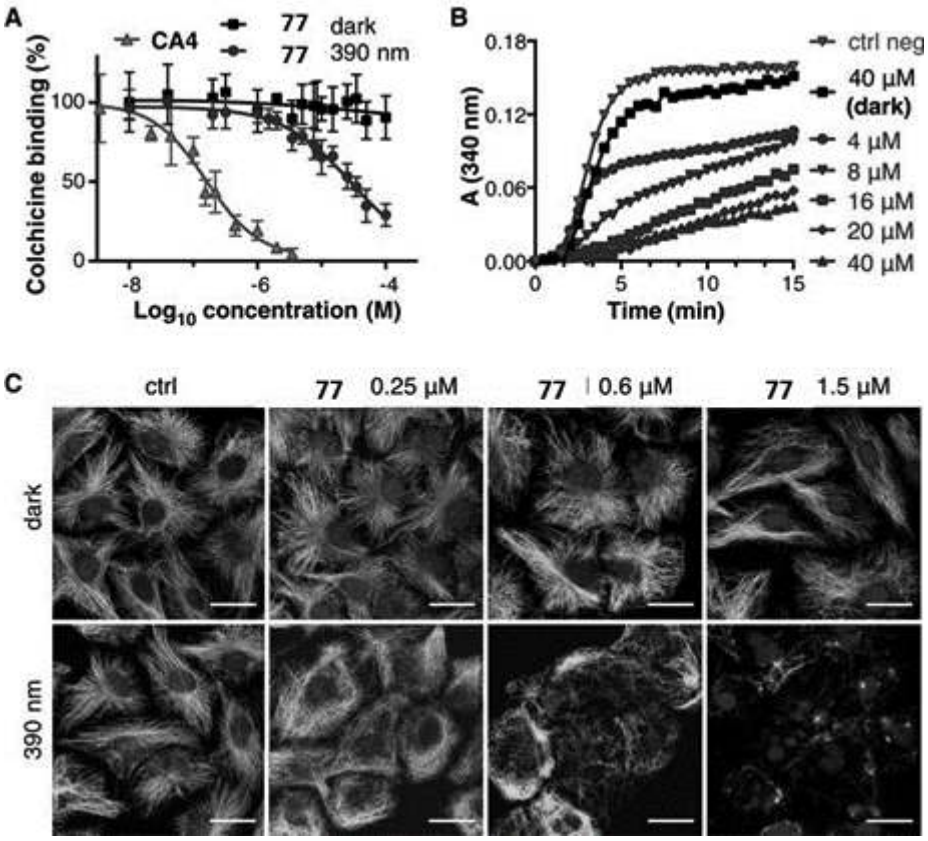

Figure 36: Binding of CA4 analogue **77** to tubulin heterodimers and inhibition of tubulin polymerization A) Results of SPA assay. B) Results of turbidimetric *in vitro* polymerization assay. C) MDA-MB-231 cells treated for 20 h with PST-1, then stained for α-tubulin. Reproduced with permission from ref. 113. Copyright 2015 Cell Press.

The research of Engdahl *et al.* focused on the evaluation of bioactivity of the same CA4 analogue **77**.[114] An *in vitro* turbidity assay with isolated tubulin was performed in order to analyze the light dependent effect of **77** on tubulin (de-)polymerization. After exposure to light of an appropriate wavelength, **77** showed similar disruptive effects like CA4 on tubulin polymerization but with slightly lower potency.[114] In the dark, no such effects were observed. In the subsequent experiment, the cytotoxicity on HeLa cells was examined. For this purpose, the viability of cells that were incubated with compound **77** for five days and irradiated with λ = 400 nm light was determined by means of an MTT assay. Irradiation led to complete cell death in the samples with concentrations of **77** of more than 500 nM. In the control samples, which were not exposed to light, compound **77** did not have toxic effects at concentrations up to 100 µM and irradiation alone did not have any effects on cell viability either.

Studies on the same photoswitchable derivative were also published by Sheldon *et al*.[115] Interestingly, photoswitching analysis gave results that are not in agreement with results published by Borowiak *et al*.[113] In fact, the half-life of the cis isomer was determined as 75-100 min in contrast to 6.2 min reported previously under the same conditions. Similarly to studies conducted by Engdahl

et al.,[114] the effect on tubulin polymerization was examined *in vitro.* In general, results are in line with those previously published. The differences in potency were defined more precisely showing an IC_{50} for pre-irradiated **77** of 5.1 µM compared to the more potent CA4 with IC_{50} = 1.9 µM. In the absence of light, **77** was 2.8 times less potent than the activated form. Besides the experiments with isolated tubulin, the authors conducted cytotoxicity studies with human umbilical vein endothelial cells (HUVECs) and MDA-MB-231 cells. The results of the assay on MDA-MB-231 were consistent with those published by Borowiak *et al*.[113] As CA4 is known to have vasculature-disrupting effects, the use of HUVECs is a reasonable addition to the cytotoxicity studies carried out before. Different pulse patterns of irradiation were applied for 48 hours in order to confirm the spontaneous isomerization from the activated *cis* back to the *trans* from. The light pulses (λ = 380 nm) were applied according to the following scheme: (i) one 1 min pulse every hour, (ii) one 1 min pulse every two hours, (iii) one 1 min pulse at the beginning of the experiment. As anticipated, the toxic effects of **77** decreased with increasing pulse intervals, For the first pulse pattern (one pulse per hour), the toxicity was 22 times higher compared to the dark control. Nevertheless, the activated aza analogue of CA4 (**77**) (IC_{50} = 0.4-0.6 µM) was not as potent as its parent drug (IC_{50} = 0.002-0.004 µM). The authors hypothesize that this difference in potency stems from metabolic instability of the aza analogue. As it is known that azobenzenes react with glutathione (GSH) in a phase II metabolism reaction,[116] the stability of **77** was evaluated revealing that both isomers are decomposed by GSH. Further LC-MS/MS investigation on the progression of the reaction with activated **77** confirmed degradation of the *cis* isomer and indicated the formation of a rearrangement product of the same mass but not accordant with the *trans* isomer. Furthermore, the transient emergence of a peak characteristic for GSH adduct was observed.

In summary, aza analogues of CA4 present promising drugs for photoactivated chemotherapy, standing out due to the possibility of being activated and also deactivated. Undoubtedly, the designed compounds are a useful tool for cell biology. However, the weak potency of the activated *cis* form compared to CA4[114] and its presumably low metabolic stability[115] might present a problem for the clinical use. In addition, the need of $\lambda \leq 400$ nm light to activate is not optimal for medical application in humans.

Another photoswitchable cytotoxic drug with an azobenzene moiety was published by Szymanski *et al*.[117] This work presents the design and analysis of twelve derivatives of the histone deacetylase (HDAC) inhibitor SAHA (vorinostat, Figure 37). HDAC inhibitor are relatively new drugs in cancer therapy. It is assumed that the cytotoxic effects are based on the inhibition of the deacetylation of chromatin. Normally, this deacetylation ensures close packing of DNA, which makes it less accessible to transcriptions factors and therefore to gene expression. Thus, inhibition of HDACs results in unregulated transcription, which may cause apoptosis.[118],[119] The hydroxamic acid moiety

of the HDAC inhibitors is crucial for the biological activity, as it binds to the zinc ion inside the enzyme's catalytic pocket. Several experiments on the photoswitching properties and inhibitory potency on different HDACs demonstrated that compound **79** was the most promising as a photoswitchable drug. Firstly, a high photostationary state (percentage of instable *cis* isomer at equilibrium under irradiation with λ = 365 nm, at c ≈ 2 mg mL^{-1} in DMSO) of 92% was measured. Secondly, analysis of the inhibition of several human HDACs showed that the *cis* isomer is the more active one (e.g. for HDAC2: IC_{50}[cis] ≈ 0.56 µM, IC_{50}[trans] ≈ 21.65 µM, IC_{50}[SAHA] ≈ 0.18 µM, see Figure 38a and b), which was not the case for most of the remaining compounds. Thirdly, derivative **79**, as well as the whole range of other aza-derivatives, was shown to be metabolically stable towards the reaction with GSH, which is the predominant biotransformation reaction of azobenzenes.[109] Next, the reversibility of isomerization of compound **79** was analyzed. Several cycles of alternate photoactivation to *cis* and deactivation to *trans* form were executed, followed by a quantification of HDAC1 activity at the end of each cycle. Results show a reversible inhibition with 59% residual activity in presence of the *cis* isomer, compared to 90% activity in the presence of the trans isomer (see Figure 38c). Subsequently, an enzymatic activity assay with HDAC2 was performed to confirm the applicability of the previous findings to the *in situ* isomerization. For this purpose, the enzyme was incubated with the *cis* form. After 30 min, the sample was exposed to white light provoking the isomerization to the *trans* form and causing a significant increase in activity (see Figure 38d). Finally, the cytotoxic effects on HeLa cells of both isomers were examined. As expected, incubation with the *cis* form lead to almost complete cell death, whereas the *trans* form did not show significant cytotoxic effects at equal concentration (100 µM) (see Figure 38e). Notably, in both cases an increase in histone acetylation indicating the inhibition of HDAC was observed. Further data analysis confirmed that inhibition of the HDACs by **79** is competitive and not irreversible. In conclusion, this research presents a promising candidate for a photoswitchable chemotherapeutic and further analysis of the biological activity is awaited in order to clarify the significance of the varying inhibitory effects on different HDAC isoforms and the *in vivo* efficiency.

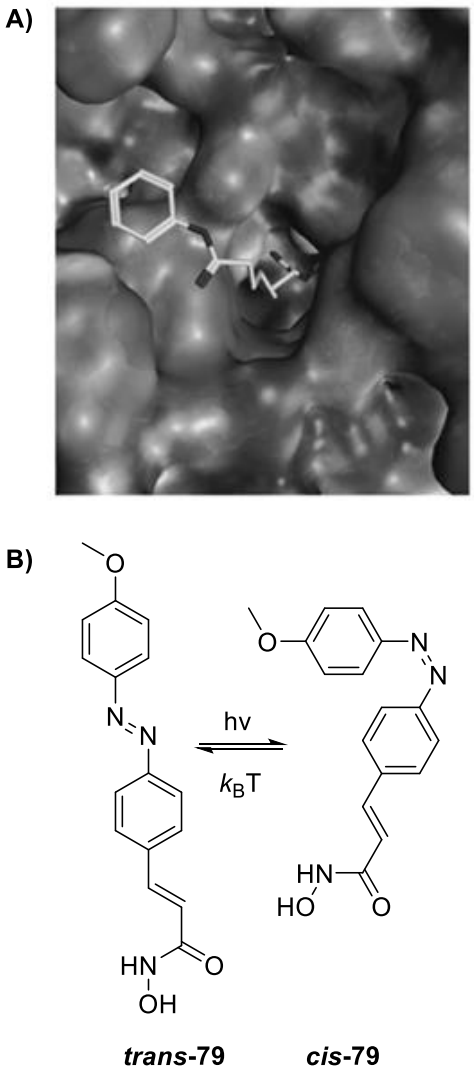

Figure 37: HDAC inhibitor SAHA and prodrug **79**. A) Binding mode and structure of SAHA; B) Structure of photoswitchable HDAC inhibitor **79**. Reproduced with permission from ref. 117. Copyright 2015 Wiley-VCH.

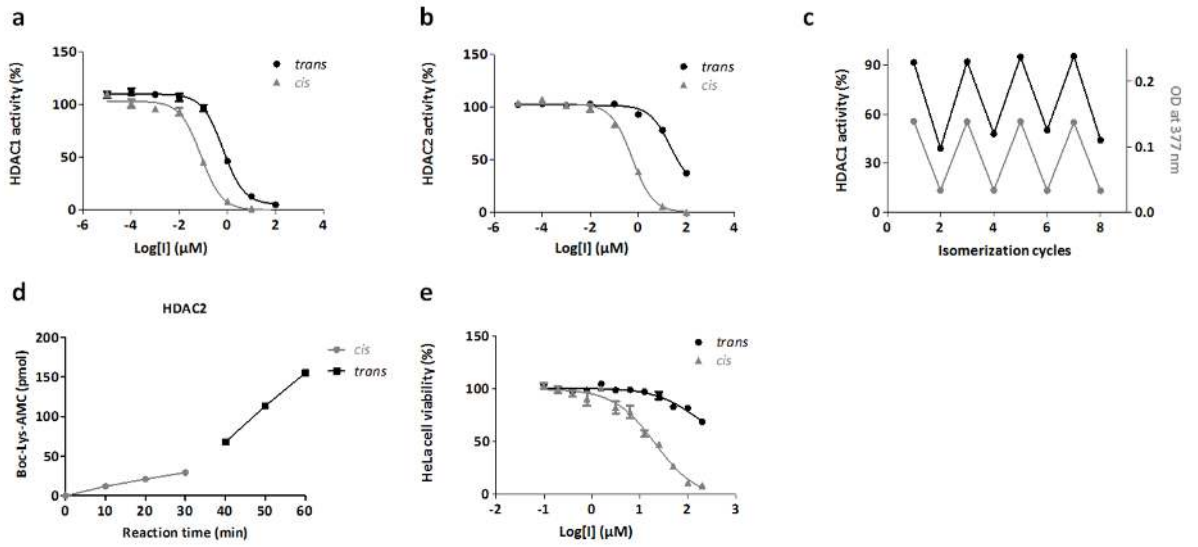

Figure 38: Studies on the performance of compound **79** as an HDAC inhibitor. The IC_{50} curves in a) HDAC1 and b) HDAC2 recombinant enzymes of *trans* and *cis* forms of the inhibitor. c) Inhibition of HDAC1 activity with 50 nM of inhibitor **79** (black) and reversible photochromism (gray) after 4 isomerization cycles. d) In situ photoisomerization of **79**, after 30 min of incubation of the *cis* form (1 µM) with HDAC2, with white light. The formation of product was monitored at the indicated times. e) HeLa cell viability was measured after 16 h of incubation with various concentrations of each isomeric form of the inhibitor. a)–e) The data are presented as mean values of three independent measurements with their respective standard deviations. Reproduced with permission from ref. 117. Copyright 2015 Wiley-VCH.

Another approach towards the development of photoswitchable chemotherapeutics was presented by Hansen *et al*. [120] This research presents the design and evaluation of photoswitchable proteasome inhibitors based on bortezomib. Proteasomes are complexes of proteolytic enzymes responsible for the degradation of ubiquitinated proteins in order to maintain cell homeostasis. Especially in tumor cells, protein synthesis rate is very high and misfolded proteins are abundant, thus inhibiting proteasomes may lead to accumulation of misfolded proteins and trigger apoptosis.[121] With the aim to preserve the biological activity and affinity to the target, the core structure of bortezomib was kept unchanged and a selection of substituted azobenzene moieties was attached to the molecule, giving six different aza-analogues (compounds **80-85**, Figure 39). Photoisomerization studies verified that it is possible to switch every derivative from the *trans* to the *cis* form by the use of light (λ = 365 nm) and that relaxation to the *trans* form occurs spontaneously with half-lives ranging from 3.8 to 7.7 hours. Furthermore, the metabolic stability towards reaction with GSH was examined. Presence of cytosolic concentrations of GSH did not show significant influence on the absorption spectrum and photoswitching properties of compound **80,** used as a model. In order to confirm the expectation that the linear *trans* form fitted better into the active site

of the proteasome complex and thus has a higher activity than that of the *cis* form, the biological activity was examined. RAJI cell lysates were incubated with the different concentrations of respective *cis* and *trans* isomers of compounds **80-85** and afterwards the binding affinity was determined by using fluorescent probes to quantify the vacant binding sites. Results showed that, in fact, the *trans* isomer has a higher affinity than the *cis* isomer (up to three times, depending on binding site and derivative), with IC_{50} values in the same range as the parent drug bortezomib. Furthermore, differences in binding affinity to the distinct binding sites were revealed. Similarly to bortezomib, the photoswitchable derivatives tend to have a higher affinity for proteasome binding sites β1 and β1i over β5. Finally, an MTT assay with HeLa cells was used to analyze the cytotoxic activity. Differences in dose-activity relation of the *cis* and *trans* isomers were observed with only minor changes in IC_{50} values. To summarize, this research again proves the concept that photoisomerization may change the biological properties of a drug. The designed bortezomib analogues, however, require further optimization to increase the difference in activity of the respective isomers. Beyond that, the fact that the *trans* form is the active isomer is not optimal for application as a photoswitchable chemotherapeutic as explained above.

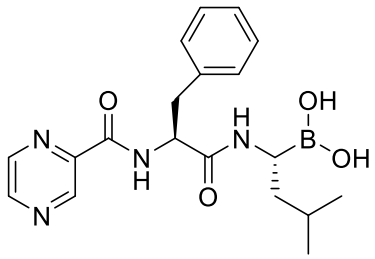

Bortezomib

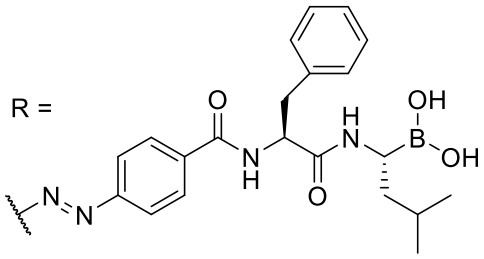

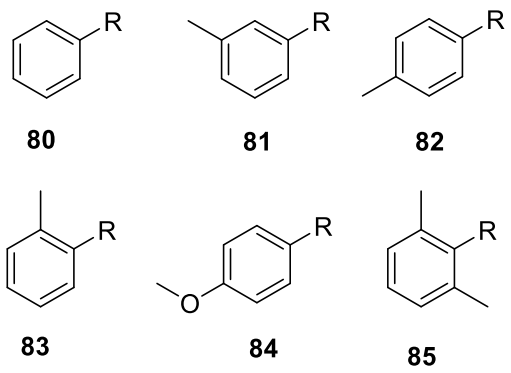

80 **81** **82** **83** **84** **85**

Figure 39: Structures of bortezomib and its analogues **80-85**.

Presa *et al.* published two photoswitchable Platinum(II) complexes employing a 1,2-dithienylethene moiety (compounds L^{86} and L^{87}, Figure 40) as a photoswitchable ligand.[122] Upon UV irradiation, the open form of the diarylethene switch isomerizes to the closed form, as shown in Figure 40. The closed form is stable in the dark and isomerization back to the open form proceeds after irradiation with visible light. Preparation of the corresponding Pt^{II} complexes was performed via the reaction of two equivalents of the photoswitchable compounds with one equivalent of cis-$[PtCl_2(DMSO)_2]$ giving *trans*-$[Pt_2Cl_4(DMSO)_2(L^{86})]$ and *trans*-$[Pt_2Cl_4(DMSO)_2(L^{87})]$ respectively. In the following we refer to these complexes as **86** and **87.** UV/Vis spectroscopy was employed to analyze the photochemical properties of the ligand and the respective complexes. Characteristic absorption bands for the open form of L^{86} and L^{87} were observed prior to irradiation. After exposure to λ = 365 nm, new bands of π-π* transitions (L^{86} : λ= 378 nm and 550 nm and L^{87}: λ= 381 nm and 592 nm) of the closed form appeared. Similar results were obtained for the corresponding Pt^{II} complexes, with the difference that absorption bands were bathochromically shifted. Subsequently, the interactions of complexes **86** and **87** with DNA were analyzed using a competitive binding assay with ethidium bromide on calf thymus DNA. Evaluation of the data revealed that **86** has a higher affinity to DNA than **87**. The authors suggest that this is caused by electronic repulsion of the fluorine atoms with the phosphate backbone of DNA. More importantly, the closed forms showed higher affinity than the respective open forms (6.5-fold binding affinity difference for **86**, and 5.5-fold for **87**). This was explained by the fact that the open form is more bulky than the closed form and thus is more sterically hindered to bind to the double helix.[122] In addition, electronic properties of the ligand after ring closure may be favorable for the binding. Next, DNA binding of the complexes was examined by analyzing electrophoretic mobility of plasmid DNA. Incubation with cisplatin, taken as a model compound, has a shortening effect on relaxed circular DNA and therefore increases the electrophoretic mobility. In contrast, **86** and **87** presumably lead to an unwinding of double helix supercoiled DNA, which decreases its mobility.[122] Overall, this effect is more distinct for the closed forms of the complexes and also more pronounced for complex **87.** Subsequently, the cytotoxic effects of the photoswitchable compounds on six different cancer cell lines were analyzed. Cells were incubated with the open and the closed forms of **86** and **87**. In contrast to results of the studies on DNA binding, neither the closed nor the open form of complex **86** had cytotoxic on any of the cell lines. On the other hand, the closed isomer of complex **87** showed inhibitory effects on the growth of most studied cell lines, whereas the open form was significantly less active. This difference in activity decreases over time, but is still visible after 72 hours of incubation. (Results for DMS53 [small lung cancer cells]: after 48 h incubation, IC_{50} [closed] = 34 μM, IC_{50} [open] = 76 μM; after 72 h incubation, IC_{50} [closed] = 30 μM, IC_{50} [open] = 55 μM). Even though the closed from of **87** shows highest activity,

it is still up to eight times less potent than cisplatin. Finally, the cellular localization of the different compounds was analyzed, exploiting the fact that the photoswitchable complexes show fluorescence. Confocal microscopy showed that all complexes are able to enter the cell. The cellular localization is in line with the results of the cytotoxicity studies, since the closed form of **87** is the only compound which is co-localized with the nucleus, while the other – less cytotoxic – complexes are located in vesicular structures. In conclusion, a new strategy in the design of photoswitchable chemotherapeutics has been developed. Broad cytotoxicity studies performed in the course of this research show the strong dependency of biological activity on the type of cell line used for examination. The relatively small differences in activity of the two isoforms and the fact that the active (closed) form is stable in the dark and will not be deactivated outside the site of action in the body are possible weaknesses of the designed Pt^{II} complexes.

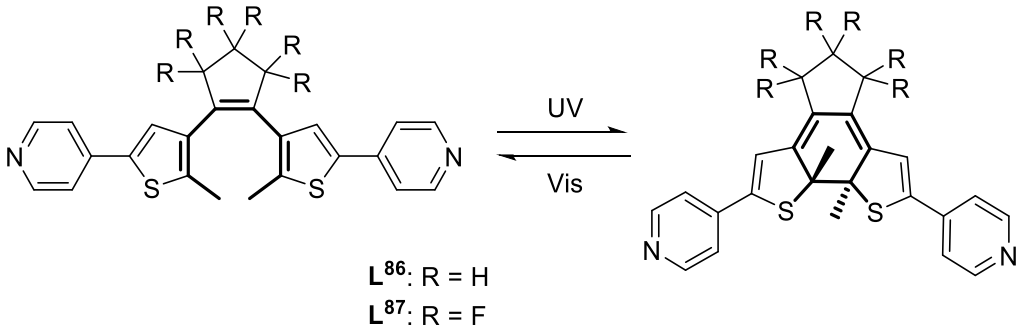

L^{86}: R = H
L^{87}: R = F

Figure 40: Structure of ligands **L^{86}** and **L^{87}** before and after photoactivation.

Taken together, the reported studies prove the principle of photoswitchable chemotherapeutic agents and highlight the advantage of reversible activation. To date, aza analogues of CA4 are the most investigated example of this approach. A possible obstacle for the application of these compounds in clinics might be the dependence on λ = 380-400 nm light. Further examination is also needed in order to determine the half-lives of the respective compounds, as this is of paramount importance for future application.

5. Conclusions

This review provides the reader with the current status of light-activated chemotherapeutic agents that are not relying on the PDT mechanism and therefore do not require oxygen for their activation. While these compounds are not yet in clinical use, we believe that a systematic overview of the field will contribute to its further development. Towards this end, we have categorized the

main strategies used for the design of light-responsive anti-cancer drugs and we have discussed their intrinsic advantages and disadvantages.

One of the main challenges for the future development of this class of drugs, which also represents a major bottleneck for their clinical implementation, is the low transparency of tissue to the UV light used to activate most of the compounds presented in this review. This is especially true for photocaged and photoswitchable designs (see Sections 3 and 4). The future application of photocaged compounds is strongly depending on the development of low-energy-light addressable photocleavable protecting groups (PPGs)[108],[123],[124] and it is anticipated that the new developments in this field will lead to molecular designs of photoactivated chemotherapeutics with high clinical relevance. What remains to be seen is the extent to which chemotherapeutics can be efficiently caged with the new PPGs and what the intrinsic toxicity of the photoreaction products is. Likewise, the implementation of photoswitchable drugs relies on the application of red-light switchable molecules, which started to emerge in the recent years.[125]–[128]

Another challenge, which is specific to the use of photoswitchable drugs, is the limited structural space which is covered with the currently employed photoswitches. At this point, azobenzene seems to be the photoswitch of choice, but in other applications of photopharmacology[109],[110],[112] also diarylethene[129],[130] and spiropyran[131] switches have been employed successfully and could provide additional benefits for chemotherapy in the future. While the reversibility of activation has been established, this field is still relying on an implementation of efficient strategies to achieve high phototherapeutic indices. This problem is connected to the relatively small photoinduced change in molecular properties, as compared to the one observed in photocaged drugs and photoactivated metal complexes. Nevertheless, we believe that the photoswitchable chemotherapeutics have great potential for clinical applications, taking full advantage of the reversible activation.

The three approaches described here may serve their purpose in different therapeutic scenarios, and with the knowledge of their strengths and limitations one will be able to choose the correct approach for a given problem. Considering this, we predict a shining future for the photoresponsive chemotherapeutic agents.

6. List of abbreviations

5CNU - 5-cyanouracil

5-FU - 5-fluorouracil

5’GMP - 5’-guanosine monophosphate

ALK - anaplastic lymphoma kinase

Arg - arginine

Asp - aspartic acid

Boc - *tert*-butyloxycarbonyl

bpm – bipyrimidine

bpy - bipyridine

CA4 - combretastatin A4

CMP - core modified porphyrin

dG - deoxy guanosine

DMSO - dimethyl sulfoxide

Dox - doxorubicin

dsDNA - double-stranded DNA

EB3 - end binding protein 3

EDANS - 5-((2-Aminoethyl)amino)naphthalene-1-sulfonic acid

EGFR - Epidermal growth factor receptor

EPR - enhanced permeability and retention

ERK - extracellular rignal-regulated kinase

FA - folic acid

FAAS - flameless atomic absorption spectroscopy

FITC - fluorescein isothiocyanate

FRET - fluorescence resonance energy transfer

G5-PAMAM - 5th generation polyamidoamine

Gly - glycine

GRPR - gastrin-releasing peptide receptor

GSH - glutathione

HDAC - histone deacetylase

His - histidine

IC_{50} - half maximal inhibitory concentration

IC_{90} - concentration at 90% of maximal inhibition

ICP MS - inductively coupled plasma mass spectrometry

IL - intraligand

IR - infrared

λ_{exc} - absorption wavelength

λ_{em} - emission wavelength

LC - liquid chromatography

LED - light emitting diode

LMCT - ligand-to-metal charge transfer

L-Trp - L-tryptophan

Met - methionine

MLCT - metal-to-ligand charge transfer

MO - molecular orbital

MS - mass spectrometry

MTT - 3-(4,5-dimethylthiazol-2-yl)-2,5-ditetrazolium bromide

MTX - methotrexate

NBP - 4-(*p*-nitrobenzyl)pyridine

NIR - near infrared

NLS - nucleus localization signaling

NOE - nuclear overhauser effect

ONP - *ortho*-nitrophenyl

PBS - phosphate buffer saline

PC - phthalocyanine

PDGF-R - platelet-derived growth factor receptor

PDT - photodynamic therapy

PEG - polyethyleneglycol

PEG-PLA - poly(ethyleneglycol)-poly(D,L-lactide)

Phen - phenantroline

PI - phototherapeutic index

PKI - protein kinase inhibitors

PPG - photocleavable protecting group

PS - photosensitizer

py - pyridine

RES - reticuloendothelial system

RGD - tripeptide Arg-Gly-Asp

Rh - rhodamine

ROS - reactive oxygen species

SAHA - suberoyl-anilide-hydroxamic acid

SBHA - suberic bishydroxamic acid

SPA - scintillation proximity assay

TDDFT - time-dependent density functional theory

UCNP - up-converting nanoparticles

UV - ultra-violet

VEGFR - Vascular endothelial growth factor receptor

7. Conflict of interest

The authors declare no conflict of interests.

8. Acknowledgments

The financial support from the Dutch Organization for Scientific Research (NWO VIDI grant no. 723.014.001 for W.S.) is gratefully acknowledged.

9. References

[1] Global and regional mortality from 235 causes of death for 20 age groups in 1990 and 2010: a systematic analysis for the Global Burden of Disease Study 2010. *Lancet* **2012**, *380*(9859), 2095–2128

[2] Edwards, R.; Aronson, J. K. Adverse Drug Reactions: Definitions, Diagnosis, and Management. *Lancet* **2000**, *356*(9237), 1255–1259.

[3] Ihbe-Heffinger, A.; Paessens, B.; Berger, K.; Shlaen, M.; Bernard, R.; von Schilling, C.; Peschel, C. The Impact of Chemotherapy-Induced Side Effects on Medical Care Usage and Cost in German Hospital Care - an Observational Analysis on Non-Small-Cell Lung Cancer Patients. *Support Care Cancer* **2013**, *21*(6), 1665–1675.

[4] Siegel, R.; DeSantis, C.; Virgo, K.; Stein, K.; Mariotto, A.; Smith, T.; Cooper, D.; Gansler, T.; Lerro, C.; Fedewa, S.; Lin, C.; Leach, C.; Spillers Cannady, R.; Cho, H.; Scoppa, S.; Hachey, M.; Kirch, R.; Jemal, A.; Ward, E. Cancer Treatment and Survivorship Statistics, 2012. *CA. Cancer J. Clin.* **2012**, *62*(4), 220–241.

[5] Hanahan, D.; Weinberg, R. A. Hallmarks of Cancer: The next Generation. *Cell* **2011**, *144* (5), 646–674.

[6] Cerqueira, B. B. S.; Lasham, A.; Shelling, A. N.; Al-Kassas, R. Nanoparticle Therapeutics: Technologies and Methods for Overcoming Cancer. *Eur. J. Pharm. Biopharm.* **2015**, *97(A)*, 140–151.

[7] van der Meel, R.; Vehmeijer, L. J. C.; Kok, R. J.; Storm, G.; van Gaal, E. V. B. Ligand-Targeted Particulate Nanomedicines Undergoing Clinical Evaluation: Current Status. *Adv. Drug Deliv. Rev.* **2013**, *65*(10), 1284–1298.

[8] Theodoulou, M.; Hudis, C. Cardiac Profiles of Liposomal Anthracyclines: Greater Cardiac Safety versus Conventional Doxorubicin? *Cancer* **2004**, *100*(10), 2052–2063.

[9] Gabizon, A. A.; Shmeeda, H.; Zalipsky, S. Pros and Cons of the Liposome Platform in Cancer Drug Targeting. *J. Liposome Res.* **2006**, *16*(3), 175–183.

[10] Robertson, C. A.; Hawkins Evans, D.; Abrahamse, H. Photodynamic Therapy (PDT): A Short Review on Cellular Mechanisms and Cancer Research Applications for PDT. *J. Photochem. Photobiol. B: Biol.* **2009**, *96*(1), 1–8.

[11] Castano, A. P.; Demidova, T. N.; Hamblin, M. R. Mechanisms in Photodynamic

Therapy: Part Three - Photosensitizer Pharmacokinetics, Biodistribution, Tumor Localization and Modes of Tumor Destruction. *Photodiagnosis Photodyn. Ther.* **2005**, *2*(2), 91–106.

[12] Noman, M. Z.; Messai, Y.; Carre, T.; Akalay, I.; Meron, M.; Janji, B.; Hasmim, M.; Chouaib, S. Microenvironmental Hypoxia Orchestrating the Cell Stroma Cross Talk, Tumor Progression and Antitumor Response. *Crit. Rev. Immunol.* **2011**, *31*(5), 357–377.

[13] Olejniczak, J.; Carling, C.-J.; Almutairi, A. Photocontrolled Release Using One-Photon Absorption of Visible or NIR Light. *J. Control. Release* **2015**, *219*, 18–30.

[14] Farrer, N. J.; Salassa, L.; Sadler, P. J. Photoactivated Chemotherapy (PACT): The Potential of Excited-State d-Block Metals in Medicine. *Dalton Trans.* **2009**, 48, 10690–10701.

[15] Schatzschneider, U. Photoactivated Biological Activity of Transition-Metal Complexes. *Eur. J. Inorg. Chem.* **2010**, *2010*(10), 1451–1467.

[16] Lucky, S. S.; Soo, K. C.; Zhang, Y. Nanoparticles in Photodynamic Therapy. *Chem. Rev.* **2015**, *115*(4), 1990–2042.

[17] Allison, R. R.; Moghissi, K. Oncologic Photodynamic Therapy: Clinical Strategies That Modulate Mechanisms of Action. *Photodiagnosis Photodyn. Ther.* **2013**, *10*(4), 331–341.

[18] Mahnken, R. E.; Billadeau, M. A.; Nikonowicz, E. P.; Morrison, H. Development of Photo *cis*-Platinum Reagents. Reaction of *cis*-dichlorobis(1,10-phenanthroline)rhodium(III) with Calf Thymus DNA, Nucleotides and Nucleosides. *J. Am. Chem. Soc.* **1992**, *114*(24), 9253–9265.

[19] Bednarski, P. J.; Grünert, R.; Zielzki, M.; Wellner, A.; Mackay, F. S.; Sadler, P. J. Light-Activated Destruction of Cancer Cell Nuclei by Platinum Diazide Complexes. *Chem. Biol.* **2006**, *13*(1), 61–67.

[20] Westendorf, A. F.; Woods, J. A.; Korpis, K.; Farrer, N. J.; Salassa, L.; Robinson, K.; Appleyard, V.; Murray, K.; Grünert, R.; Thompson, A. M.; Sadler, P. J.; Bednarski, P. J. *trans,trans,trans*-[$Pt^{IV}(N_3)_2(OH)_2(py)(NH_3)$]: A Light-Activated Antitumor Platinum Complex That Kills Human Cancer Cells by an Apoptosis-Independent Mechanism. *Mol. Cancer Ther.* **2012**, *11*(9), 1894–1904.

[21] Ronconi, L.; Sadler, P. J. Photoreaction Pathways for the Anticancer Complex *Trans,trans,trans*-[$Pt(N_3)_2(OH)_2(NH_3)_2$]. *Dalt. Trans.* **2011**, *40*(1), 262–268.

[22] Farrer, N. J.; Sadler, P. J. Photochemotherapy: Targeted Activation of Metal Anticancer Complexes. *Aust. J. Chem.* **2008**, *61*(9), 669-674

[23] Bednarski, P. J.; Mackay, F. S.; Sadler, P. J. Photoactivatable Platinum Complexes. *Anti-cancer Agents Med. Chem.* **2007**, *7*(1), 75–93.

[24] Kratochwil, N. A.; Parkinson, J. A.; Bednarski, P. J.; Sadler, P. J. Nucleotide Platination Induced by Visible Light. *Angew. Chemie Int. Ed. Engl.* **1999**, *38*(10), 1460–1463.

[25] Kratochwil, N. A.; Zabel, M.; Range, K. J.; Bednarski, P. J. Synthesis and X-Ray Crystal Structure of *trans,cis*-[$Pt(OAc)_2I_2(en)$]: A Novel Type of Cisplatin Analog That Can Be

Photolyzed by Visible Light to DNA-Binding and Cytotoxic Species in Vitro. *J. Med. Chem.* **1996**, *39*(13), 2499–2507.

[26] Müller, P.; Schröder, B.; Parkinson, J. A.; Kratochwil, N. A.; Coxall, R. A.; Parkin, A.; Parsons, S.; Sadler, P. J. Nucleotide Cross-Linking Induced by Photoreactions of Platinum(IV)-Azide Complexes. *Angew. Chem. Int. Ed. Engl.* **2003**, *42*(3), 335–339.

[27] Farrer, N. J.; Woods, J. A.; Munk, V. P.; Mackay, F. S.; Sadler, P. J. Photocytotoxic *trans* -Diam(m)ine Platinum(IV) Diazido Complexes More Potent than Their *cis* Isomers. *Chem. Res. Toxicol.* **2010**, *23*(2), 413–421.

[28] Mackay, F. S.; Woods, J. A.; Moseley, H.; Ferguson, J.; Dawson, A.; Parsons, S.; Sadler, P. J. A Photoactivated *trans*-Diammine Platinum Complex as Cytotoxic as Cisplatin. *Chemistry* **2006**, *12*(11), 3155–3161.

[29] Farrer, N. J.; Woods, J. A.; Salassa, L.; Zhao, Y.; Robinson, K. S.; Clarkson, G.; Mackay, F. S.; Sadler, P. J. A Potent *Trans*-Diimine Platinum Anticancer Complex Photoactivated by Visible Light. *Angew. Chem. Int. Ed. Engl.* **2010**, *49*(47), 8905–8908.

[30] Mackay, F. S.; Woods, J. A.; Heringová, P.; Kašpárková, J.; Pizarro, A. M.; Moggach, S. A.; Parsons, S.; Brabec, V.; Sadler, P. J. A Potent Cytotoxic Photoactivated Platinum Complex. *Proc. Natl. Acad. Sci. U. S. A.* **2007**, *104*(52), 20743–20748.

[31] Min, Y.; Li, J.; Liu, F.; Yeow, E. K. L.; Xing, B. Near-Infrared Light-Mediated Photoactivation of a Platinum Antitumor Prodrug and Simultaneous Cellular Apoptosis Imaging by Upconversion-Luminescent Nanoparticles. *Angew. Chem. Int. Ed. Engl.* **2014**, *53*(4), 1012–1016.

[32] Chen, G.; Qiu, H.; Prasad, P. N.; Chen, X. Upconversion Nanoparticles: Design, Nanochemistry, and Applications in Theranostics. *Chem. Rev.* **2014**, *114*(10), 5161–5214.

[33] Crespy, D.; Landfester, K.; Schubert, U. S.; Schiller, A. Potential Photoactivated Metallopharmaceuticals: From Active Molecules to Supported Drugs. *Chem. Commun.* **2010**, *46*(36), 6651-6662.

[34] Farrer, N. J.; Sadler, P. J. Photochemotherapy: Targeted Activation of Metal Anticancer Complexes. *Aust. J. Chem.* **2008**, *61*(9), 669-674.

[35] Smith, N. A.; Sadler, P. J. Photoactivatable Metal Complexes: From Theory to Applications in Biotechnology and Medicine. *Philos. Trans. A. Math. Phys. Eng. Sci.* **2013**, *371*(1995), 20120519.

[36] Howerton, B. S.; Heidary, D. K.; Glazer, E. C. Strained Ruthenium Complexes Are Potent Light-Activated Anticancer Agents. *J. Am. Chem. Soc.* **2012**, *134*(20), 8324–8327.

[37] Singh, T. N.; Turro, C. Photoinitiated DNA Binding by *cis*-$[Ru(bpy)_2(NH_3)_2]^{2+}$. *Inorg. Chem.* **2004**, *43*(23), 7260–7262.

[38] Zhou, Q.-X.; Lei, W.-H.; Hou, Y.-J.; Chen, Y.-J.; Li, C.; Zhang, B.-W.; Wang, X.-S. BODIPY-Modified Ru(II) Arene Complex - a New Ligand Dissociation Mechanism and a Novel Strategy to Red Shift the Photoactivation Wavelength of Anticancer Metallodrugs. *Dalton Trans.* **2013**, *42*(8), 2786–2791.

[39] Wachter, E.; Heidary, D. K.; Howerton, B. S.; Parkin, S.; Glazer, E. C. Light-Activated Ruthenium Complexes Photobind DNA and Are Cytotoxic in the Photodynamic Therapy Window. *Chem. Commun.* **2012**, *48*(77), 9649–9651.

[40] Aird, R. E.; Cummings, J.; Ritchie, A. A.; Muir, M.; Morris, R. E.; Chen, H.; Sadler, P. J.; Jodrell, D. I. *In Vitro* and *in Vivo* Activity and Cross Resistance Profiles of Novel Ruthenium (II) Organometallic Arene Complexes in Human Ovarian Cancer. *Br. J. Cancer* **2002**, *86*(10), 1652–1657.

[41] Chen, H.; Parkinson, J. A.; Parsons, S.; Coxall, R. A.; Gould, R. O.; Sadler, P. J. Organometallic Ruthenium(II) Diamine Anticancer Complexes: Arene-Nucleobase Stacking and Stereospecific Hydrogen-Bonding in Guanine Adducts. *J. Am. Chem. Soc.* **2002**, *124*(12), 3064–3082.

[42] Betanzos-Lara, S.; Salassa, L.; Habtemariam, A.; Sadler, P. J. Photocontrolled Nucleobase Binding to an Organometallic Ru^{II} Arene Complex. *Chem. Commun.* **2009**, 6622–6624.

[43] Lutterman, D. A.; Fu, P. K.-L.; Turro, C. *cis*-$[Rh_2(\mu\text{-}O_2CCH_3)_2(CH_3CN)_6]^{2+}$ as a Photoactivated Cisplatin Analog. *J. Am. Chem. Soc.* **2006**, *128*(3), 738–739.

[44] Loganathan, D.; Morrison, H. Effect of Ring Methylation on the Photophysical, Photochemical and Photobiological Properties of *cis*-Dichlorobis(1,10-Phenanthroline)Rhodium(III)Chloride. *Photochem. Photobiol. 82*(1), 237–247.

[45] Siddik, Z. H. Cisplatin: Mode of Cytotoxic Action and Molecular Basis of Resistance. *Oncogene* **2003**, *22*(47), 7265–7279.

[46] Takahara, P. M.; Frederick, C. A.; Lippard, S. J. Crystal Structure of the Anticancer Drug Cisplatin Bound to Duplex DNA. *J. Am. Chem. Soc.* **1996**, *118*(49), 12309–12321.

[47] Magennis, S. W.; Habtemariam, A.; Novakova, O.; Henry, J. B.; Meier, S.; Parsons, S.; Oswald, I. D. H.; Brabec, V.; Sadler, P. J. Dual Triggering of DNA Binding and Fluorescence via Photoactivation of a Dinuclear ruthenium(II) Arene Complex. *Inorg. Chem.* **2007**, *46*(12), 5059–5068.

[48] Brabec, V.; Leng, M. DNA Interstrand Cross-Links of *trans*-diamminedichloroplatinum(II) Are Preferentially Formed between Guanine and Complementary Cytosine Residues. *Proc. Natl. Acad. Sci.* **1993**, *90*(11), 5345–5349.

[49] Barragán, F.; López-Senín, P.; Salassa, L.; Betanzos-Lara, S.; Habtemariam, A.; Moreno, V.; Sadler, P. J.; Marchán, V. Photocontrolled DNA Binding of a Receptor-Targeted Organometallic Ruthenium(II) Complex. *J. Am. Chem. Soc.* **2011**, *133*(35), 14098–14108.

[50] Zhao, Y.; Woods, J. A.; Farrer, N. J.; Robinson, K. S.; Pracharova, J.; Kasparkova, J.; Novakova, O.; Li, H.; Salassa, L.; Pizarro, A. M.; Clarkson, G. J.; Song, L.; Brabec, V.; Sadler, P. J. Diazido Mixed-Amine Platinum(IV) Anticancer Complexes Activatable by Visible-Light Form Novel DNA Adducts. *Chem. Eur. J.* **2013**, *19*(29), 9578–9591.

[51] Kasparkova, J.; Kostrhunova, H.; Novakova, O.; Křikavová, R.; Vančo, J.; Trávníček, Z.; Brabec, V. A Photoactivatable Platinum(IV) Complex Targeting Genomic DNA and Histone Deacetylases. *Angew. Chem. Int. Ed. Engl.* **2015**, *54*(48), 14478-14482.

[52] Garner, R. N.; Gallucci, J. C.; Dunbar, K. R.; Turro, C. $[Ru(bpy)_2(5\text{-cyanouracil})_2]^{2+}$ as a Potential Light-Activated Dual-Action Therapeutic Agent. *Inorg. Chem.* **2011**, *50*(19), 9213–9215.

[53] Ronconi, L.; Sadler, P. J. Unprecedented Carbon–Carbon Bond Formation Induced by Photoactivation of a Platinum(IV)-Diazido Complex. *Chem. Commun.* **2008**, 235–237.

[54] Phillips, H. I. A.; Ronconi, L.; Sadler, P. J. Photoinduced Reactions of *cis,trans,cis*-$[Pt^{IV}(N_3)_2(OH)_2(NH_3)_2)$ with 1-Methylimidazole. *Chem. Eur. J.* **2009**, *15*(7), 1588–1596.

[55] Zhao, Y.; Farrer, N. J.; Li, H.; Butler, J. S.; McQuitty, R. J.; Habtemariam, A.; Wang, F.; Sadler, P. J. De Novo Generation of Singlet Oxygen and Ammine Ligands by Photoactivation of a Platinum Anticancer Complex. *Angew. Chem. Int. Ed. Engl.* **2013**, *52*(51), 13633–13637.

[56] Butler, J. S.; Woods, J. A.; Farrer, N. J.; Newton, M. E.; Sadler, P. J. Tryptophan Switch for a Photoactivated Platinum Anticancer Complex. *J. Am. Chem. Soc.* **2012**, *134*(40), 16508–16511.

[57] Dasari, S.; Tchounwou, P. B. Cisplatin in Cancer Therapy: Molecular Mechanisms of Action. *Eur. J. Pharmacol.* **2014**, *740*, 364-378.

[58] Pizarro, A. M.; McQuitty, R. J.; Mackay, F. S.; Zhao, Y.; Woods, J. A.; Sadler, P. J. Cellular Accumulation, Lipophilicity and Photocytotoxicity of Diazido Platinum(IV) Anticancer Complexes. *ChemMedChem* **2014**, *9*(6), 1169–1175.

[59] Westendorf, A. F.; Zerzankova, L.; Salassa, L.; Sadler, P. J.; Brabec, V.; Bednarski, P. J. Influence of Pyridine versus Piperidine Ligands on the Chemical, DNA Binding and Cytotoxic Properties of Light Activated *trans,trans,trans*-$[Pt(N_3)_2(OH)_2(NH_3)(L)]$. *J. Inorg. Biochem.* **2011**, *105*(5), 652–662.

[60] Hidayatullah, A. N.; Wachter, E.; Heidary, D. K.; Parkin, S.; Glazer, E. C. Photoactive Ru(II) Complexes with Dioxinophenanthroline Ligands Are Potent Cytotoxic Agents. *Inorg. Chem.* **2014**, *53*(19), 10030–10032.

[61] Dickerson, M.; Sun, Y.; Howerton, B.; Glazer, E. C. Modifying Charge and Hydrophilicity of Simple Ru(II) Polypyridyl Complexes Radically Alters Biological Activities: Old Complexes, Surprising New Tricks. *Inorg. Chem.* **2014**, *53*(19), 10370–10377.

[62] Heidary, D. K.; Howerton, B. S.; Glazer, E. C. Coordination of Hydroxyquinolines to a Ruthenium Bis-Dimethyl-Phenanthroline Scaffold Radically Improves Potency for Potential as Antineoplastic Agents. *J. Med. Chem.* **2014**, *57*(21), 8936–8946.

[63] Reinhard, R.; Schmidt, B. F. Nitrobenzyl-Based Photosensitive Phosphoramide Mustards: Synthesis and Photochemical Properties of Potential Prodrugs for Cancer Therapy. *J. Org. Chem.* **1998**, *63*(8), 2434–2441.

[64] Wei, Y.; Yan, Y.; Pei, D.; Gong, B. A Photoactivated Prodrug. *Bioorg. Med. Chem. Lett.* **1998**, *8*(18), 2419–2422.

[65] Ciesienski, K. L.; Hyman, L. M.; Yang, D. T.; Haas, K. L.; Dickens, M. G.; Holbrook, R. J.; Franz, K. J. A Photo-Caged Platinum(II) Complex That Increases Cytotoxicity upon Light Activation. *Eur. J. Inorg. Chem.* **2010**, *2010*(15), 2224–2228.

[66] Crider, S. E.; Holbrook, R. J.; Franz, K. J. Coordination of Platinum Therapeutic Agents

to Met-Rich Motifs of Human Copper Transport protein1. *Metallomics* **2010**, *2*(1), 74–83.

[67] Ciesienski, K. L.; Haas, K. L.; Dickens, M. G.; Tesema, Y. T.; Franz, K. J. A Photolabile Ligand for Light-Activated Release of Caged Copper. *J. Am. Chem. Soc.* **2008**, *13*(37), 12246–12247.

[68] Ciesienski, K. L.; Haas, K. L.; Franz, K. J. Development of next-Generation Photolabile Copper Cages with Improved Copper Binding Properties. *Dalton Trans.* **2010**, *39*(40), 9538–9546.

[69] Kumbhar, A. A.; Franks, A. T.; Butcher, R. J.; Franz, K. J. Light Uncages a Copper Complex to Induce Nonapoptotic Cell Death. *Chem. Commun. (Camb).* **2013**, 2460–2462.

[70] Filomeni, G.; Cerchiaro, G.; Da Costa Ferreira, A. M.; De Martino, A.; Pedersen, J. Z.; Rotilio, G.; Ciriolo, M. R. Pro-Apoptotic Activity of Novel Isatin-Schiff Base Copper(II) Complexes Depends on Oxidative Stress Induction and Organelle-Selective Damage. *J. Biol. Chem.* **2007**, *282*(16), 12010–12021.

[71] Margalioth, E. J.; Schenker, J. G.; Chevion, M. Copper and Zinc Levels in Normal and Malignant Tissues. *Cancer* **1983**, *52*(5), 868–872.

[72] Leonidova, A.; Pierroz, V.; Rubbiani, R.; Lan, Y.; Schmitz, A. G.; Kaech, A.; Sigel, R. K. O.; Ferrari, S.; Gasser, G. Photo-Induced Uncaging of a Specific Re(I) Organometallic Complex in Living Cells. *Chem. Sci.* **2014**, *5*(10), 4044-4056.

[73] Amoroso, A. J.; Coogan, M. P.; Dunne, J. E.; Fernández-Moreira, V.; Hess, J. B.; Hayes, A. J.; Lloyd, D.; Millet, C.; Pope, S. J. A.; Williams, C. Rhenium Fac Tricarbonyl Bisimine Complexes: Biologically Useful Fluorochromes for Cell Imaging Applications. *Chem. Commun. (Camb).* **2007**, 3066–3068.

[74] Joshi, T.; Pierroz, V.; Mari, C.; Gemperle, L.; Ferrari, S.; Gasser, G. A bis(dipyridophenazine)(2-(2-Pyridyl)pyrimidine-4-Carboxylic acid)ruthenium(II) Complex with Anticancer Action upon Photodeprotection. *Angew. Chem. Int. Ed. Engl.* **2014**, *53*(11), 2960–2963.

[75] Mitra, K.; Gautam, S.; Kondaiah, P.; Chakravarty, A. R. The *cis*-Diammineplatinum(II) Complex of Curcumin: A Dual Action DNA Crosslinking and Photochemotherapeutic Agent. *Angew. Chem. Int. Ed. Engl.* **2015**, *54*(47), 13989–13993.

[76] Esatbeyoglu, T.; Huebbe, P.; Ernst, I. M. A.; Chin, D.; Wagner, A. E.; Rimbach, G. Curcumin-From Molecule to Biological Function. *Angew. Chem. Int. Ed. Engl.* **2012**, *51*(22), 5308–5332.

[77] Prasad, S.; Tyagi, A. K.; Aggarwal, B. B. Recent Developments in Delivery, Bioavailability, Absorption and Metabolism of Curcumin: The Golden Pigment from Golden Spice. *Cancer Res. Treat.* **2014**, *46*(1), 2–18.

[78] Dahl, T. A.; Bilski, P.; Reszka, K. J.; Chignell, C. F. Photocytotoxicity of Curcumin. *Photochem. Photobiol.* **1994**, *59*(3), 290–294.

[79] Bio, M.; Rajaputra, P.; Nkepang, G.; You, Y. Far-Red Light Activatable, Multifunctional Prodrug for Fluorescence Optical Imaging and Combinational Treatment. *J. Med.*

Chem. **2014**, *57*(8), 3401–3409.

[80] Bio, M.; Rajaputra, P.; Nkepang, G.; Awuah, S. G.; Hossion, A. M. L.; You, Y. Site-Specific and Far-Red-Light-Activatable Prodrug of Combretastatin A-4 Using Photo-Unclick Chemistry. *J. Med. Chem.* **2013**, *56*(10), 3936–3942.

[81] Noguchi, M.; Skwarczynski, M.; Prakash, H.; Hirota, S.; Kimura, T.; Hayashi, Y.; Kiso, Y. Development of Novel Water-Soluble Photocleavable Protective Group and Its Application for Design of Photoresponsive Paclitaxel Prodrugs. *Bioorg. Med. Chem.* **2008**, *16*(10), 5389–5397.

[82] Yu, H.; Li, J.; Wu, D.; Qiu, Z.; Zhang, Y. Chemistry and Biological Applications of Photo-Labile Organic Molecules. *Chem. Soc. Rev.* **2010**, *39*(2), 464–473.

[83] Šolomek, T.; Wirz, J.; Klán, P. Searching for Improved Photoreleasing Abilities of Organic Molecules. *Acc. Chem. Res.* **2015**, 48(12), 3064–3072.

[84] Dcona, M. M.; Yu, Q.; Capobianco, J. A.; Hartman, M. C. T. Near Infrared Light Mediated Release of Doxorubicin Using Upconversion Nanoparticles. *Chem. Commun. (Camb).* **2015**, *51*(40), 8477–8479.

[85] Tietze, L. F.; Müller, M.; Duefert, S.-C.; Schmuck, K.; Schuberth, I. Photoactivatable Prodrugs of Highly Potent Duocarmycin Analogues for a Selective Cancer Therapy. *Chem. Eur. J.* **2013**, *19*(5), 1726–1731.

[86] Lin, W.; Peng, D.; Wang, B.; Long, L.; Guo, C.; Yuan, J. A Model for Light-Triggered Porphyrin Anticancer Prodrugs Based on Ano-Nitrobenzyl Photolabile Group. *Eur. J. Org. Chem.* **2008**, *2008*(5), 793–796.

[87] Tanaka, F. UFT (tegafur and Uracil) as Postoperative Adjuvant Chemotherapy for Solid Tumors (carcinoma of the Lung, Stomach, Colon/rectum, and Breast): Clinical Evidence, Mechanism of Action, and Future Direction. *Surg. Today* **2007**, *37*(11), 923–943.

[88] Kessel, D.; Chou, T.-H. Tumor-Localizing Components of the Porphyrin Preparation Hematoporphyrin Derivative. *Cancer Res.* **1983**, *43*(5), 1994–1999.

[89] Zhang, Z.; Hatta, H.; Ito, T.; Nishimoto, S. Synthesis and Photochemical Properties of Photoactivated Antitumor Prodrugs Releasing 5-Fluorouracil. *Org. Biomol. Chem.* **2005**, *3* (4), 592–596.

[90] Ellerby, H. M.; Arap, W.; Ellerby, L. M.; Kain, R.; Andrusiak, R.; Rio, G. D.; Krajewski, S.; Lombardo, C. R.; Rao, R.; Ruoslahti, E.; Bredesen, D. E.; Pasqualini, R. Anti-Cancer Activity of Targeted pro-Apoptotic Peptides. *Nat. Med.* **1999**, *5*(9), 1032–1038.

[91] Swierkot, J.; Szechiński, J. Methotrexate in Rheumatoid Arthritis. *Pharmacol. Rep.* *58*(4), 473–492.

[92] Choi, S. K.; Thomas, T. P.; Li, M.-H.; Desai, A.; Kotlyar, A.; Baker, J. R. Photochemical Release of Methotrexate from Folate Receptor-Targeting PAMAM Dendrimer Nanoconjugate. *Photochem. Photobiol. Sci.* **2012**, *11*(4), 653–660.

[93] Choi, S. K.; Thomas, T.; Li, M.-H.; Kotlyar, A.; Desai, A.; Baker, J. R. Light-Controlled Release of Caged Doxorubicin from Folate Receptor-Targeting PAMAM Dendrimer Nanoconjugate. *Chem. Commun. (Camb).* **2010**, *46*(15), 2632–2634.

[94] Gewirtz, D. A. A Critical Evaluation of the Mechanisms of Action Proposed for the Antitumor Effects of the Anthracycline Antibiotics Adriamycin and Daunorubicin. *Biochem. Pharmacol.* **1999**, *57*(7), 727–741.

[95] Thorn, C. F.; Oshiro, C.; Marsh, S.; Hernandez-Boussard, T.; McLeod, H.; Klein, T. E.; Altman, R. B. Doxorubicin Pathways: Pharmacodynamics and Adverse Effects. *Pharmacogenet. Genomics* **2011**, *21*(7), 440–446.

[96] Vejpongsa, P.; Yeh, E. T. H. Prevention of Anthracycline-Induced Cardiotoxicity: Challenges and Opportunities. *J. Am. Coll. Cardiol.* **2014**, *64*(9), 938–945.

[97] Ibsen, S.; Zahavy, E.; Wrasdilo, W.; Berns, M.; Chan, M.; Esener, S. A Novel Doxorubicin Prodrug with Controllable Photolysis Activation for Cancer Chemotherapy. *Pharm. Res.* **2010**, *27*(9), 1848–1860.

[98] Lewis, A. D.; Lau, D. H. M.; Duran, G. E.; Wolf, C. R.; Sikic, B. I. Role of Cytochrome P-450 from the Human CYP3A Gene Family in the Potentiation of Morpholino Doxorubicin by Human Liver Microsomes. *Cancer Res.* **1992**, *52*(16), 4379–4384.

[99] Ibsen, S.; Zahavy, E.; Wrasidlo, W.; Hayashi, T.; Norton, J.; Su, Y.; Adams, S.; Esener, S. Localized in Vivo Activation of a Photoactivatable Doxorubicin Prodrug in Deep Tumor Tissue. *Photochem. Photobiol.* **2013**, *89*(3), 698–708.

[100] Dcona, M. M.; Mitra, D.; Goehe, R. W.; Gewirtz, D. A.; Lebman, D. A.; Hartman, M. C. T. Photocaged Permeability: A New Strategy for Controlled Drug Release. *Chem. Commun. (Camb).* **2012**, 4755–4757.

[101] Shawver, L. K.; Slamon, D.; Ullrich, A. Smart Drugs: Tyrosine Kinase Inhibitors in Cancer Therapy. *Cancer Cell* **2002**, *1*(2), 117–123.

[102] Zindler, M.; Pinchuk, B.; Renn, C.; Horbert, R.; Döbber, A.; Peifer, C. Design, Synthesis, and Characterization of a Photoactivatable Caged Prodrug of Imatinib. *ChemMedChem* **2015**, *10*(8), 1335–1338.

[103] Baker, S. J.; Reddy, E. P. Targeted Inhibition of Kinases in Cancer Therapy. *Mt. Sinai J. Med. 77*(6), 573–586.

[104] Bollag, G.; Tsai, J.; Zhang, J.; Zhang, C.; Ibrahim, P.; Nolop, K.; Hirth, P. Vemurafenib: the First Drug Approved for BRAF-Mutant Cancer. *Nat. Rev. Drug Discov.* **2012**, *11*(11), 873–886.

[105] Horbert, R.; Pinchuk, B.; Davies, P.; Alessi, D.; Peifer, C. Photoactivatable Prodrugs of Antimelanoma Agent Vemurafenib. *ACS Chem. Biol.* **2015**, *10*(9), 2099–2107.

[106] Skwarczynski, M.; Noguchi, M.; Hirota, S.; Sohma, Y.; Kimura, T.; Hayashi, Y.; Kiso, Y. Development of First Photoresponsive Prodrug of Paclitaxel. *Bioorg. Med. Chem. Lett.* **2006**, *16*(17), 4492–4496.

[107] Greish, K. Enhanced Permeability and Retention (EPR) Effect for Anticancer Nanomedicine Drug Targeting. *Methods Mol. Biol.* **2010**, *624*, 25–37.

[108] Hansen, M. J.; Velema, W. A.; Lerch, M. M.; Szymanski, W.; Feringa, B. L. Wavelength-Selective Cleavage of Photoprotecting Groups: Strategies and Applications in Dynamic Systems. *Chem. Soc. Rev.* **2015**, *44*(11), 3358–3377.

[109] Velema, W. A.; Szymanski, W.; Feringa, B. L. Photopharmacology: Beyond Proof of Principle. *J. Am. Chem. Soc.* **2014**, *136*(6), 2178–2191.

[110] Broichhagen, J.; Frank, J. A.; Trauner, D. A Roadmap to Success in Photopharmacology. *Acc. Chem. Res.* **2015**, *48*(7), 1947–1960.

[111] Pettit, G. R.; Rhodes, M. R.; Herald, D. L.; Hamel, E.; Schmidt, J. M.; Pettit, R. K. Antineoplastic Agents. 445. Synthesis and Evaluation of Structural Modifications of (*Z*)- and (*E*)-Combretastatin A-4. *J. Med. Chem.* **2005**, *48*(12), 4087–4099.

[112] Szymański, W.; Beierle, J. M.; Kistemaker, H. A. V; Velema, W. A.; Feringa, B. L. Reversible Photocontrol of Biological Systems by the Incorporation of Molecular Photoswitches. *Chem. Rev.* **2013**, *113*(8), 6114–6178.

[113] Borowiak, M.; Nahaboo, W.; Reynders, M.; Nekolla, K.; Jalinot, P.; Hasserodt, J.; Rehberg, M.; Delattre, M.; Zahler, S.; Vollmar, A.; Trauner, D.; Thorn-Seshold, O. Photoswitchable Inhibitors of Microtubule Dynamics Optically Control Mitosis and Cell Death. *Cell* **2015**, *162*(2), 403–411.

[114] Engdahl, A. J.; Torres, E. A.; Lock, S. E.; Engdahl, T. B.; Mertz, P. S.; Streu, C. N. Synthesis, Characterization, and Bioactivity of the Photoisomerizable Tubulin Polymerization Inhibitor Azo-Combretastatin A4. *Org. Lett.* **2015**, *17*(18), 4546–4549.

[115] Sheldon, J. E.; Dcona, M. M.; Lyons, C. E.; Hackett, J. C.; Hartman, M. C. T. Photoswitchable Anticancer Activity *via trans-cis* Isomerization of a Combretastatin A-4 Analog. *Org. Biomol. Chem.* **2016**, *14*, 40–49.

[116] Boulègue, C.; Löweneck, M.; Renner, C.; Moroder, L. Redox Potential of Azobenzene as an Amino Acid Residue in Peptides. *ChemBioChem* **2007**, *8*(6), 591–594.

[117] Szymanski, W.; Ourailidou, M. E.; Velema, W. A.; Dekker, F. J.; Feringa, B. L. Light-Controlled Histone Deacetylase (HDAC) Inhibitors: Towards Photopharmacological Chemotherapy. *Chem. Eur. J.* **2015**, *21*(46), 16517–16524.

[118] Mottamal, M.; Zheng, S.; Huang, T. L.; Wang, G. Histone Deacetylase Inhibitors in Clinical Studies as Templates for New Anticancer Agents. *Molecules* **2015**, *20*(3), 3898–3941.

[119] Somech, R.; Izraeli, S.; J Simon, A. Histone Deacetylase Inhibitors-a New Tool to Treat Cancer. *Cancer Treat. Rev.* **2004**, *30*(5), 461–472.

[120] Hansen, M. J.; Velema, W. A.; de Bruin, G.; Overkleeft, H. S.; Szymanski, W.; Feringa, B. L. Proteasome Inhibitors with Photocontrolled Activity. *ChemBioChem* **2014**, *15*(14), 2053–2057.

[121] Goldberg, A. L. Functions of the Proteasome: From Protein Degradation and Immune Surveillance to Cancer Therapy. *Biochem. Soc. Trans.* **2007**, *35*(1), 12–17.

[122] Presa, A.; Brissos, R. F.; Caballero, A. B.; Borilovic, I.; Korrodi-Gregório, L.; Pérez-Tomás, R.; Roubeau, O.; Gamez, P. Photoswitching the Cytotoxic Properties of Platinum(II) Compounds. *Angew. Chem. Int. Ed. Engl.* **2015**, *54*(15), 4561–4565.

[123] Palao, E.; Slanina, T.; Muchová, L.; Šolomek, T.; Vítek, L.; Klán, P. Transition-Metal-Free CO-Releasing BODIPY Derivatives Activatable by Visible to NIR Light as Promising Bioactive Molecules. *J. Am. Chem. Soc.* **2016**, *138*(1), 126–133.

[124] Goswami, P. P.; Syed, A.; Beck, C. L.; Albright, T. R.; Mahoney, K. M.; Unash, R.; Smith, E. A.; Winter, A. H. BODIPY-Derived Photoremovable Protecting Groups Unmasked with Green Light. *J. Am. Chem. Soc.* **2015**, *137*(11), 3783–3786.

[125] Bléger, D.; Schwarz, J.; Brouwer, A. M.; Hecht, S. *o*-Fluoroazobenzenes as Readily Synthesized Photoswitches Offering Nearly Quantitative Two-Way Isomerization with Visible Light. *J. Am. Chem. Soc.* **2012**, *134*(51), 20597–20600.

[126] Dong, M.; Babalhavaeji, A.; Samanta, S.; Beharry, A. A.; Woolley, G. A. Red-Shifting Azobenzene Photoswitches for in Vivo Use. *Acc. Chem. Res.* **2015**, *48*(10), 2662-2670.

[137] Siewertsen, R.; Neumann, H.; Buchheim-Stehn, B.; Herges, R.; Näther, C.; Renth, F.; Temps, F. Highly Efficient Reversible *Z-E* Photoisomerization of a Bridged Azobenzene with Visible Light through Resolved $S_1(n\pi^*)$ Absorption Bands. *J. Am. Chem. Soc.* **2009**, *131*(43), 15594–15595.

[138] Yang, Y.; Hughes, R. P.; Aprahamian, I. Near-Infrared Light Activated Azo-BF_2 Switches. *J. Am. Chem. Soc.* **2014**, *136*(38), 13190–13193.

[129] Chen, X.; Wehle, S.; Kuzmanovic, N.; Merget, B.; Holzgrabe, U.; König, B.; Sotriffer, C. A.; Decker, M. Acetylcholinesterase Inhibitors with Photoswitchable Inhibition of β-Amyloid Aggregation. *ACS Chem. Neurosci.* **2014**, *5*(5), 377–389.

[130] Reisinger, B.; Kuzmanovic, N.; Löffler, P.; Merkl, R.; König, B.; Sterner, R. Exploiting Protein Symmetry to Design Light-Controllable Enzyme Inhibitors. *Angew. Chem. Int. Ed. Engl.* **2014**, *53*(2), 595–598.

[131] Velema, W. A.; Hansen, M. J.; Lerch, M. M.; Driessen, A. J. M.; Szymanski, W.; Feringa, B. L. Ciprofloxacin-Photoswitch Conjugates: a Facile Strategy for Photopharmacology. *Bioconjugate Chem.* **2015**, *26*(12), 2592–2597.